

DISSERTATION

UNRAVELING PRIONS: THE COMPLEXITIES BETWEEN THE PRION PROTEIN,
COMPLEMENT, AND B CELLS IN DIVERSE PATHOGENIC SETTINGS

Submitted by

Sarah Kane

Graduate Degree Program in Cell and Molecular Biology

In partial fulfillment of the requirements

For the Degree of Doctor of Philosophy

Colorado State University

Fort Collins, Colorado

Fall 2017

Doctoral Committee:

Advisor: Mark Zabel

James Bamburg
Ronald Tjalkens
Anne Avery

Copyright by Sarah Jo Kane 2017

All Rights Reserved

ABSTRACT

UNRAVELING PRIONS: THE COMPLEXITIES BETWEEN THE PRION PROTEIN, COMPLEMENT, AND B CELLS IN DIVERSE PATHOGENIC SETTINGS

Prions diseases affect numerous mammalian species and may arise spontaneously; from genetic predisposition of the prion protein, PrP^C, to misfold and aggregate; or from contacted with prion-contaminated materials. The first described prion disease, scrapie, manifests in sheep, and records date back to the 18th century. Other mammalian species susceptible to prion diseases include humans, cats, mink, cervids (deer, elk, and moose), and cattle. The term Transmissible Spongiform Encephalopathy (TSE) arose to describe this new class of infectious diseases which exhibit spongiform degeneration in the central nervous system (CNS). TSEs are invariably fatal diseases, and only herd culling or breeding resistance mitigate disease spreading. However, chronic wasting disease (CWD) in cervids represents the first known TSE to occur in free-ranging wildlife, and the apparent facile spread demands strategies to halt its spread and prevent species eradication.

Human prion disease characterization dates back to the 1920s. However, the bovine spongiform encephalopathy (BSE or mad cow disease) outbreak and subsequent transmission into a small number of humans in the 1980s and 90s pressed the need to understand the TSE agent. Many researchers since the 1960s postulated protein at least partially comprised the agent, but Stanley Prusiner provided the first

experimental evidence of protein composition correlating with infectivity. Further, he coined the term proteinaceous particle, or prion. Follow-up research elegantly highlighted a host protein requisite to cause disease. Researchers now broadly accept the disease mechanism involves misfolded prions perverting the cellular prion protein to alter its conformation and join the highly stable prion aggregate.

Upon peripheral exposure, most prion strains propagate in the lymphoreticular system prior to invading the CNS. Many elegant studies reveal the Complement system promotes initial prion trafficking and propagation in spleen and lymph nodes because mice deficient in various Complement proteins or receptors exhibit delayed or no disease. Once in the LRS, many postulate prions retrogradely infect the brain via sympathetic nerve fibers and the spinal cord. Once in the brain, prions provoke astrogliosis, neurodegeneration, and invariable death.

While prion researchers made great strides in characterizing TSEs within a short few decades, many fundamental questions remain unaddressed. For example: what additional host factors foster prion pathogenesis? What is the normal function of the properly-folded, cellular prion protein? Lastly, do prion binding partners provide therapeutic targets? Data presented in this dissertation highlight crucial roles for Complement regulatory protein Factor H and Complement receptor CD21 in scrapie pathogenesis, suggest C1q may strain-specifically impact prion disease, highlight PrP^C as a crucial mediator in the adaptive immune system, and provide potential therapeutic tools and targets to combat prion disease.

ACKNOWLEDGMENTS

The work presented in this dissertation culminated from numerous collaborations, round-table discussions, and friendly debates. I would like to personally thank Taylor Farley, Elizabeth Gordon, Joshua Estep, Dana Hill, Brady Michel, Heather Bender, and Eric Swanson for providing assistance in generating data presented here. Members of the Prion Research Center, particularly Glenn Telling, Richard Bessen, Jifeng Bian, and Julie Moreno, provided intellectual insight and overall positive reinforcement throughout the years. The Telling, Bartz, Bessen, Hannan, Ghebrehiwet, and Hoover labs provided invaluable research tools. The entire Zabel laboratory, both past and present, offer a collaborative and constructive environment, and without their support this work would severely lack. I would also like to thank Drs. Jim Bamburg, Ron Tjalkens, and Anne Avery for serving on my committee and providing insight and support.

My family and friends attended talks, dealt with scientific rants, and supported me throughout my entire life and career. I sincerely believe my career blossomed due to a handful of people believing in me. I would like to specifically thank Ian Foreman and Haley Elkin for providing emotional support throughout the dissertation writing process.

Lastly, I would like to acknowledge Drs. Joe Koke and Mark Zabel. These two crucial influences formed me into the scientist and person I am today. Thank you for dealing with my odd work hours, allowing me to make mistakes and learn from them, and most importantly, thank you for believing in me.

DEDICATION

I would like to dedicate this work to all the research animals whose invaluable lives helped generate the enclosed dissertation.

TABLE OF CONTENTS

ABSTRACT	ii
ACKNOWLEDGEMENTS	iv
DEDICATION	v
LIST OF FIGURES	viii
CHAPTER 1 – INTRODUCTION	1
REFERENCES	22
CHAPTER 2 – COMPLEMENT REGULATORY PROTEIN FACTOR H PARADOXICALLY PROMOTES PRION DISEASE	31
Summary	31
Introduction	32
Materials and Methods	35
Results	41
Discussion	58
REFERENCES	64
CHAPTER 3 – RELATIVE IMPORTANCE OF COMPLEMENT RECEPTORS CD21/35 (CR2/1) IN SCRAPIE PATHOGENESIS	68
Summary	68
Introduction	69
Materials and Methods	72
Results	78
Discussion	85
REFERENCES	89
CHAPTER 4 – CLASSICAL COMPLEMENT ACTIVATOR C1Q MAY IMPACT PRION DISEASES IN A STRAIN-SPECIFIC MANNER	93
Summary	93
Introduction	94
Materials and Methods	96
Results	101
Discussion	107
REFERENCES	110
CHAPTER 5 – PRP ^C , LIKELY IN COOPERATION WITH CD21/35, PROMOTES HUMORAL IMMUNITY	112
Summary	112
Introduction	113
Materials and Methods	116
Results	122
Discussion	135
REFERENCES	142
CHAPTER 6 – GENERATION OF PRION-SPECIFIC NANOBODIES: BIOCHEMICAL TOOLS AND POTENTIAL THERAPEUTICS TO COMBAT PRION DISEASE	147
Summary	147

Introduction	147
Materials and Methods.....	153
Results	158
Discussion.....	170
REFERENCES	173
OVERALL SUMMARY	175

LIST OF FIGURES

Figure 1.1 – Structure of human PrP ^C	15
Figure 2.1 – Factor H directly interacts with prion amyloid	42
Figure 2.2 – Example of fH mouse genotyping	43
Figure 2.3 – Experimental design of fH gene-dose study	44
Figure 2.4 – Factor H wild type, hemizygous, and knockout mice do not differ in splenic prion loads by 30dpi	45
Figure 2.5– Factor H hemizygous and knockout mice contain lower splenic prion loads at 60dpi	46
Figure 2.6 – Factor H hemizygous and knockout mice contain lower splenic prion loads at 90dpi	47
Figure 2.7 – Factor H hemizygous and knockout mice contain lower splenic prion loads at 120dpi	48
Figure 2.8 – Factor H hemizygous and knockout mice contain similar splenic prion loads as wild type by 150dpi	49
Figure 2.9 – Analysis of prion loads in brain at early time points	50
Figure 2.10 – Mice of all fH genotypes contain detectable PK-resistant prions in their brain by 180dpi	51
Figure 2.11 – Cumulative early time point data	52
Figure 2.12 – Factor H knockout mice resist the onset of terminal disease longer than wild type or hemizygous mice	53
Figure 2.13 – Histological brain examination from Factor H terminal disease study	53
Figure 2.14– The RML5 sex difference depends on route of inoculation	54
Figure 2.15 – Preliminary data: fH may select for certain prion strains	55
Figure 2.16 – C3 may confound the Factor H study	57
Figure 2.17 – C3 promotes prion pathogenesis in the central nervous system	58
Figure 3.1 – Illustration of murine splice variants CD35 and CD21	71
Figure 3.2 – CD21 and CD35 both bind prion amyloid	79
Figure 3.3 – CD21 promotes splenic accumulation at 30dpi	80
Figure 3.4– CD21-deficient mice resist terminal disease onset longer than wild type, hemizygous, or CD35-deficient mice	81
Figure 3.5 – Soluble CD21 may serve as a therapeutic	82
Figure 3.6 – CD19 alterations depend on CD21	84
Figure 3.7 – PrP ^C is not a confounding variable	84
Figure 4.1 – C1q directly interacts with prion amyloid	102
Figure 4.2 – C1q paradoxically limits CWD splenic accumulation, yet promotes RML5 accumulation	103
Figure 4.3 – C1q slightly enhances splenic CWD accumulation and early propagation in Tg5037;C1q ^{+/+} mice	104
Figure 4.4 – <i>In vitro</i> prion infection assays may help ascertain C1q’s role in prion disease	105
Figure 4.5– C1q prevents the onset of terminal disease in a transgenic mouse model of CWD	107

Figure 5.1 – Cell-surface PrP ^C levels reduce after <i>in vitro</i> stimulation.....	123
Figure 5.2 – Splenic lymphocyte proportions and naïve, non-vaccinated survival against <i>E. coli</i> infection depends on mouse background, not <i>Prnp</i> status	125
Figure 5.3 – PrP ^C augments early events in B cell activation	127
Figure 5.4– PrP ^C bolsters humoral immunity after vaccination.....	129
Figure 5.5 – Vaccination does not entirely protect PrP KO from infection with live <i>E. coli</i>	130
Figure 5.6 – PrP ^C forms a complex and co-localizes with B cell co-receptor member CD21	131
Figure 5.7 – PrP ^C may regulate CD21 translocation efficiency.....	133
Figure 5.8 – PrP ^C deficiency increases CD19 protein levels	135
Figure 6.1 – Cartoon diagram of camelid antibodies discussed in this chapter.....	149
Figure 6.2 – Nanobody library construction experimental design.....	152
Figure 6.3 – Alpaca serum contains highly-reactive antibodies after the 6 th boost	159
Figure 6.4– Phage display vector pMESy4 vector map and analysis.....	160
Figure 6.5 – Initial screens show low percentage of clones containing true nanobody inserts	161
Figure 6.6 – Large-scale library production and phage packaging	162
Figure 6.7 – Phage panning round 1	163
Figure 6.8 – Phage panning number 2 enriched specificity by an undefined amount .	164
Figure 6.9 – Library master plate analysis	165
Figure 6.10 – CDR3 sequence homology analysis	167
Figure 6.11 – Two positive clones may specifically recognize infected brain.....	169

CHAPTER 1 – INTRODUCTION

Historical relevance. The advent of bovine spongiform encephalopathy, AKA mad cow disease or BSE, and the subsequent transmission into a small number of humans (Hill et al. 1997) in the 1980s and '90s, respectively, generated a great need to characterize and decipher the disease etiology. Many researchers asserted the pathogen exhibited characteristics of a slow-acting virus, and the race to detect and sequence the virus ensued. However, it would take a heretical and highly controversial study from Stanley Prusiner's laboratory to classify an entirely new class of infectious agent, which he termed proteinaceous particle, or prion.

The first record of this unusual type of disease dates back to 1732 in Great Britain. Sheep and goats infected with this disease, termed scrapie, display odd behavioral signs, including blank stares and rubbing along fences until they scrape off their wool or hair. Other hallmark signs of scrapie include weight loss and ataxia, a clinical term for incoordination. Brain lesions indicative of spongiform encephalopathy were first described in 1898 (reviewed in Wang et al. 2015).

Other animals, often in situations of captivity, may also succumb to this type of disease. For example, Wisconsin ranch-raised mink farmers first observed a neurological disease similar to scrapie in 1947 (Hartsough and Burger 1965). Cervids, including deer, reindeer, elk, and moose, can succumb to chronic wasting disease (CWD), named after the overt weight-loss phenotype. CWD gained much attention in the media due to

the following worrisome characteristics: 1) the first prion disease known to affect free-ranging animals, 2) the rapid spread into several states in the Continental United States and 3) the appearance (or perhaps first detection) in reindeer and moose in Scandinavia in 2016 (Benestad et al. 2016). CWD spreading mechanisms and origin(s) remain largely unknown. Some propose CWD arose from a spontaneous case which infected other cervids via contact with contaminated plants or soil; others propose all prion diseases come from the first described prion disease, scrapie.

Perhaps one of the most unique features of scrapie is environmental persistence. Georgsson et al. (2006) analyzed Icelandic records regarding scrapie recurrence after herd culling. One farmer culled his entire flock in 1982 and housed a different flock in a new building until 1998. Sixteen years after culling the old flock, the farmer transferred 4-5 lambs into the former sheep house, and one lamb developed scrapie within two years. These worrisome data suggest the scrapie pathogen can persist in the environment for at least 16 years. Studies suggest scrapie persists in soil (Seidel et al. 2007) or dust (Gough et al. 2015). CWD appears to persist in the environment as well. Wyckoff et al. (2016) reported CWD transmission into model organisms housed on soil naturally contaminated with CWD. Collectively, these data highlight scrapie and CWD environmental persistence and begin to unravel the difficulty in producing efficient mitigation strategies.

Human prion diseases. Pathologists Creutzfeld and Jakob characterized a distinctive neurological disease in the early 1920s. As reviewed in Wolfgang (1968), Creutzfeldt

first described a 23 year-old woman with a neurological disease lasting 2.5 years. Postmortem examination showed previously undescribed alterations in subcortical nuclei and grey matter in the cerebral cortex. Jakob described three similar cases the following year and termed the disease “spastic pseudosclerosis” in 1923. The name was later changed to Cruetzfeldt-Jakob disease (CJD) after the two pathologists who initially described the disease. We now recognize CJD as a human prion disease, but researchers did not appreciate the parallels between CJD and the other animal prion disease for several decades.

Humans prion diseases occur due to polymorphisms in the *PRNP* gene, from spontaneous misfolding and aggregation of the *PRNP* protein product, PrP^C, from ingestion of prion-contaminated tissues, or from iatrogenic exposure in surgery or blood transfusions. To date, there are 3 known genetic prion diseases. While spontaneous Creutzfeld-Jakob disease (sCJD) remains an enigma, heterozygosity at *PRNP* codon 129 appears to offer some resistance to both spontaneous and acquired CJD (Palmer et al. 1991; Saba and Booth 2013). Lastly, humans can acquire CJD via ingestion or medical practices involving prion-contaminated tissues/blood or instruments.

Genetic prion diseases include: familial CJD, Gerstmann-Straussler-Scheinker (GSS) disease, and fatal familial insomnia (FFI). Several *PRNP* polymorphisms correlate with phenotypes associated with genetic prion diseases (Mastrianni 2014). Genotype-phenotype correlations in familial CJD include: Asp178Asn concomitant with 129V; Val180Ile; Thr183Ala; Glu200Lys; Arg208His; Val210Ile; or Met232Arg. GSS variants

include Pro102Leu, Pro105Leu, Ala117Val, Tyr145Stop, Gln160Stop, Phe198Ser, and Gln217Arg. Only one polymorphism is associated with FFI: Asp178Asn concomitant with 129M. Clinical manifestations of genetic prion diseases include: dementia, autonomic disturbances (such as insomnia in FFI), chorea, and ataxia. Due to clinical manifestations overlapping with more common Alzheimer's disease (AD), many prion disease cases are likely misdiagnosed as AD. Thus, genetic testing aids in identifying genetic prion disease, but not sporadic or acquired CJD. Post-mortem analyses confirm prion disease diagnoses, including spongiform degeneration, astrogliosis, and anti-PrP positive amyloid plaques.

As the name implies, spontaneous CJD (sCJD) seems to occur spontaneously. While there are no known causative *PRNP* polymorphisms associated with sCJD, heterozygosity at codon 129 seems to protect individuals from developing sCJD. In other words, individuals homozygous at codon 129 for either Methionine (M) or Valine (V) develop sCJD more frequently than heterozygous individuals. While M or V at codon129 does not alter the structure or folding of PrP^C (Hosszu et al. 2004), heterozygosity likely alters downstream misfolding mechanism. Perhaps homozygous individuals with 100% of PrP^C containing identical structure are more prone to self-associate. However, this remains largely unexplored. Purified PrP is prone to aggregate under acidic conditions (Swietnicki et al. 2000). Therefore, perhaps one could study whether a pure sample of PrP containing 129M or 129V spontaneously misfolds at a faster rate than a mixture of equimolar PrP containing 129M and 129V.

Humans may also acquire prion disease from ingesting prion-contaminated cattle tissues. As mentioned above, most widely accept variant CJD (vCJD) arose due to BSE entering the human food chain. Similarly to sCJD, the main genetic factor known to increase the risk of acquiring vCJD is homozygosity at codon 129. In fact, only one known vCJD case occurred in an individual heterozygous at codon 129 (Kaski et al. 2009). Although entirely devastating to patients and families, the World Health Organization reported only 175 total vCJD cases in the United Kingdom and 49 cases in other countries by 2012. Similarly, Diack et al. (2014) reported 177 cases in the UK and 51 cases from other countries (228 total). However, recent estimates indicate 1:2,000 people in the UK carry vCJD prions in their appendix. Many prions exhibit lymphotropism prior to invading the central nervous system (CNS), and Hilton et al. (1998) reported prion immunoreactivity in appendix prior to clinical onset. Therefore, Gill et al. (2013) screened archived formalin-fixed, paraffin-embedded appendix samples. Of the 32,441 samples tested, 16 showed prion immunoreactivity. This study begs the question: does subclinical infection equate to eventual clinical disease?

Other examples of human prion disease transmission involve medical procedures or ritualistic cannibalism. Rudge et al. (2015) reported 77 cases of iatrogenic CJD after cadaver-derived pituitary-derived growth hormone treatment. These patients received growth hormone during childhood, and the onset of clinical signs occurred at 43 years of age (mean). Further, three iatrogenic CJD cases occurred after patients received blood transfusions contaminated with vCJD prions (Llewelyn et al. 2004, Peden et al. 2004, and Dietz et al. 2007), and humans can iatrogenically acquire prions [likely] from dura

mater grafts (Thadani et al. 1988 and Kim et al. 2011). Lastly, the prion disease Kuru arose in the Fore tribe in Papua New Guinea due to ritualistic cannibalism of deceased loved ones (reviewed in Liberski 2013), and Hadlow noticed similarities between Kuru and scrapie in 1959. Similarly to spontaneous and variant CJD, heterozygosity of codon 129 confers prolonged incubation times or resistance to Kuru (Mead et al. 2008).

Proteinaceous infectious only. After the BSE and vCJD outbreaks, the race to discover the pathogen ensued. Carleton Gajdusek, one of the primary researchers involved in describing Kuru, argued the pathogen exhibited characteristics of a slow-acting virus (Gajdusek 1967; Gajdusek and Gibbs 1968). In fact, most scientists and clinicians believed the agent was viral until the 1980s, and the Gajdusek laboratory continued to label the CJD pathogen a virus up to one year prior to Prusiner's Nobel Prize award (Kordek et al. 1996).

Many researchers noted the scrapie agent resisted viral inactivation procedures, such as formalin fixation (Pattinson 1965). However, it took Stanley Prusiner's highly controversial publication (Prusiner 1982) to experimentally show the scrapie agent not only required, but is comprised of, protein. Prusiner argued the scrapie agent (termed proteinaceous particle, or prion) is much smaller than a virus and resists most nucleic acid inactivating procedures, including ultraviolet irradiation and formalin fixation (Prusiner et al. 1981 and 1982). As mentioned previously, Prusiner's work and receiving a Nobel Prize was highly controversial. First, the concept of a protein pathogen did not sit right with virologists, and Prusiner received public ridicule (described in Mallucci

2014). Secondly, Prusiner was not the first to describe the scrapie agent's resistance to nucleic acid inactivation (Alper et al. 1967, among others). Lastly, Alper et al. proposed the scrapie agent replicates without nucleic acid in 1967, and the hypothesis of self-replicating proteins derived from host machinery was first described by Griffith (1967). Prusiner (1982) cited Griffith's 1967 article, attributing the origin of replicating protein hypothesis to Griffith. Despite this citation, many felt as though Prusiner "piggy-backed" on others' theoretical breakthroughs.

However, the first experimental evidence of infectious proteins did indeed come from Prusiner's laboratory. In 1981, Prusiner et al. showed proteinase K (PK, 100 µg/mL for 2 hours) treatment reduced scrapie infectivity, whereas RNase or DNase minimally impacted infectivity. At this time, Prusiner et al. concluded a protein at least partially comprised the scrapie agent. McKinley, Bolton, and Prusiner (1983) showed the amount of scrapie protein component, termed PrP, directly correlated with infectivity.

Specifically, they reported reduced titer corresponding to increased PK digestion. In other words, mild protease digestion did not affect scrapie infectivity, but complete digestion with PK ablated infectivity. These data, along with the evidence showing nucleic acid inactivation did not reduce scrapie infectivity, compelled Prusiner to present a new mechanism of information transfer outside of the central dogma of biology (DNA -> RNA -> protein).

While Prusiner and Griffith both implicated the involvement of host protein(s) in scrapie pathogenesis, it wasn't confirmed until Oesch et al. (1985) sequenced PrP 27-30

(named for the relative molecular weight after gel electrophoresis). Briefly, Oesch et al. purified prions and separated the fragments by high pressure liquid chromatography (HPLC). The sequence was obtained by gas-phase sequencing, and they determined RNA sequence by reverse translation. They then revealed the sequence was present in the hamster genome via southern blotting, and mRNA transcript was detected in both infected and non-infected brains via northern blotting. This seminal work provided the first experimental evidence that the host genome indeed encoded PrP (named in Prusiner 1982). It wasn't until 1993 that Bueler et al. showed the dependence on host PrP^C to generate prion disease. In summary, *Prnp* knockout (PrP KO) mice resisted disease when inoculated with scrapie prions. They rescued this effect by crossing PrP KO mice to express the Syrian hamster transgene, rendering the mice susceptible to hamster prions. This groundbreaking study highlighted the importance of a host protein in scrapie pathogenesis.

Interestingly, PrP KO mice are able to develop humoral (antibody) responses against scrapie prions (Prusiner et al. 1993). This phenomenon is easily explained by the built-in regulatory mechanism to prevent autoimmunity. During development, T and B lymphocytes which recognize host proteins are rendered anergic. While this mechanism prevents auto-immunity, this limits vaccination paradigms against prions since the disease relies on host protein expression. B cell-mediated humoral immune responses are either T- dependent or independent. T-dependent antigens require not only B cell antigen recognition, but also cognate T cell antigen recognition. In summary, B cells (and other antigen presenting cells) load peptides into MHC II complexes, and if T cells

simultaneously recognize antigens from the same pathogen via their T cell receptor (TCR), the B cell activates to produce antibody. However, antigens loaded into MHC II complexes are comprised of linear epitopes. Therefore, any T cell which recognizes a linear epitope from PrP^C would be negatively selected against during development. Thus, the only hope to elicit an adaptive immune response against prions would arise from T-independent B cell activation. T-independent antigens are usually structural or repeating in nature. For example, lipopolysaccharide (LPS) from *Escherichia coli* is a repeating, polysaccharide structure which can elicit T-independent antibody responses.

Perhaps vaccinating animals with prions in conjunction with a T-independent adjuvant, such as saponin (White et al. 1991) could aid in eliciting humoral immune responses against prions. However, vaccinating animals with prions raises the concern of infecting the animals with the vaccine. In fact, Gordon (1946) attempted to vaccinate animals with formalin-fixed scrapie prions, only to find all sheep succumbed to prion disease within two years. Future directions include determining a way to abolish prion infectivity yet maintain structural integrity. For more information regarding the complexities of prion vaccines, see Zabel and Avery (2015).

Alternatively to vaccination, other antibody therapeutic options for combatting prion disease may exist. Perhaps vaccinating PrP KO mice with prions, then humanizing said antibodies, could provide a viable treatment. Further, Pardon et al. (2014) outlined a molecular biology technique to generate camelid “nanobodies” which share high homology with human variable domains. Nanobodies preferentially bind structural

epitopes, may spontaneously cross the blood brain barrier, and thus offer potential for treating prion disease. For more information, see Chapter 6.

Prions and the immune system. While prions fail to elicit adaptive (B- or T- cell mediated) immunity, certain cells and proteins in the innate immune system recognize prions and counter-intuitively aid in initial spread and replication. Specifically, Michel et al. (2012) showed macrophages are the main cell-type to capture and/or retain prion rods in the peritoneal cavity and mediastinal lymph nodes. Once in the lymph node, cell:cell prion rod transfer occurs to B cells ~6 hours post-exposure.

Several lines of evidence highlight a crucial role for follicular dendritic cells (FDCs) and B cells in prion disease pathogenesis. FDCs abundantly express PrP^C, and limiting PrP^C expression to FDCs alone sufficiently caused prion infection in spleen upon peripheral exposure (McCulloch et al. 2011). Further, juxtaposing FDCs to sympathetic nerve fibers in CXCR5^{-/-} mice enhanced prion neuroinvasion (Prinz et al. 2003). Klein et al. (1997) showed B cell deficiency (μ MT) prevented prion disease in a scrapie mouse model. Further, Mok et al. (2012) showed B cells distribute prions from draining lymph nodes to secondary lymphoid organs (SLOs) because specifically preventing B cell egress via sphingosine 1-phosphate receptor 1 deficiency prevented prion transport and propagation to SLOs. Intriguingly, however, PrP^C expression on B cells is dispensable for establishing disease because PrP^C deficiency specifically in B cells did not prevent neuroinvasion (Klein et al. 1998). These data suggest B cells utilize a mechanism beyond PrP^C to capture and spread prions. Data presented within suggest Complement

Receptors 2/1 (CR2/1 or CD21/35) may be the putative peripheral prion receptor. For more information, see Chapter 3.

Prions require an intact Complement system to establish disease because mice deficient in various Complement proteins either partially or entirely resist prion disease. Deficiency in C3, arguably the key player in Complement, causes a delay in prion accumulation and onset of clinical symptoms in CWD and scrapie mouse models (Michel et al. 2012b and Mabbott et al. 2001). Deficiency in the classical Complement cascade activator C1q also increases survival time in mouse model of scrapie (Mabbott et al. 2001). Dendritic cells (DCs) largely require C3 and C1q to capture and traffic prions to sites of replication because DCs from mice deficient in C1q or C3 capture fewer prions (Michel et al. 2012). Interestingly, Complement receptors CD21/35 promote prion disease more-so than their endogenous ligand, C3. Mice deficient in CD21/35 display prolonged survival (Zabel et al. 2007) or entirely resist disease (Michel et al. 2012) in mouse models of scrapie or CWD, respectively, whereas transgenic mice lacking C3 eventually succumbed to disease. Collectively, these data highlight Complement's critical role in prion disease pathogenesis, and suggest CD21/35 impact prion disease independent of C3.

Glial cells in prion disease. Glial cells in the CNS include astrocytes, microglia, and oligodendrocytes. Astrocytes express PrP^C and are thereby susceptible to prion infection. In fact, astrocyte-restricted PrP^C is sufficient to cause infection after intracerebral inoculation (Raeber et al. 1997). Further, prion infection induces

astrogliosis, or the transition from quiescence to an inflammatory state. Several lines of evidence suggest neuroinflammation promotes neurodegeneration and eventual death. Kordek et al. (1996) reported mouse-adapted CJD infection induced ~200-fold TNF-alpha increase in mice compared to non-infected controls. Astrocytes are known to produce TNF-alpha in response to various immunological stimuli (Chung and Benveniste 1990). Further, mice deficient in anti-inflammatory cytokine interleukin 10 (IL-10) succumb to prion disease faster than IL-10 sufficient mice (Thackray et al. 2004). IL-10 dampens the inflammatory response, and these data suggest IL-10 prolongs survival during prion disease. Intriguingly, these effects were seen after both intracerebral and peripheral inoculation, suggesting IL-10 impacts both peripheral and CNS infection. Collectively, these data suggest neuroinflammation negatively impacts prion disease outcome, and perhaps promoting an anti-inflammatory state may prolong the life of a patient with prion disease.

Microglia express PrP^C (Brown et al. 1998) and likely also promote inflammation and subsequent neuronal death. Bate, Boshuizen, and Williams (2005) reported microglia induce neuronal death via a CD14-dependent mechanism. CD14 cooperatively signals with the LPS receptor, TLR4. Perplexingly, TLR4 mutant mice display accelerated prion disease onset regardless of inoculation route. These data suggest TLR4 signaling combats prion infection, yet also promotes neuronal cell-death via CD14. TLR4 and CD14 signaling in microglia appear to be a double-edged sword. Perhaps TLR4 promotes prion phagocytosis by microglia, which helps remove prions, but the resulting inflammation, perhaps mediated by TNF-alpha (Wu et al. 2009), promotes neuronal cell

death. If so, perhaps future directions could include promoting TLR-mediated phagocytosis without the resulting cytokine response.

Prion strains. Prions appear to undergo selection mechanisms and may display differential tropism and adaptation. While the concept of viral strains is intuitive based on differential genetic information and tropisms, the definition of prion strains remains murky. Prion strains exhibit distinct pathological phenotypes, but what “encodes” the differences between prion strains? For example, Bessen and Marsh (1992) reported transmissible mink encephalopathy (TME) inoculated into hamsters caused two distinct disease phenotypes after three passages. In one cohort, the hamsters displayed lymphotropism, hyperactive clinical signs, and succumbed to disease at 65 days (mean). The authors termed this phenotype hyper-TME (HY-TME). The hamsters in the second cohort did not display lymphotropism, exhibited lethargic behavior, and succumbed to disease at 168 days (mean). The authors termed this phenotype drowsy-TME (DY-TME)

These data suggest prions may exist as different strains, but considering prions do not differ in primary sequence, does strain information exist at the conformational or post-translational modification level? Do host factors preferentially select certain conformers within the milieu of original inoculum? Perhaps the answer may involve a combination of both. For example, the Caughey and Telling labs revealed differential conformational stabilities between different prion strains. Specifically, certain strains resist higher concentrations of guanidinium hydrochloride denaturation than others and show

differential antibody binding capacities (Saijo et al. 2016). However, Sjoberg et al. (2008) reported Factor H, a Complement regulatory protein, differentially binds prion conformers. Specifically, Factor H appeared to bind PrP oligomers to a greater extent than PrP fibrils. Thus, Factor H may bind certain conformers, and thus dictate which conformers evade Complement recognition and subsequent trafficking/propagation *in vivo*. For more information, see Chapter 2. In summary, prion strains remain enigmatic, although the selection mechanisms likely involve a combination of conformer stabilities and host selection mechanisms.

Prion protein (PrP^C) physiology. Human *PRNP* on chromosome 20 contains 3 exons. Exon 3 encodes the open reading frame (ORF) and thus protein product (See Figure 1.1). Zahn et al. (2000) resolved the human prion protein NMR structure. The N-terminal domain contains copper-binding octapeptide repeats (Riek et al. 1996) and is largely flexible and disordered, while the globular, structured domain contains secondary alpha helices and anti-parallel beta sheet. The three alpha helices comprise residues 144-154, 173-194, and 200-228. Residues 128-131 and 161-164 comprise the anti-parallel beta sheet. The prion protein exists in three glycosylation states: diglycosylated, monoglycosylated, or un-glycosylated. N-linked glycan occupation occurs at asparagine residues 181 and 197 in humans (first described in Liao et al. 1986) or 180 and 196 in mouse (Locht et al. 1986). Riek et al. (1996) reported a disulfide bond between cysteine residues 179 and 214. Lastly, PrP^C anchors to cholesterol-rich lipid raft domains via glycosylphosphatidylinositol (GPI) addition (Stahl et al. 1987) on the C-terminus.

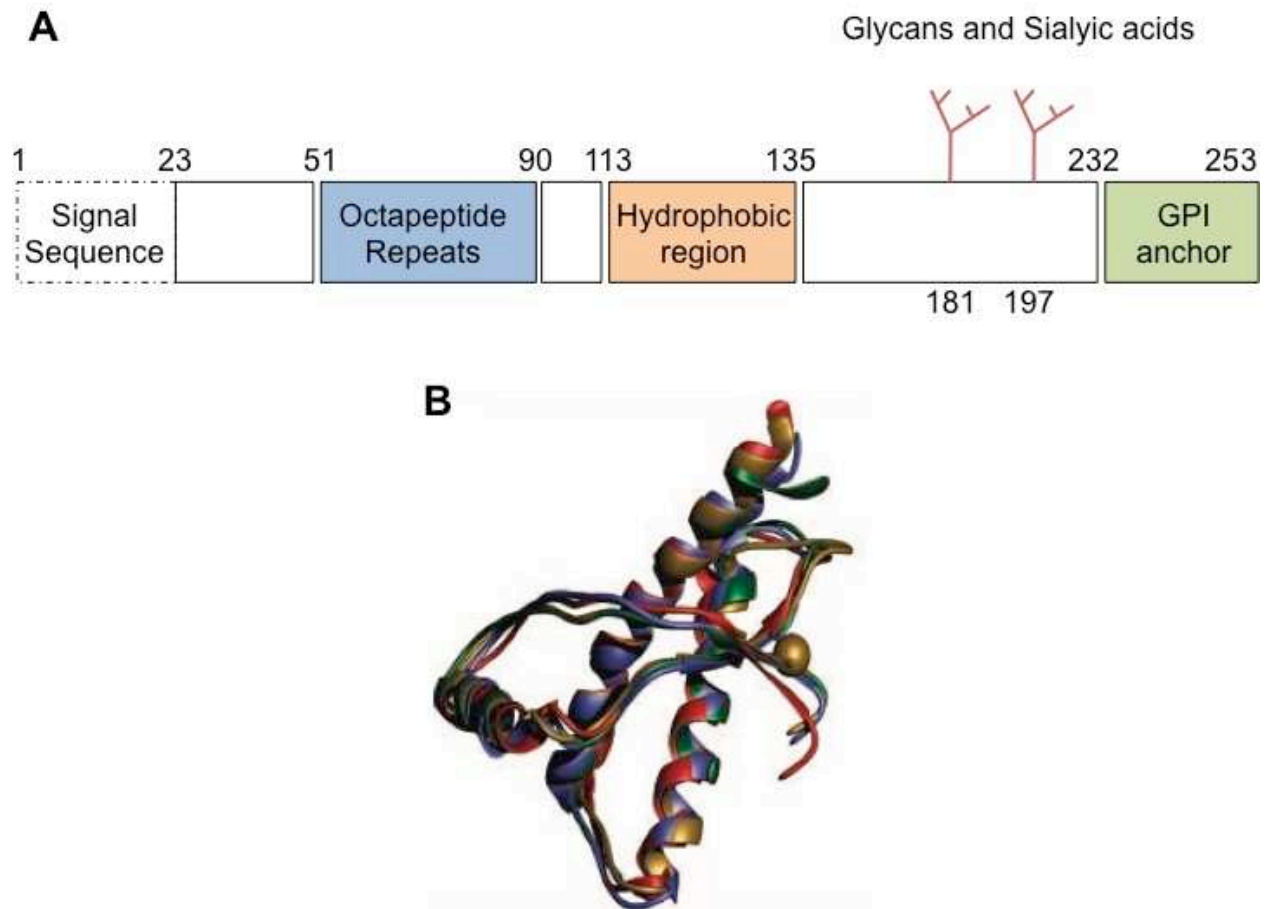


Figure 1.1. Structure of human PrP^C. Human *PRNP* on chromosome 20 contains 3 exons, and exon 3 encodes the ORF. The first 23 amino acids of PrP^C (A, modeled from Acevedo-Morantes and Wille 2014) encode the signal sequence which is not found in fully processed protein. The octapeptide repeat region binds copper and other divalent cations. N-linked glycans may occupy Asn residues at 181 and 197 (red). PrP^C anchors to the outer leaflet of the plasma membrane via glycosylphosphatidylinositol (GPI) addition on the C-terminus. NMR and crystal structures of human PrP^C (B, from Hosszu et al. 2004) show that polymorphism at 129 (sphere) does not alter protein structure (129V: yellow; 129M: red; crystal structure: green).

Mammals, from mice to men, abundantly express PrP^C, and most notably in the lymphoid and nervous systems. However, the precise physiological function of PrP^C remains elusive because *Prnp*^{-/-} transgenic (PrP KO) mice appear to develop normally (Prusiner et al. 1993). However, PrP KO mice display deficiencies in long term potentiation during development (Caiati et al. 2013), and the Strittmatter group reports

synaptic signaling via the metabotropic glutamate receptor involves PrP^C (Haas et al. 2016). Further, PrP^C promotes neurite outgrowth via interactions with neural cell adhesion molecule (NCAM) and Fyn kinase (Santuccione et al. 2005). These data suggest that while PrP KO mice appear to develop normally, PrP^C may play a role in synaptic transmission.

PrP^C appears to potentiate T cell proliferation and/or immunological synapse formation between antigen presenting cells (APCs) and T cells. Specifically, Mabbott et al (1997) showed primary mouse lymphocyte proliferation in response to Con-A partially depended on PrP^C because anti-PrP antibodies abrogated proliferation. Further, T cell mitogen PHA caused PrP^C upregulation in human T cells, and T cell proliferation in response to anti-CD3 was abrogated by anti-PrP antibody 8H4 (Li et al. 2001).

Cashman et al. (1990) also reported cell-activation increased surface levels of PrP^C, and anti-PrP antibodies suppressed proliferation. However, antibody treatment could potentially disrupt cell:cell interactions necessary for stimulation. Interestingly, however, PrP-deficient dendritic cells (DCs) exhibited impaired PrP^{+/+} T cell stimulation, suggesting PrP^C may exert its effect via APCs at the level of the immunological synapse (Ballerini et al. 2006).

Several studies show PrP^C regulation during cell stress/immunological responses. For example, Shyu et al. (2002) reported *Prnp* mRNA upregulation in response to heat shock. Interestingly, Lotscher et al. (2003) also reported increased PrP^C immunodetection in germinal centers and follicular dendritic cell networks after vesicular

stomatitis viral infection. Ballerini et al. (2006) reported increased cell-surface PrP^C in activated T cells, and inhibitory antibody SAF83 against PrP reduced proliferation after stimulation. Logic therefore serves to suggest PrP^C plays a role in CD8+ cell signaling in response to an intracellular pathogen. However, Genoud et al. (2004) reported no deficiency in CD8+ T cell responses against cytotoxic lymphocytic choriomeningitis virus (LCMV) or vesicular stomatitis virus (VSV) in mice deficient in PrP^C and its homolog Doppel. This was observed by LCMV-specific cytotoxic T lymphocyte numbers in blood, as well as antibody responses after vaccination. Collectively, these results suggest PrP^C may participate in immunological events leading to lymphocyte activation, but the precise roles and functions remain unclear.

B cells can generate humoral (antibody) responses both dependent and independent of T cell help. Lipopolysaccharide (LPS) is an example of a T-independent antigen due to repeating structures capable of activating B cells even without cognate T cell help. Interestingly, PrP KO mice show increased susceptibility to LPS-induced septic shock (Liu et al. 2015). Furthermore, PrP^C cross-linking induced calcium flux and ERK phosphorylation in Jurkat T cells (Stuermer et al. 2004). Interestingly, ERK phosphorylation and calcium flux also occur in the process of B cell activation. Lastly, PrP^C was found to co-precipitate with Fyn kinase (Shi et al. 2013), another known member involved in B cell activation downstream of antigen recognition. However, further biochemical experiments such as surface plasmon resonance are required to conclude this direct interaction. Collectively, PrP^C appears to augment T cell proliferation, yet T-dependent immunological responses to viral infection do not appear

to depend on the expression PrP^C (Genoud et al. 2004). Thus, the role of PrP^C in an adaptive immune response remains unclear. Data generated in Chapter 5 aimed to address the role of PrP^C in B cell activation.

Physiologically-relevant prions. Not all protein aggregation associates with disease. In fact, protein aggregation appears to serve a biological purpose across kingdoms. In bacteria, the Rho transcription terminator no longer halts transcription in its aggregated state (Yuan and Hochschild 2017). A similar phenomenon occurs in yeast cells, albeit through a different mechanism and involving a different protein (Wickner 1994, reviewed in Wickner et al. 2007). These findings naturally incite various questions regarding misfolded proteins associated with disease. Do these proteins aggregate in response to the true culprit underpinning disease? In other words, could PrP^C aggregation provide a biological signal, but occasionally become non-resolvable and infectious? One could easily test this hypothesis using techniques employed by yeast prion researchers. For example, semi-denaturing detergent agarose gel electrophoresis (SDD-AGE) employs the use of partial denaturation with a detergent such as sodium dodecyl sulfate (SDS) to distinguish between soluble protein and higher-order aggregates. Perhaps PrP^C aggregates in response to insult. Experiments to address this hypothesis are currently underway.

Prion detection/diagnostics. Perhaps the largest hurdle in prion diagnostics involves discriminating prions from PrP^C. Historically, researchers relied on prion resistance to protease digestion. Proteinase K (PK) digestion ranging between 10 – 100 µg/mL for

30-120 minutes digests PrP^C but leaves the resistant prion core intact. This core fragment, termed PrP^{RES}, is readily detected via western blotting and runs with apparent differences in molecular weight depending on BSE or CJD type (Hill et al. 1997 and Casalone et al. 2004). Further, prion histological detection relies on formic acid denaturation and/or PK digestion. Experiments from our laboratory suggest different prion strains, for example mouse-adapted scrapie vs transgenic CWD models, require different protocols for IHC detection and thus highlight stability differences between prion strains as discussed previously.

The aforementioned techniques require relatively high prion loads for detection, and sub-threshold prion levels may go undetected and thus prone to type-II error. Therefore, Claudio Soto's laboratory (Saborio et al. 2001) developed an amplification technique, termed protein misfolding cyclic amplification (PMCA), which provides substrate for sub-threshold prion seeds to amplify *in vitro*. Briefly, PMCA employs the use of perfused brain homogenate derived from mice which over-express PrP^C to amplify prions in a 37°C sonicator water bath. Growing prion seeds undergo 24 hour rounds with sonication bursts every 30 minutes to break up the prion aggregate into smaller seeds. Samples undergo serial rounds after 1:2 dilution into fresh normal brain homogenate (NBH). Each round is assessed for PrP^{RES} via traditional PK digestion and western blotting. The Zabel laboratory translated Soto's PMCA protocol to detect CWD using NBH from transgenic mice which overexpress the elk prion protein (Meyerett et al. 2008). Further, the Zabel laboratory designed a PMCA scoring paradigm which correlates round to positivity with initial prion load (Pulford et al. 2012) and offers a way

to run statistical analyses. In other words, tissues with higher prion loads will become positive via western blot at earlier rounds than tissues with lower initial prion loads.

The Nishida laboratory developed another prion amplification technique (Atarashi et al. 2011) termed real-time quaking induced conversion (RT-Quic). Unlike PMCA, RT-Quic uses soluble, recombinant PrP as the substrate for amplifying sub-threshold quantities of prion seed. To date, researchers used RT-Quic to amplify prions derived from cerebral spinal fluid (Atarashi et al. 2011), brain, urine, and feces (John et al. 2013). While one could argue PMCA is more sensitive due to serial amplifications, RT-Quic minimizes animal use and is less time-consuming.

Prion-like diseases. Several host proteins present amyloid formation associated with neurodegenerative diseases. For example, Alzheimer's, Parkinson's, and Huntington's diseases all contain a protein-misfolding component. While each disease displays unique manifestations and associated amyloid-forming protein, Verma et al. (2015) proposed a unifying mechanism of protein-based information transfer. Specifically, a native host protein undergoes a conformational transition and self-aggregates. A small number of misfolded protein units comprise oligomers, whereas fibrils are much larger. Fibrils associate to form plaques, and plaque depositions are a hallmark characteristic of the aforementioned neurodegenerative diseases. However, whether the protein misfolding underlie disease manifestations or are simply correlated with the true cause of disease remains unknown.

In summary, prions may affect various mammalian species and require host protein expression to cause disease. While prion researchers made great strides in understanding this newly discovered mode of information transfer, several questions remain unaddressed. For example, what cellular factors promote prion disease? What is the physiological function of the cellular prion protein? Lastly, how can we treat the invariably fatal prion diseases? Data presented in this dissertation aimed to at least begin to address these questions and provide evidence of various therapeutic targets and research tools.

REFERENCES

- Acevedo-Morantes CY, Wille H. The structure of human prions: from biology to structural models-considerations and pitfalls. *Viruses*. 2014 Oct 20;6(10):3875-92. doi: 10.3390/v6103875. Review. PubMed PMID: 25333467; PubMed Central PMCID: PMC4213568.
- Alper T, Cramp WA, Haig DA, Clarke MC. Does the agent of scrapie replicate without nucleic acid? *Nature*. 1967 May 20;214(5090):764-6. PubMed PMID: 4963878.
- Atarashi R, Satoh K, Sano K, Fuse T, Yamaguchi N, Ishibashi D, Matsubara T, Nakagaki T, Yamanaka H, Shirabe S, Yamada M, Mizusawa H, Kitamoto T, Klug G, McGlade A, Collins SJ, Nishida N. Ultrasensitive human prion detection in cerebrospinal fluid by real-time quaking-induced conversion. *Nat Med*. 2011 Feb;17(2):175-8. doi: 10.1038/nm.2294. Epub 2011 Jan 30. PubMed PMID: 21278748.
- Ballerini C, Gourdain P, Bachy V, Blanchard N, Levavasseur E, Grégoire S, Fontes P, Aucouturier P, Hivroz C, Carnaud C. Functional implication of cellular prion protein in antigen-driven interactions between T cells and dendritic cells. *J Immunol*. 2006 Jun 15;176(12):7254-62. PubMed PMID: 16751368.
- Bate C, Boshuizen R, Williams A. Microglial cells kill prion-damaged neurons in vitro by a CD14-dependent process. *J Neuroimmunol*. 2005 Dec 30;170(1-2):62-70. Epub 2005 Oct 11. PubMed PMID: 16225933.
- Benestad SL, Mitchell G, Simmons M, Ytrehus B, Vikøren T. First case of chronic wasting disease in Europe in a Norwegian free-ranging reindeer. *Vet Res*. 2016 Sep 15;47(1):88. doi: 10.1186/s13567-016-0375-4. PubMed PMID: 27641251; PubMed Central PMCID: PMC5024462.
- Bessen RA, Marsh RF. Biochemical and physical properties of the prion protein from two strains of the transmissible mink encephalopathy agent. *J Virol*. 1992 Apr;66(4):2096-101. PubMed PMID: 1347795; PubMed Central PMCID: PMC289000.
- Brown DR, Besinger A, Herms JW, Kretzschmar HA. Microglial expression of the prion protein. *Neuroreport*. 1998 May 11;9(7):1425-9. PubMed PMID: 9631441.
- Büeler H, Aguzzi A, Sailer A, Greiner RA, Autenried P, Aguet M, Weissmann C. Mice devoid of PrP are resistant to scrapie. *Cell*. 1993 Jul 2;73(7):1339-47. PubMed PMID: 8100741.
- Caiati MD, Safiulina VF, Fattorini G, Sivakumaran S, Legname G, Cherubini E. PrPC controls via protein kinase A the direction of synaptic plasticity in the immature

hippocampus. *J Neurosci*. 2013 Feb 13;33(7):2973-83. doi: 10.1523/JNEUROSCI.4149-12.2013. PubMed PMID: 23407955.

Cashman NR, Loertscher R, Nalbantoglu J, Shaw I, Kascsak RJ, Bolton DC, Bendheim PE. Cellular isoform of the scrapie agent protein participates in lymphocyte activation. *Cell*. 1990 Apr 6;61(1):185-92. PubMed PMID: 1969332.

Chung IY, Benveniste EN. Tumor necrosis factor-alpha production by astrocytes. Induction by lipopolysaccharide, IFN-gamma, and IL-1 beta. *J Immunol*. 1990 Apr 15;144(8):2999-3007. PubMed PMID: 2109008.

Diack AB, Head MW, McCutcheon S, Boyle A, Knight R, Ironside JW, Manson JC, Will RG. Variant CJD. 18 years of research and surveillance. *Prion*. 2014;8(4):286-95. doi: 10.4161/pri.29237. Epub 2014 Nov 1. Review. PubMed PMID: 25495404; PubMed Central PMCID: PMC4601215.

Dietz K, Raddatz G, Wallis J, Müller N, Zerr I, Duerr HP, Lefèvre H, Seifried E, Löwer J. Blood transfusion and spread of variant Creutzfeldt-Jakob disease. *Emerg Infect Dis*. 2007 Jan;13(1):89-96. PubMed PMID: 17370520; PubMed Central PMCID: PMC2725807.

Gajdusek DC, Gibbs CJ Jr. Slow, latent and temperate virus infections of the central nervous system. *Res Publ Assoc Res Nerv Ment Dis*. 1968;44:254-80. PubMed PMID: 4978852.

Gajdusek DC. Slow-virus infections of the nervous system. *N Engl J Med*. 1967 Feb 16;276(7):392-400. PubMed PMID: 6066787.

Genoud N, Behrens A, Miele G, Robay D, Heppner FL, Freigang S, Aguzzi A. Disruption of Doppel prevents neurodegeneration in mice with extensive Prnp deletions. *Proc Natl Acad Sci U S A*. 2004 Mar 23;101(12):4198-203. Epub 2004 Mar 8. PubMed PMID: 15007175; PubMed Central PMCID: PMC384718.

Georgsson G, Sigurdarson S, Brown P. Infectious agent of sheep scrapie may persist in the environment for at least 16 years. *J Gen Virol*. 2006 Dec;87(Pt 12):3737-40. PubMed PMID: 17098992.

Gill ON, Spencer Y, Richard-Loendt A, Kelly C, Dabaghian R, Boyes L, Linehan J, Simmons M, Webb P, Bellerby P, Andrews N, Hilton DA, Ironside JW, Beck J, Poulter M, Mead S, Brandner S. Prevalent abnormal prion protein in human appendixes after bovine spongiform encephalopathy epizootic: large scale survey. *BMJ*. 2013 Oct 15;347:f5675. doi: 10.1136/bmj.f5675. PubMed PMID: 24129059; PubMed Central PMCID: PMC3805509.

GORDON WS. Advances in veterinary research. *Vet Rec*. 1946 Nov 23;58(47):516-25. PubMed PMID: 20279638.

Gough KC, Baker CA, Simmons HA, Hawkins SA, Maddison BC. Circulation of prions within dust on a scrapie affected farm. *Vet Res.* 2015 Apr 16;46:40. doi: 10.1186/s13567-015-0176-1. PubMed PMID: 25889731; PubMed Central PMCID: PMC4397813.

Griffith JS. Self-replication and scrapie. *Nature.* 1967 Sep 2;215(5105):1043-4. PubMed PMID: 4964084.

Haas LT, Salazar SV, Kostylev MA, Um JW, Kaufman AC, Strittmatter SM. Metabotropic glutamate receptor 5 couples cellular prion protein to intracellular signalling in Alzheimer's disease. *Brain.* 2016 Feb;139(Pt 2):526-46. doi: 10.1093/brain/awv356. Epub 2015 Dec 14. PubMed PMID: 26667279; PubMed Central PMCID: PMC4840505.

Hadlow W.J. Scrapie and kuru. *Lancet.* 1959:289–290.

Hartsough GR, Burger D. Encephalopathy of mink. I. Epizootiologic and clinical observations. *J Infect Dis.* 1965 Oct;115(4):387-92. PubMed PMID: 5891240.

Hill AF, Desbruslais M, Joiner S, Sidle KC, Gowland I, Collinge J, Doey LJ, Lantos P. The same prion strain causes vCJD and BSE. *Nature.* 1997 Oct 2;389(6650):448-50, 526. PubMed PMID: 9333232.

Hilton DA, Fathers E, Edwards P, Ironside JW, Zajicek J. Prion immunoreactivity in appendix before clinical onset of variant Creutzfeldt-Jakob disease. *Lancet.* 1998 Aug 29;352(9129):703-4. PubMed PMID: 9728989.

Hosszu LL, Jackson GS, Trevitt CR, Jones S, Batchelor M, Bhelt D, Prodromidou K, Clarke AR, Waltho JP, Collinge J. The residue 129 polymorphism in human prion protein does not confer susceptibility to Creutzfeldt-Jakob disease by altering the structure or global stability of PrPC. *J Biol Chem.* 2004 Jul 2;279(27):28515-21. Epub 2004 Apr 27. PubMed PMID: 15123682.

John TR, Schätzl HM, Gilch S. Early detection of chronic wasting disease prions in urine of pre-symptomatic deer by real-time quaking-induced conversion assay. *Prion.* 2013 May-Jun;7(3):253-8. doi: 10.4161/pri.24430. PubMed PMID: 23764839; PubMed Central PMCID: PMC3783112.

Kaski D, Mead S, Hyare H, Cooper S, Jampana R, Overell J, Knight R, Collinge J, Rudge P. Variant CJD in an individual heterozygous for PRNP codon 129. *Lancet.* 2009 Dec 19;374(9707):2128. doi: 10.1016/S0140-6736(09)61568-3. PubMed PMID: 20109837.

Kim HL, Do JY, Cho HJ, Jeon YC, Park SJ, Ma HI, Song JH, Lee Y, Choi H, Choi KC, Kim YS, Zerr I, Kallenberg K, Kim YJ. Dura mater graft-associated Creutzfeldt-Jakob disease: the first case in Korea. *J Korean Med Sci.* 2011 Nov;26(11):1515-7. doi:

10.3346/jkms.2011.26.11.1515. Epub 2011 Oct 27. PubMed PMID: 22065911; PubMed Central PMCID: PMC3207058.

Klein MA, Frigg R, Flechsig E, Raeber AJ, Kalinke U, Bluethmann H, Bootz F, Suter M, Zinkernagel RM, Aguzzi A. A crucial role for B cells in neuroinvasive scrapie. *Nature*. 1997 Dec 18-25;390(6661):687-90. PubMed PMID: 9414161.

Klein MA, Frigg R, Raeber AJ, Flechsig E, Hegyi I, Zinkernagel RM, Weissmann C, Aguzzi A. PrP expression in B lymphocytes is not required for prion neuroinvasion. *Nat Med*. 1998 Dec;4(12):1429-33. PubMed PMID: 9846583.

Kordek R, Nerurkar VR, Liberski PP, Isaacson S, Yanagihara R, Gajdusek DC. Heightened expression of tumor necrosis factor alpha, interleukin 1 alpha, and glial fibrillary acidic protein in experimental Creutzfeldt-Jakob disease in mice. *Proc Natl Acad Sci U S A*. 1996 Sep 3;93(18):9754-8. PubMed PMID: 8790403; PubMed Central PMCID: PMC38501.

Kordek R, Nerurkar VR, Liberski PP, Isaacson S, Yanagihara R, Gajdusek DC. Heightened expression of tumor necrosis factor alpha, interleukin 1 alpha, and glial fibrillary acidic protein in experimental Creutzfeldt-Jakob disease in mice. *Proc Natl Acad Sci U S A*. 1996 Sep 3;93(18):9754-8. PubMed PMID: 8790403; PubMed Central PMCID: PMC38501.

Li R, Liu D, Zanusso G, Liu T, Fayen JD, Huang JH, Petersen RB, Gambetti P, Sy MS. The expression and potential function of cellular prion protein in human lymphocytes. *Cell Immunol*. 2001 Jan 10;207(1):49-58. PubMed PMID: 11161453.

Liao YC, Lebo RV, Clawson GA, Smuckler EA. Human prion protein cDNA: molecular cloning, chromosomal mapping, and biological implications. *Science*. 1986 Jul 18;233(4761):364-7. PubMed PMID: 3014653.

Liberski PP. Kuru: a journey back in time from papua new Guinea to the neanderthals' extinction. *Pathogens*. 2013 Jul 18;2(3):472-505. doi: 10.3390/pathogens2030472. Review. PubMed PMID: 25437203; PubMed Central PMCID: PMC4235695.

Liu J, Zhao D, Liu C, Ding T, Yang L, Yin X, Zhou X. Prion protein participates in the protection of mice from lipopolysaccharide infection by regulating the inflammatory process. *J Mol Neurosci*. 2015 Jan;55(1):279-287. doi: 10.1007/s12031-014-0319-2. Epub 2014 May 20. PubMed PMID: 24838383.

Llewelyn CA, Hewitt PE, Knight RS, Amar K, Cousens S, Mackenzie J, Will RG. Possible transmission of variant Creutzfeldt-Jakob disease by blood transfusion. *Lancet*. 2004 Feb 7;363(9407):417-21. PubMed PMID: 14962520.

Locht C, Chesebro B, Race R, Keith JM. Molecular cloning and complete sequence of prion protein cDNA from mouse brain infected with the scrapie agent. *Proc Natl Acad*

Sci U S A. 1986 Sep;83(17):6372-6. PubMed PMID: 3462700; PubMed Central PMCID: PMC386505.

Lötscher M, Recher M, Hunziker L, Klein MA. Immunologically induced, complement-dependent up-regulation of the prion protein in the mouse spleen: follicular dendritic cells versus capsule and trabeculae. *J Immunol*. 2003 Jun 15;170(12):6040-7. PubMed PMID: 12794132.

Mabbott NA, Brown KL, Manson J, Bruce ME. T-lymphocyte activation and the cellular form of the prion protein. *Immunology*. 1997 Oct;92(2):161-5. PubMed PMID: 9415021; PubMed Central PMCID: PMC1364053.

Mabbott NA, Bruce ME, Botto M, Walport MJ, Pepys MB. Temporary depletion of complement component C3 or genetic deficiency of C1q significantly delays onset of scrapie. *Nat Med*. 2001 Apr;7(4):485-7. PubMed PMID: 11283677.

Mallucci, G. Medicine: Outside the fold. *Nature* 2014 April; 508(7495):180-181

Mastrianni JA. The genetics of prion diseases. *Genet Med*. 2010 Apr;12(4):187-95. doi: 10.1097/GIM.0b013e3181cd7374. Review. PubMed PMID: 20216075.

McCulloch L, Brown KL, Bradford BM, Hopkins J, Bailey M, Rajewsky K, Manson JC, Mabbott NA. Follicular dendritic cell-specific prion protein (PrP) expression alone is sufficient to sustain prion infection in the spleen. *PLoS Pathog*. 2011 Dec;7(12):e1002402. doi: 10.1371/journal.ppat.1002402. Epub 2011 Dec 1. PubMed PMID: 22144895; PubMed Central PMCID: PMC3228802.

McKinley MP, Bolton DC, Prusiner SB. A protease-resistant protein is a structural component of the scrapie prion. *Cell*. 1983 Nov;35(1):57-62. PubMed PMID: 6414721.

Mead S, Whitfield J, Poulter M, Shah P, Uphill J, Beck J, Campbell T, Al-Dujaily H, Hummerich H, Alpers MP, Collinge J. Genetic susceptibility, evolution and the kuru epidemic. *Philos Trans R Soc Lond B Biol Sci*. 2008 Nov 27;363(1510):3741-6. doi: 10.1098/rstb.2008.0087. PubMed PMID: 18849290; PubMed Central PMCID: PMC2576515.

Meyerett C, Michel B, Pulford B, Spraker TR, Nichols TA, Johnson T, Kurt T, Hoover EA, Telling GC, Zabel MD. In vitro strain adaptation of CWD prions by serial protein misfolding cyclic amplification. *Virology*. 2008 Dec 20;382(2):267-76. doi: 10.1016/j.virol.2008.09.023. Epub 2008 Oct 25. PubMed PMID: 18952250.

Michel B, Ferguson A, Johnson T, Bender H, Meyerett-Reid C, Pulford B, von Teichman A, Seelig D, Weis JH, Telling GC, Aguzzi A, Zabel MD. Genetic depletion of complement receptors CD21/35 prevents terminal prion disease in a mouse model of chronic wasting disease. *J Immunol*. 2012 Nov 1;189(9):4520-7. doi:

10.4049/jimmunol.1201579. Epub 2012 Sep 21. PubMed PMID: 23002439; PubMed Central PMCID: PMC3478448.

Michel B, Meyerett-Reid C, Johnson T, Ferguson A, Wyckoff C, Pulford B, Bender H, Avery A, Telling G, Dow S, Zabel MD. Incunabular immunological events in prion trafficking. *Sci Rep.* 2012;2:440. doi: 10.1038/srep00440. Epub 2012 Jun 6. PubMed PMID: 22679554; PubMed Central PMCID: PMC3368226.

Mok SW, Proia RL, Brinkmann V, Mabbott NA. B cell-specific S1PR1 deficiency blocks prion dissemination between secondary lymphoid organs. *J Immunol.* 2012 May 15;188(10):5032-40. doi: 10.4049/jimmunol.1200349. Epub 2012 Apr 13. PubMed PMID: 22504650; PubMed Central PMCID: PMC3364719.

Oesch B, Westaway D, Wälchli M, McKinley MP, Kent SB, Aebersold R, Barry RA, Tempst P, Teplow DB, Hood LE, et al. A cellular gene encodes scrapie PrP 27-30 protein. *Cell.* 1985 Apr;40(4):735-46. PubMed PMID: 2859120.

Palmer MS, Dryden AJ, Hughes JT, Collinge J. Homozygous prion protein genotype predisposes to sporadic Creutzfeldt-Jakob disease. *Nature.* 1991 Jul 25;352(6333):340-2. Erratum in: *Nature* 1991 Aug 8;352(6335):547. PubMed PMID: 1677164.

Pardon E, Laeremans T, Triest S, Rasmussen SG, Wohlkönig A, Ruf A, Muyldermans S, Hol WG, Kobilka BK, Steyaert J. A general protocol for the generation of Nanobodies for structural biology. *Nat Protoc.* 2014 Mar;9(3):674-93. doi: 10.1038/nprot.2014.039. Epub 2014 Feb 27. PubMed PMID: 24577359; PubMed Central PMCID: PMC4297639.

Pattinson IH. RESISTANCE OF THE SCRAPIE AGENT TO FORMALIN. *J Comp Pathol.* 1965 Apr;75:159-64. PubMed PMID: 14317615.

Peden AH, Head MW, Ritchie DL, Bell JE, Ironside JW. Preclinical vCJD after blood transfusion in a PRNP codon 129 heterozygous patient. *Lancet.* 2004 Aug 7-13;364(9433):527-9. PubMed PMID: 15302196.

Prinz M, Heikenwalder M, Junt T, Schwarz P, Glatzel M, Heppner FL, Fu YX, Lipp M, Aguzzi A. Positioning of follicular dendritic cells within the spleen controls prion neuroinvasion. *Nature.* 2003 Oct 30;425(6961):957-62. Epub 2003 Oct 15. PubMed PMID: 14562059.

Prusiner SB, Groth D, Serban A, Koehler R, Foster D, Torchia M, Burton D, Yang SL, DeArmond SJ. Ablation of the prion protein (PrP) gene in mice prevents scrapie and facilitates production of anti-PrP antibodies. *Proc Natl Acad Sci U S A.* 1993 Nov 15;90(22):10608-12. PubMed PMID: 7902565; PubMed Central PMCID: PMC47826.

Prusiner SB, McKinley MP, Groth DF, Bowman KA, Mock NI, Cochran SP, Masiarz FR. Scrapie agent contains a hydrophobic protein. *Proc Natl Acad Sci U S A.* 1981 Nov;78(11):6675-9. PubMed PMID: 6273882; PubMed Central PMCID: PMC349112.

Prusiner SB. Novel proteinaceous infectious particles cause scrapie. *Science*. 1982 Apr 9;216(4542):136-44. PubMed PMID: 6801762.

Pulford B, Spraker TR, Wyckoff AC, Meyerett C, Bender H, Ferguson A, Wyatt B, Lockwood K, Powers J, Telling GC, Wild MA, Zabel MD. Detection of PrPCWD in feces from naturally exposed Rocky Mountain elk (*Cervus elaphus nelsoni*) using protein misfolding cyclic amplification. *J Wildl Dis*. 2012 Apr;48(2):425-34. PubMed PMID: 22493117.

Raeber AJ, Race RE, Brandner S, Priola SA, Sailer A, Bessen RA, Mucke L, Manson J, Aguzzi A, Oldstone MB, Weissmann C, Chesebro B. Astrocyte-specific expression of hamster prion protein (PrP) renders PrP knockout mice susceptible to hamster scrapie. *EMBO J*. 1997 Oct 15;16(20):6057-65. PubMed PMID: 9321385; PubMed Central PMCID: PMC1326289.

Riek R, Hornemann S, Wider G, Billeter M, Glockshuber R, Wüthrich K. NMR structure of the mouse prion protein domain PrP(121-231). *Nature*. 1996 Jul 11;382(6587):180-2. PubMed PMID: 8700211.

Rudge P, Jaunmuktane Z, Adlard P, Bjurstrom N, Caine D, Lowe J, Norsworthy P, Hummerich H, Druyeh R, Wadsworth JD, Brandner S, Hyare H, Mead S, Collinge J. Iatrogenic CJD due to pituitary-derived growth hormone with genetically determined incubation times of up to 40 years. *Brain*. 2015 Nov;138(Pt 11):3386-99. doi: 10.1093/brain/awv235. Epub 2015 Aug 11. PubMed PMID: 26268531; PubMed Central PMCID: PMC4620512.

Saba R, Booth SA. The genetics of susceptibility to variant Creutzfeldt-Jakob disease. *Public Health Genomics*. 2013;16(1-2):17-24. doi: 10.1159/000345203. Epub 2013 Mar 18. Review. PubMed PMID: 23548713.

Saborio GP, Permanne B, Soto C. Sensitive detection of pathological prion protein by cyclic amplification of protein misfolding. *Nature*. 2001 Jun 14;411(6839):810-3. PubMed PMID: 11459061.

Saijo E, Hughson AG, Raymond GJ, Suzuki A, Horiuchi M, Caughey B. PrP^{Sc}-Specific Antibody Reveals C-Terminal Conformational Differences between Prion Strains. *J Virol*. 2016 Apr 29;90(10):4905-13. doi: 10.1128/JVI.00088-16. Print 2016 May 15. PubMed PMID: 26937029; PubMed Central PMCID: PMC4859706.

Santuccione A, Sytnyk V, Leshchyns'ka I, Schachner M. Prion protein recruits its neuronal receptor NCAM to lipid rafts to activate p59^{fyn} and to enhance neurite outgrowth. *J Cell Biol*. 2005 Apr 25;169(2):341-54. PubMed PMID: 15851519; PubMed Central PMCID: PMC2171870.

Seidel B, Thomzig A, Buschmann A, Groschup MH, Peters R, Beekes M, Terytze K. Scrapie Agent (Strain 263K) can transmit disease via the oral route after persistence

in soil over years. PLoS One. 2007 May 9;2(5):e435. PubMed PMID: 17502917; PubMed Central PMCID: PMC1855989.

Shyu WC, Harn HJ, Saeki K, Kubosaki A, Matsumoto Y, Onodera T, Chen CJ, Hsu YD, Chiang YH. Molecular modulation of expression of prion protein by heat shock. Mol Neurobiol. 2002 Aug;26(1):1-12. PubMed PMID: 12392052.

Sjöberg AP, Nyström S, Hammarström P, Blom AM. Native, amyloid fibrils and beta-oligomers of the C-terminal domain of human prion protein display differential activation of complement and bind C1q, factor H and C4b-binding protein directly. Mol Immunol. 2008 Jun;45(11):3213-21. doi: 10.1016/j.molimm.2008.02.023. Epub 2008 Apr 11. PubMed PMID: 18406463.

Stahl N, Borchelt DR, Hsiao K, Prusiner SB. Scrapie prion protein contains a phosphatidylinositol glycolipid. Cell. 1987 Oct 23;51(2):229-40. PubMed PMID: 2444340.

Stuermer CA, Langhorst MF, Wiechers MF, Legler DF, Von Hanwehr SH, Guse AH, Plattner H. PrPc capping in T cells promotes its association with the lipid raft proteins reggie-1 and reggie-2 and leads to signal transduction. FASEB J. 2004 Nov;18(14):1731-3. Epub 2004 Sep 2. PubMed PMID: 15345693.

Swietnicki W, Morillas M, Chen SG, Gambetti P, Surewicz WK. Aggregation and fibrillization of the recombinant human prion protein huPrP90-231. Biochemistry. 2000 Jan 18;39(2):424-31. PubMed PMID: 10631004.

Thackray AM, McKenzie AN, Klein MA, Lauder A, Bujdoso R. Accelerated prion disease in the absence of interleukin-10. J Virol. 2004 Dec;78(24):13697-707. PubMed PMID: 15564479; PubMed Central PMCID: PMC533935.

Thadani V, Penar PL, Partington J, Kalb R, Janssen R, Schonberger LB, Rabkin CS, Prichard JW. Creutzfeldt-Jakob disease probably acquired from a cadaveric dura mater graft. Case report. J Neurosurg. 1988 Nov;69(5):766-9. PubMed PMID: 3054015.

Verma M, Vats A, Taneja V. Toxic species in amyloid disorders: Oligomers or mature fibrils. Ann Indian Acad Neurol. 2015 Apr-Jun;18(2):138-45. doi: 10.4103/0972-2327.144284. Review. PubMed PMID: 26019408; PubMed Central PMCID: PMC4445186.

Wang J, Wang X, Gao X, Vortmeyer A. Prion diseases and their Prpsc-based molecular diagnostics. Journal of Neurology and Neuroscience. 2015. Dec 30; 6(4).

White AC, Cloutier P, Coughlin RT. A purified saponin acts as an adjuvant for a T-independent antigen. Adv Exp Med Biol. 1991;303:207-10. PubMed PMID: 1805566.

Wickner RB, Edskes HK, Shewmaker F, Nakayashiki T. Prions of fungi: inherited structures and biological roles. *Nat Rev Microbiol.* 2007 Aug;5(8):611-8. Review. PubMed PMID: 17632572; PubMed Central PMCID: PMC2376760.

Wickner RB. [URE3] as an altered URE2 protein: evidence for a prion analog in *Saccharomyces cerevisiae*. *Science.* 1994 Apr 22;264(5158):566-9. PubMed PMID: 7909170.

Wolfgang, MW. Creutzfeldt-Jakob disease. *Acta Neurol. Scandinav.* 1968 44:1-32
Wu R, Liu L, Peng ZW, Duan XL, Wang BR, Jin YP, Kuang F. [Toll-like receptor 4 expression and cytokine secretion in microglial cells induced by IgG stimulation]. *Xi Bao Yu Fen Zi Mian Yi Xue Za Zhi.* 2009 Mar;25(3):201-3. Chinese. PubMed PMID: 19257980.

Wyckoff AC, Kane S, Lockwood K, Seligman J, Michel B, Hill D, Ortega A, Mangalea MR, Telling GC, Miller MW, Vercauteren K, Zabel MD. Clay Components in Soil Dictate Environmental Stability and Bioavailability of Cervid Prions in Mice. *Front Microbiol.* 2016 Nov 23;7:1885. eCollection 2016. PubMed PMID: 27933048; PubMed Central PMCID: PMC5120086.

Yuan AH, Hochschild A. A bacterial global regulator forms a prion. *Science.* 2017 Jan 13;355(6321):198-201. doi: 10.1126/science.aai7776. PubMed PMID: 28082594; PubMed Central PMCID: PMC5460984.

Zabel MD, Avery AC. Prions--not your immunologist's pathogen. *PLoS Pathog.* 2015 Feb 19;11(2):e1004624. doi: 10.1371/journal.ppat.1004624. eCollection 2015 Feb. Review. PubMed PMID: 25695738; PubMed Central PMCID: PMC4335031.

Zabel MD, Heikenwalder M, Prinz M, Arrighi I, Schwarz P, Kranich J, von Teichman A, Haas KM, Zeller N, Tedder TF, Weis JH, Aguzzi A. Stromal complement receptor CD21/35 facilitates lymphoid prion colonization and pathogenesis. *J Immunol.* 2007 Nov 1;179(9):6144-52. PubMed PMID: 17947689.

Zahn R, Liu A, Lührs T, Riek R, von Schroetter C, López García F, Billeter M, Calzolari L, Wider G, Wüthrich K. NMR solution structure of the human prion protein. *Proc Natl Acad Sci U S A.* 2000 Jan 4;97(1):145-50. PubMed PMID: 10618385; PubMed Central PMCID: PMC26630.

CHAPTER 2 – COMPLEMENT REGULATORY PROTEIN FACTOR H PARADOXICALLY PROMOTES PRION DISEASE¹

Summary

Several Complement proteins and receptors exacerbate mouse models of prion disease, including C3, C1q, and CD21/35. These proteins of the Complement cascade likely increase uptake, trafficking, and retention of prions in the lymphoreticular system, hallmark sites of early PrP^{Sc} propagation. Complement regulatory protein Factor H (fH) binds post-translationally modified host proteins and lipids to prevent C3b deposition and thus autoimmune cell lysis. Previous reports show fH binds various conformations of the cellular prion protein, leading us to question the role of fH in prion disease. We report a biophysical interaction between purified fH and prion amyloid (“prion rods”) enriched from prion-diseased brain. Further, in a scrapie mouse model, we report transgenic mice lacking *Cfh* alleles unexpectedly resist prion accumulation and onset of terminal disease in a gene-dose manner. We conclude from these data and previous findings that the interplay between Complement and prions likely involves a complex balance of prion sequestration and destruction via local tissue macrophages, prion trafficking by B and dendritic cells within the lymphoreticular system, intranodal prion replication by B and Follicular Dendritic cells, and potential prion strain selection through Factor H. Collectively, these findings shed new light onto the paradoxical role of Complement regulatory proteins in prion disease.

¹ A version of this chapter was recently accepted: Kane, SJ *et al.* Complement Regulatory Protein Factor H is a Soluble Prion Receptor That Potentiates Peripheral Prion Pathogenesis *J Immunol.* (2017). Figures were modified for clarity.

Introduction

Prions encipher and transmit pathogen information via structural conversion of the soluble, cellular prion protein, PrP^C, to a misfolded and aggregated prion. Examples of prion diseases include Creutzfeldt-Jakob disease in humans; scrapie in sheep and goats; bovine spongiform encephalopathy (BSE) in cattle; chronic wasting disease (CWD) in deer, elk, and moose; and transmissible mink spongiform encephalopathy (TME) in mink. Hallmark clinical signs of prion diseases can include dementia, ataxia, and weight loss. Neuropathological manifestations of prion disease include astrogliosis, spongiform degeneration, and prion amyloid deposition. Many prion strains propagate in lymphoid tissues during a clinically silent carrier phase prior to neuroinvasion and clinical manifestations. Interestingly, BSE and Drowsy TME prion strains lack this phenotype, implicating an alternate route to the central nervous system independent of lymphoid propagation (Somerville et al. 1997; Bartz et al. 2005).

The (in)ability of certain prions to breach species barriers, as well as distinct biochemical and pathological characteristics among prions derived from the same PrP^C primary sequence (Bessen and Marsh 1992) suggest prions can exist as different strains or quasi-species. However, whether these prion strains arise from enhanced thermodynamic stability of certain conformations in the original inoculum, or host factors preferentially promote certain prion conformations, remains inconclusive. Interestingly, prions derived from spleen display broader species tropism when compared to prions from brain (Beringue et al. 2012). These data highlight strain selection capacity within a single host and suggest certain host factors likely select for certain prion strains during

the transition between establishing infection in extraneural tissues to ultimate neuroinvasion. However, whether selection occurs at the protein conformational level, post-translational modification status, protein:protein interactions, or cell-type level, remains unknown.

Several elegant studies implicate a branch of the innate immune system, Complement, as a facilitator of early prion spread and propagation. CD21/35- and PrP^C-expressing follicular dendritic (FDC) and B cells capture pathogens opsonized with C3 and C4 cleavage products and decrease the threshold to activate B cells to induce antibody production. Both FDCs and B cells promote prion disease (Klein et al. 1998; Brown et al. 1999; Montrasio et al. 2000, Klein et al. 2001; Zabel et al. 2007, McCulloch et al. 2011) despite the failure of adaptive immunity against prions. Many studies suggest Complement promotes trafficking of infectious prions to cells expressing PrP^C, a substrate for the growing prion aggregate, in lymphoid follicles. Specifically, mice deficient in C3, C4, C1q, and Complement receptors CD21/35 accumulate less splenic prions early in disease and partially or completely resist terminal disease (Zabel et al. 2007; Michel et al. 2012).

Considering the largely nonspecific nature of the Complement cascade, hosts require regulatory mechanisms to prevent self-recognition and subsequent autoimmunity. Complement Regulatory protein Factor H (β 1H globulin, CFH, or fH) prevents Complement activation on host tissues by binding sialic acids and polyanionic carbohydrates, such as glycosaminoglycan (GAG), which are largely absent on

pathogen surfaces. Although C3b marks virtually all cell surfaces in circulation, Factor H bound to host polyanionic carbohydrates mediates C3b inactivation through co-factor activity with Factor I, as well as limits activity of the C3 convertase, C3bBb (Carroll et al. 2011). Not surprisingly, mutations or deficiency in Factor H lead to autoimmune diseases such as membranoproliferative glomerulonephritis, atypical hemolytic uremic syndrome and age-related macular degeneration (Pickering et al. 2002, Zipfel et al. 2007; Hageman et al. 2005).

Both PrP^C and PrP^{Sc} contain sialic acid residues, and splenic PrP^{Sc} is more sialylated than brain PrP^{Sc} (Srivastava et al. 2015). Furthermore, Factor H binds various conformations of recombinant PrP^C free of all post-translational modifications (PTMs), suggesting Factor H potentially impacts prion disease outcomes via direct interactions with PrP^{Sc} (Mitchell et al 2007; Sjöberg et al. 2008). We confirmed a direct interaction between fH and recombinant PrP using surface plasmon resonance (SPR; data not shown), and for the first time demonstrate Factor H interacts with prion amyloid enriched from prion-infected brain. Collectively, these previous findings led us to investigate the role of fH in a mouse model of scrapie.

Inactivation of the *Cfh* gene renders mice deficient in plasma C3 (Pickering et al. 2002 and confirmed in serum of mice reported here; data not shown). Since C3 promotes prion disease (Mabbott et al. 2001; Michel et al. 2013), its absence in mice also lacking fH confounds the ability to assess the role of fH in prion pathogenesis. To ascertain the specific effect of Factor H deficiency, we peripherally inoculated mice with a high dose

of mouse-adapted scrapie which affects C3 knockout mice nearly identically to wild type mice (Klein et al. 2001). Transgenic mice expressing zero, one, or two allelic copies of Factor H exhibited a gene-dose effect in early prion accumulation and onset of terminal disease after challenge with a high dose of RML5 prions. Knockout and hemizygous mice accumulated fewer splenic and brain prions at early time points and resisted the onset of terminal disease in comparison to their fH sufficient cohorts. Overall, these surprising data demonstrate fH may play a direct role in prion disease by promoting certain prion strains' lymphotropism and subsequent neuroinvasion.

Materials and Methods

Mice. All mice were bred and maintained at Lab Animal Resources, accredited by the Association for Assessment and Accreditation of Lab Animal Care International and approved on January 14, 2016 by the Institutional Animal Care and Use Committee at Colorado State University. Factor H knockout mice on the C57/Bl6 background were kindly provided by Dr. Joshua Thurman (University of Colorado – Denver). We crossed *Cfh*^{-/-} mice to hemizyosity with C57/Bl6 wild type mice from Jackson Laboratories. Hemizygous breeders generated pups of various *Cfh* genotypes.

Protocol ID: 09-1580A. We determined *Cfh* genotype from extracted tail clip DNA (Qiagen 69504) using the following primers: 5' CTACAAATGCCGCCCTGGAT 3' (mzBAP3), 5' CTGCCAGCCTAAAGGACCC 3' (mzBAP4r), 5' GTAAAGGTCCTCCTCCAAGAG 3' (fHReg200), and 5' GGGGATCGGCAATAAAAAGAC 3' (NEO). mzBAP3 and mzBAP4r primers were

designed using NCBI's primer design website and blasted against the available C57BL/6 genome to ensure specificity. PCR conditions were as follows for 35 cycles: denaturation at 95°C, annealing at 55°C, and elongation at 72°C. PCR products were resolved using agarose gel electrophoresis. Amplicons of 400 bp (fHReg200 and NEO) indicated the presence of a knockout allele, and amplicons of 451 bp (BAP3/4) indicated the presence of a wild type allele.

Mouse inoculations and clinical sign scoring. Age- and sex- matched mice ($n \geq 6$ per genotype) ranging from 6 weeks to 1 year received 100 μL of approximately 10^6 lethal dose₅₀ units of mouse-adapted scrapie strain RML5 prions into the peritoneal cavity. Mice were monitored daily and sacrificed at the onset of terminal disease or specified timepoints. We employed a scoring system to assess the severity of disease, including: tail rigidity (0-2), akinesia (0-4), ataxia (0-4), tremors (0-4), and weight loss (0-2). Mice scored above 10 (total) or with a 4 or above in one category were euthanized via CO₂ inhalation replacing 20% of air per minute to effect.

Tissue collection and analysis. After euthanasia, the following samples were collected and frozen or fixed in 4% formaldehyde in 1X PBS: serum, spleen (half fixed, half frozen), kidneys (one fixed, one frozen), tail clip, and brain (half fixed, half frozen). We assessed the presence of protease-resistant prions (PrP^{RES}) in 10% (w/v) homogenate after proteinase K (Roche) digestion (10 $\mu\text{g}/\text{mL}$ for spleen and 50 $\mu\text{g}/\text{mL}$ for brain) and western blotting using anti-PrP monoclonal antibody BAR224 (Cayman) conjugated to horseradish peroxidase (HRP). Blots were developed using chemiiluminescent

substrates hydrogen peroxide and luminol for 5 minutes at room temperature and visualized using a GE digital imager and ImageQuant software. Tissues negative for PrP^{RES} on western blots were subjected to serial protein misfolding cyclic amplification (PMCA; Saborio and Soto, 2001). Briefly, PMCA uses 10% normal brain homogenate in PMCA buffer (1X PBS, 1% Triton X-100, 4 mM EDTA and 150 mM NaCl) from PrP^C over-expressing transgenic mice, strain TgA20, as substrate for amplification of previously undetectable prions. Twenty-five microliters of normal brain homogenate (NBH) and 25 μ L 10% sample homogenate, underwent a 40 second pulse of sonication at ~150 watts, followed by a 30 minute incubation, and repeated for 24 hours (one round). Serial rounds were set up similarly, transferring 25 μ L of the previous round's sample to 25 μ L of fresh NBH. Fresh positive controls of 0.05% RML5 prions served as positive control for each PMCA round. Each biological sample was run in at least technical duplicates, and round-to-positivity was determined by PK digestion and western blotting. Relative PMCA units were assigned as previously described (Pulford et al. 2012). Non-amplified samples containing detectable PrP^{RES} via western blot were not subjected to PMCA.

Prion rod preparation and surface plasmon resonance. Prion rods were enriched from infected brain as previously described (Michel et al. 2012, Safar et al. 1990). Briefly, brains from animals infected with chronic wasting disease (E2), hyper- or drowsy-transmissible spongiform encephalopathies (HY- or DY-TME) were homogenized in 1X PBS to 10% (w/v) concentration. Sucrose (1.2 M) was added to 10 mL of clarified tissue to a final concentration of 165.5 mM, and samples were ultracentrifuged (100,000 x g)

for one hour at 4°C. Pellets were resuspended to a final protein concentration of 5.0 mg/mL in 1X TBS containing 2.0% Triton X-100 (TBST) and incubated on ice for 30 minutes. Samples were subjected to another round of ultracentrifugation for 20 minutes at 0°C, washed twice in 1X TBST, and twice with 1X TBS. The pellets were then resuspended in 1X PBS containing 1% sarcosyl and protease inhibitor cocktail (Roche). Vortexed samples were incubated on a heated shaker at 37°C for two hours at 800 rpm. Samples were then gently overlaid on a 0.32 M sucrose in PMCA buffer 1 (PMCA buffer without Triton-X 100) cushion, ultracentrifuged for one hour at 4°C, and supernatants removed. Pellets were resuspended in 2.3 M NaCl, 5% sarcosyl in 1X PBS, centrifuges at 13,000 x g, washed three times in 50 mM Tris 150 mM NaCl, and were either stored dry or suspended in PBS at -80°C. The presence of PK resistant prion rods was confirmed by western blot.

Highly enriched prion rods were coupled to CM-5 sensor chips outside of the instrument after generating the reference flow cells within the instrument by activating with EDC/NHS and deactivating with ethanolamine three to five times. The chip was then removed from the instrument and the gold chip disassembled from the cassette. The entire surface was activated with 100 µL of EDC/NHS for 12 minutes. A pellet of rods was resuspended in 100 µL of 10 mM sodium acetate pH 5.4, sonicated at 37°C for 40 seconds, and incubated on the gold chip at room temperature for one hour. The chip was then briefly rinsed with 1X PBS, and remaining active groups were deactivated with ethanolamine for 7 minutes. Prior to use in interaction analyses, startup cycles of 50

mM sodium hydroxide served to remove any nonspecifically bound prion rods from the surface.

All SPR experiments involved recombinant PrP (rPrP) or prion rod enriched from infected brain as the ligand coated to a CM5 Series S sensor chip, and commercially-available Factor H (CompTech) as the analyte. Factor H was buffer exchanged in Amicon filter devices into 1X Running Buffer (50 mM Tris HCl, 150 mM NaCl, pH 7.42). The rPrP-coated chip was kindly provided by Dr. Hae-Eun Kang in the Telling lab. Briefly, flow cells were first activated with 0.2 M 1-ethyl-3-(3-dimethylaminopropyl) carbodiimide hydrochloride (EDC) and 0.05 M N-hydroxysuccinimide (NHS) for seven minutes at 10 μ L/min. Amine coupling recombinant cervid or murine PrP^C in 10 mM sodium acetate pH 5.5 was accomplished by flowing 20 μ g/mL of ligand over the activated chip for seven minutes at 10 μ L/min. Excess activated groups were deactivated with 1 M ethanolamine HCl pH 8.5 for seven minutes at 10 μ L/min. Reference flow cells, built-in negative controls for this system, underwent rounds of activation and deactivation without the addition of protein ligand.

Cell culture prion infection. N2a mouse neuroblastoma cells were grown in RPMI medium containing 10% fetal bovine serum and 1% penicillin/streptomycin. RML5 infected brain homogenate was UV-sterilized prior to infecting cells. RML5 was pre-incubated with PBS or fH (5 μ g/mL final) for 25 minutes prior to infecting cells. N2a cells (passage 3) were seeded at 100,000 cells per well in a 12 well plate and infected with 0.3% RML5 containing PBS or fH. Cells were grown at 37°C and 5% CO₂ for 4 days.

Wells were rinsed 2X in 1X PBS, and cells were detached from the plate using 5 mM EDTA in 1X PBS for 10 minutes. Cell pellets were resuspended in 100 μ L PMCA buffer containing 1% Triton X-100 and lysed on ice for 30 minutes. Lysates were assessed for PrP^{RES} using traditional PK digestion and western blotting techniques.

C3 ELISA. C3 in brain in serum was quantified in serum and brain using a commercially-available ELISA and confirmed via western blot. Briefly, heart stick samples were allowed to clot at room temperature for 10 minutes, centrifuged at 1,000 x g (3600 rpm) for ten minutes at 4°C, and serum was pipetted off and stored separately at -20 or -80°C. Serum and 10% brain homogenate were diluted 1:50,000 and 1:10, respectively, in provided diluent prior to ELISA. After interpolating absorbance values from the known standard curves, the concentrations were multiplied by the dilution factor.

Statistical analyses. All statistical analyses were performed using GraphPad Prism software. One- or two- way ANOVAs were run to compare genotype, sex, or the interaction between these two variables. P-values < 0.05 were considered significantly different. In the terminal disease study, we observed one male outlier and subsequently removed this data point. Technical duplicates or triplicates from each biological replicate were averaged, and the mean value of each biological replicate was considered an n of 1.

Results

fH directly binds PrP^C and prion amyloid. Previous reports indicate a molecular interaction between various conformations of recombinant PrP and fH, but whether fH binds *in vivo*-derived prion amyloid remained unknown. We performed a previously published protocol which removes soluble PrP^C and highly enriches insoluble prion rods (Safar et al. 1990; Johnson et al. 2010; Michel et al. 2012). We then coupled these prion rods to a CM5 sensor chip and tested an interaction with fH as an analyte. Intriguingly, fH was shown to bind both HY- and DY- TME with similar affinities, despite their differential lymphotropism (Figure 2.1). These data may highlight a role for fH impacting prion disease in a mechanism other than lymphotropism.

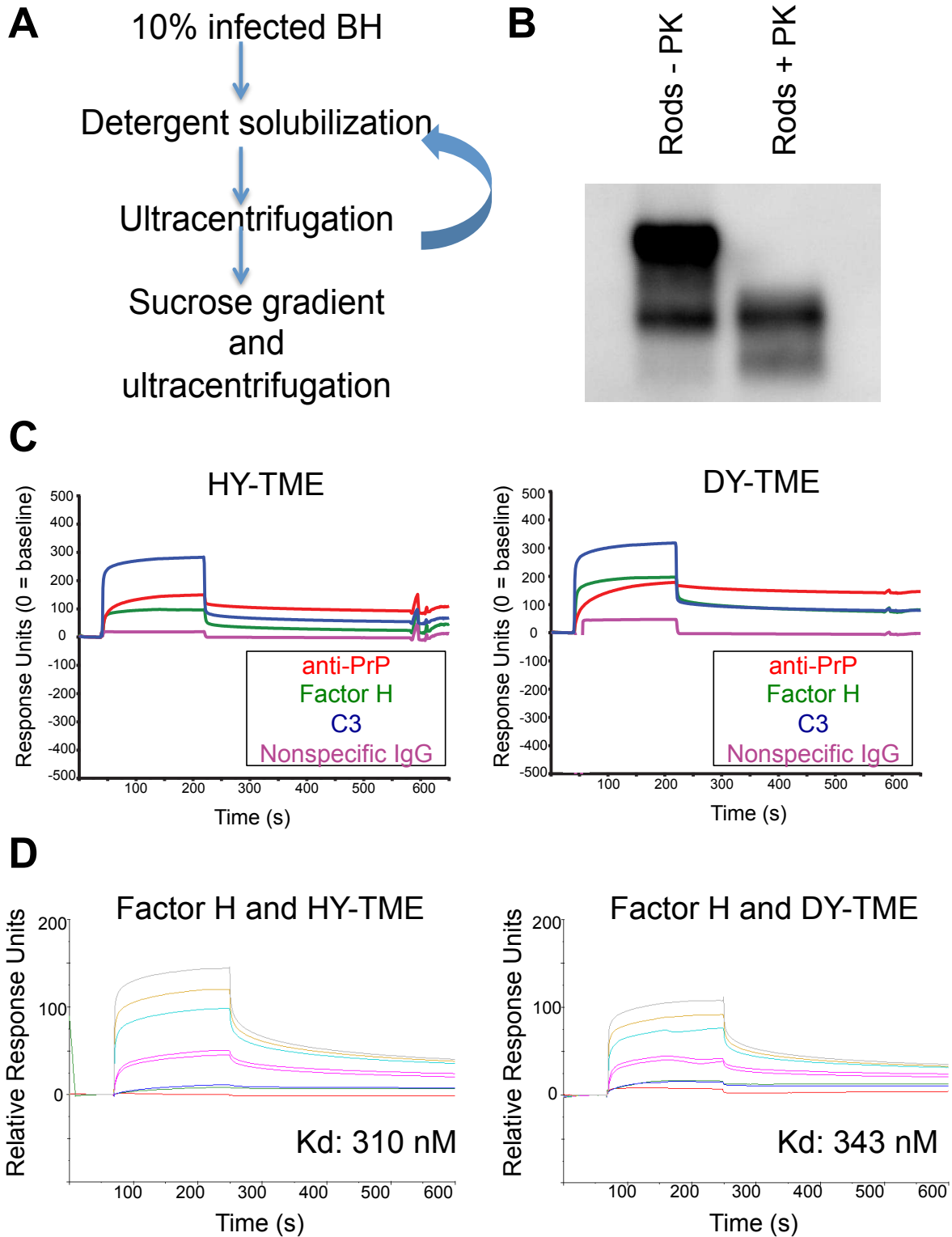


Figure 2.1. Factor H directly interacts with prion amyloid. Prion rods were enriched from infected brain homogenate as previously described (A) and contain PK-resistant material (B). Surface plasmon resonance (SPR) analyses reveal that Complement component C3 opsonizes prion amyloid, but Factor H can bind prion amyloid with

similar affinities (D) and potentially protect from C3 opsonization. Factor H analyte concentrations tested include 0 (red), 5 (blue), 100 (magenta), 500 (teal), 1000 (gold), and 2000 (gray) nM.

fH does not affect splenic prion loads at 30dpi. To assess the role of *fH* in early scrapie trafficking and lymphoid propagation, we intraperitoneally inoculated littermates of various *Cfh* genotypes (Figure 2.2 and 2.3) with 10^6 LD₅₀ units of RML5 and assessed for prion loads in brain and spleens. Interestingly, prion loads did not differ between genotypes at 30dpi (Figure 2.4), suggesting trafficking and early stages of replication do not depend on Factor H.

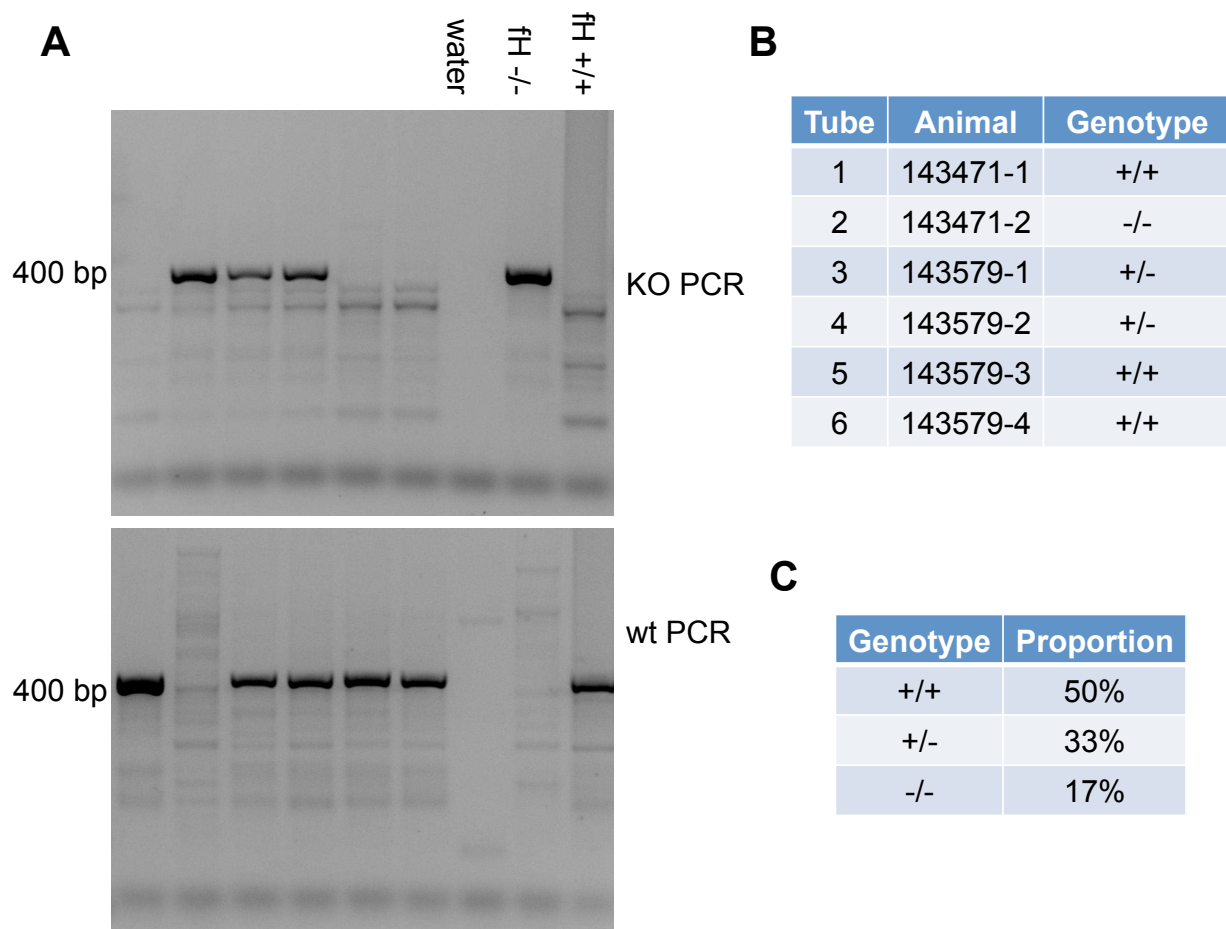


Figure 2.2. Example of *fH* mouse genotyping. Extracted DNA from tail clips were subjected to two separate PCR reactions (A). PCR reactions containing *fH*Reg200 and

NEO primers (A, top panel) generated a 400bp amplicon in the presence of a knockout allele, and PCR reactions containing BAP3 and BAP4 primers (A, bottom panel) generated a 451bp amplicon in the presence of a wild type allele. Panel B summarizes the genotyping results in A, and C shows the relative proportions of genotypes in this subset of animals.

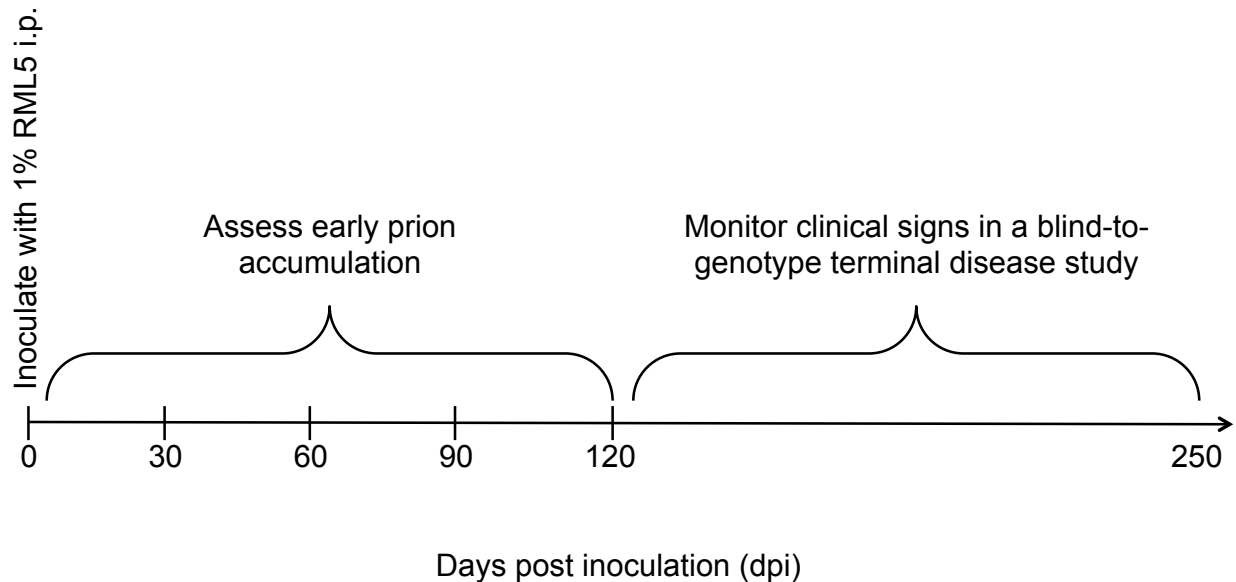


Figure 2.3. Experimental design of fH gene-dose study. Hemizygous breeders generated wild type, hemizygous, or knockout littermates. After determining the genotypes via PCR, mice received mouse-adapted scrapie in their peritoneal cavity. Specifically, mice received 100 μ L of 1% CD-1 brain homogenate infected with Rocky Mountain Laboratory mouse-adapted scrapie 5 (RML5) prions. Mice (n=5+ per genotype) were sacrificed at 30, 60, 90, and 120 days post inoculation (dpi), and splenic prion loads determined via protein misfolding cyclic amplification (PMCA). In a blind-to-genotype study, mice were observed daily for clinical signs of prion disease and sacrificed at the onset of terminal disease.

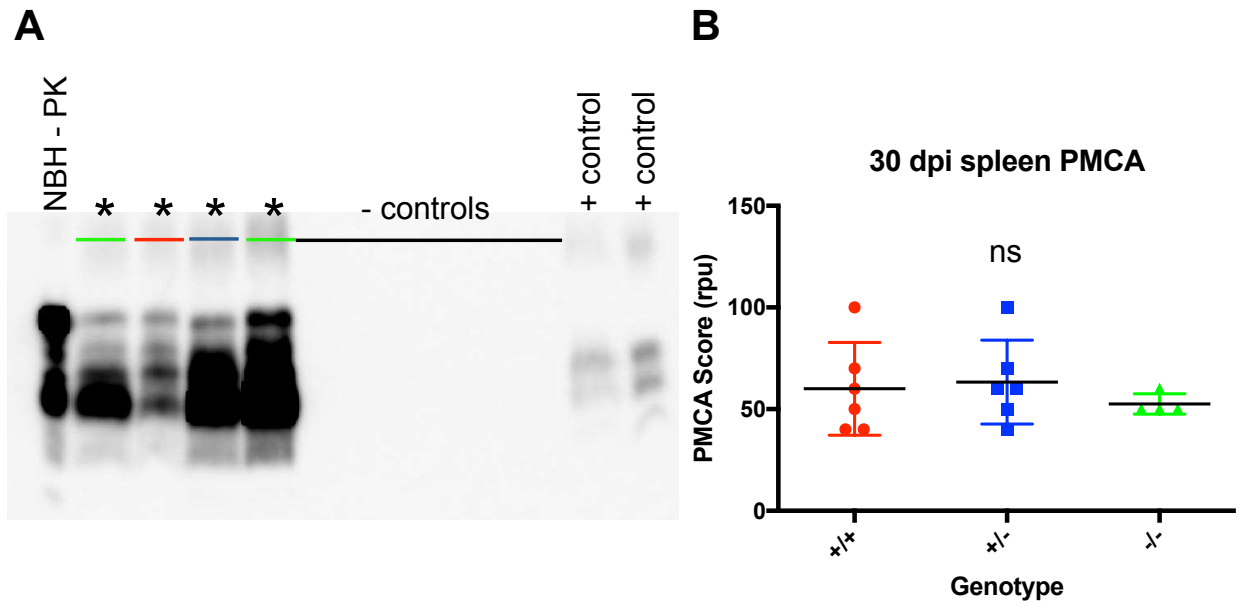


Figure 2.4. Factor H wild type, hemizygous, and knockout mice do not differ in splenic prion loads at 30dpi. Mice (n=5+ per genotype) received 100 μ L of 1% RML5 and were sacrificed at 30dpi. Spleens (10% w/v) were subjected to serial rounds of PMCA in duplicate and analyzed via proteinase K (PK) digestion and western blot. Normal brain homogenate without PK digestion served as a control for western-blot transfer and band-shift after PK digestion. Example PMCA data (A) shows roughly equal genotype proportions positive for PK-resistant prions in their spleen at round E. Relative PMCA units (rpu) were assigned to each animal and analyzed as described previously (Pulford et al. 2012). One-way ANOVA analysis revealed no statistical difference among fH genotypes ($p=0.4883$).

fH does affect splenic prion loads after 30dpi. Splenic load increases corresponded with increased *Cfh* gene dosage after 30dpi (Figure 2.10A). We found statistically significant differences between genotypes analyzed at 60dpi (Figure 2.5), 90dpi (Figure 2.6), and 120dpi (Figure 2.7). However, knockout mice reached wild type and hemizygous levels by 150dpi (Figure 2.8).

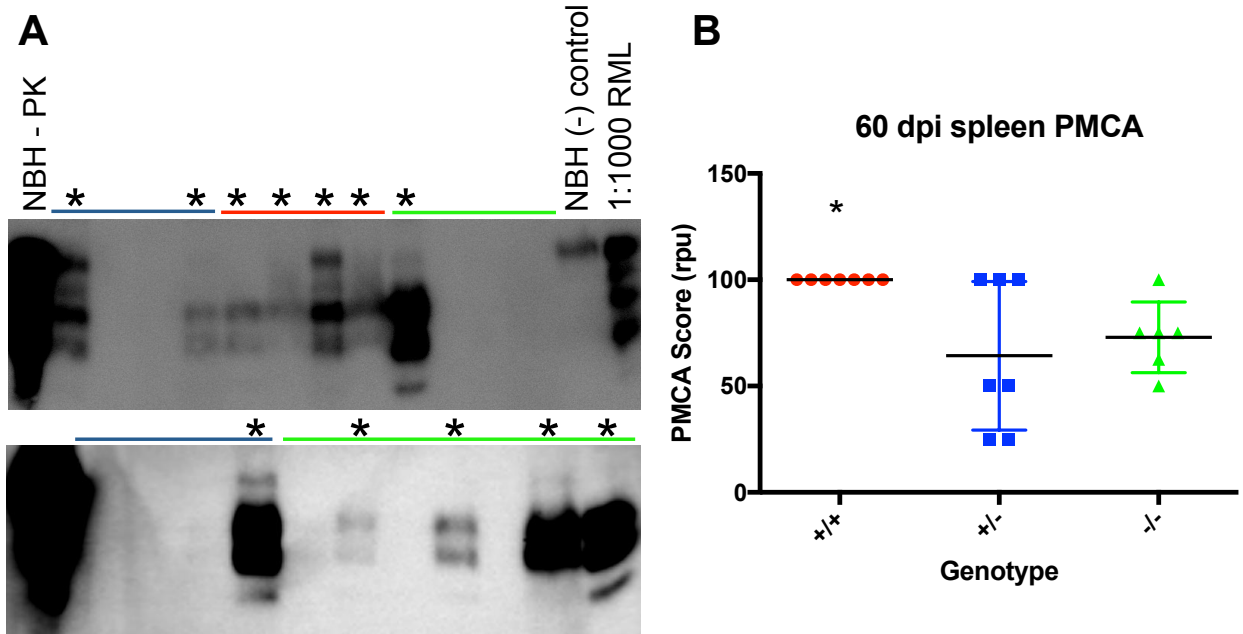


Figure 2.5. Factor H hemizygous and knockout mice contain lower splenic prion loads at 60dpi. Mice (n=6+ per genotype) received 100 μ L of 1% RML5 and were sacrificed at 60dpi. Spleens (10% w/v) were subjected to serial rounds of PMCA in duplicate and analyzed via proteinase K (PK) digestion and western blot. Normal brain homogenate without PK digestion served as a control for western-blot transfer and band-shift after PK digestion. Example PMCA data (A) shows a higher proportion of wild type mice as positive for PK-resistant prions in their spleen at round A (top panel), whereas hemizygous and knockout mice required additional rounds (bottom panel) of PMCA to detect prions, indicating a lower prion load. Relative PMCA units (rpu) were assigned to each animal and analyzed as described previously (Pulford et al. 2012). One-way ANOVA analysis revealed a statistically significant difference among fH genotypes ($p=0.0236$).

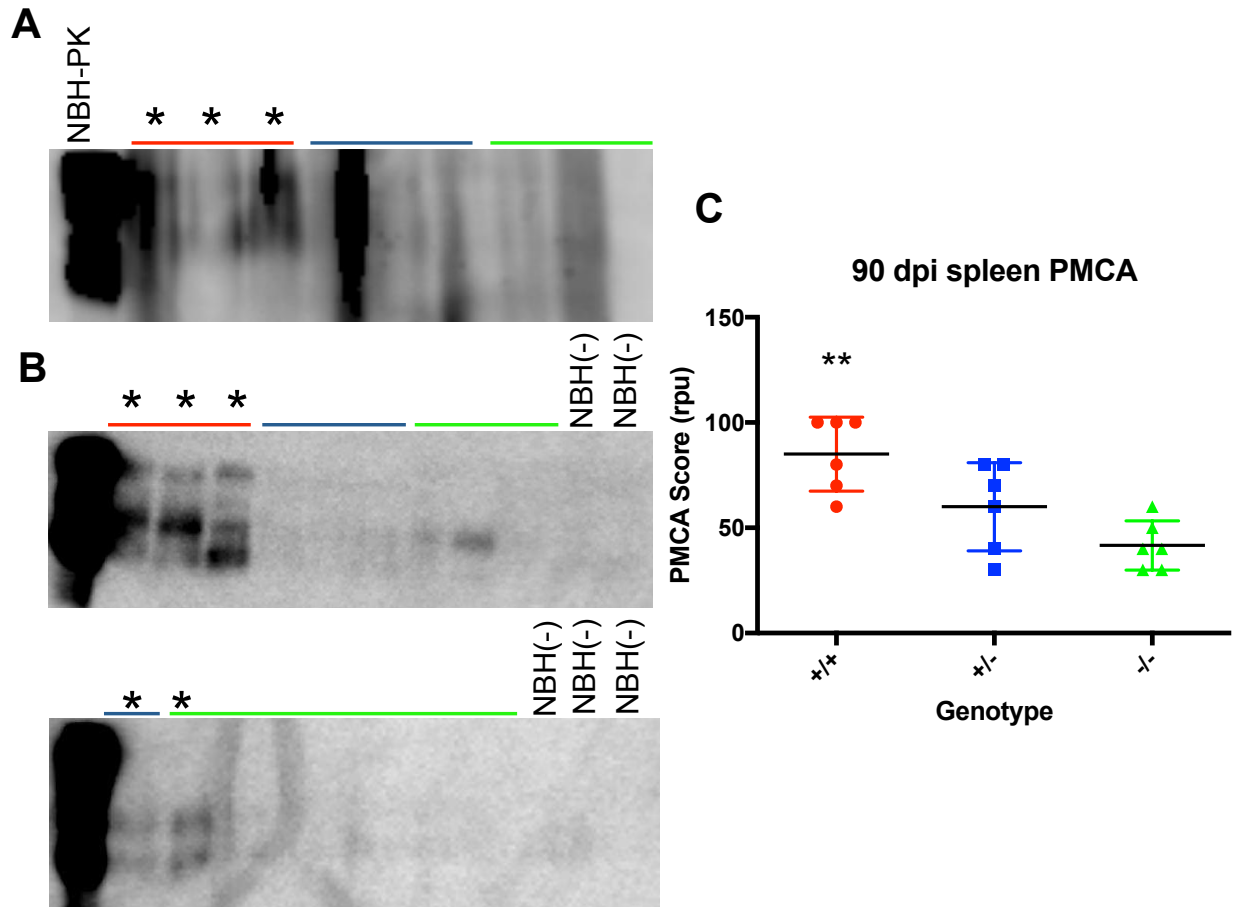


Figure 2.6. Factor H hemizygous and knockout mice contain lower splenic prion loads at 90dpi. Mice (n=6+ per genotype) received 100 μ L of 1% RML5 and were sacrificed at 90dpi. Spleens (10% w/v) were first analyzed for PK-resistant prions in their spleen after 10 μ g/mL PK digestion and western blotting (A). Samples positive for PrP^{RES} by straight western blotting were assigned 200 rpu, and negative samples were subjected to serial rounds of PMCA until positive by western blot (B). Example PMCA data (B) shows a higher proportion of wild type mice as positive for PK-resistant prions in their spleen at round A (top panel), whereas hemizygous and knockout mice required additional rounds (bottom panel) of PMCA to detect prions, indicating a lower prion load. One-way ANOVA analysis revealed a statistically significant difference among fH genotypes ($p=0.0021$).

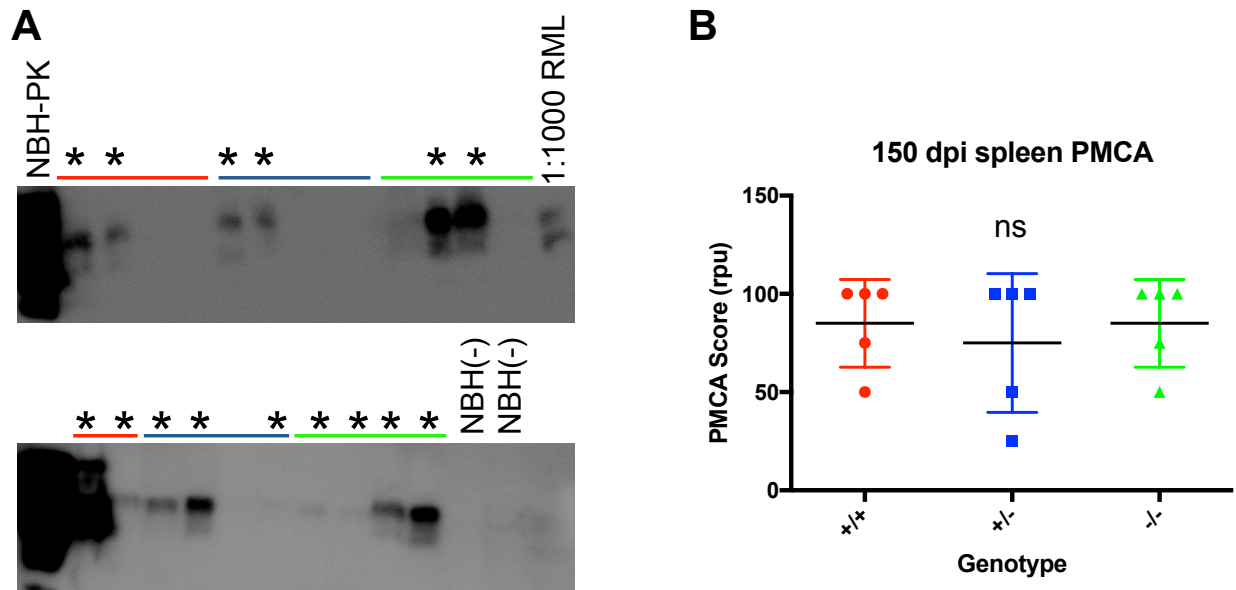


Figure 2.8. Factor H hemizygous and knockout mice contain similar splenic prion loads as wild type by 150dpi. Mice (n=6+ per genotype) received 100 μ L of 1% RML5 and were sacrificed at 90dpi. Spleens (10% w/v) were subjected to serial rounds of PMCA until positive by western blot. Example PMCA data (A) shows roughly equal proportions of mice positive for PK-resistant prions in their spleens at round A (top panel) and B (bottom panel). Relative PMCA units (rpu) were assigned to each animal, and one-way ANOVA analyses revealed no statistical differences.

fH promotes prion neuroinvasion. To determine the temporal pattern of neuroinvasion in response to *fH* status, we assessed prion loads in brain at 90dpi, 120dpi, and 150dpi using sPMCA. Similar to the trend observed in spleen, prion loads in brain corresponded to *Cfh* status after i.p. challenge (Figure 2.9). Interestingly, knockout mice reached hemizygous and wild type prion levels in both spleen and brain by 150dpi.

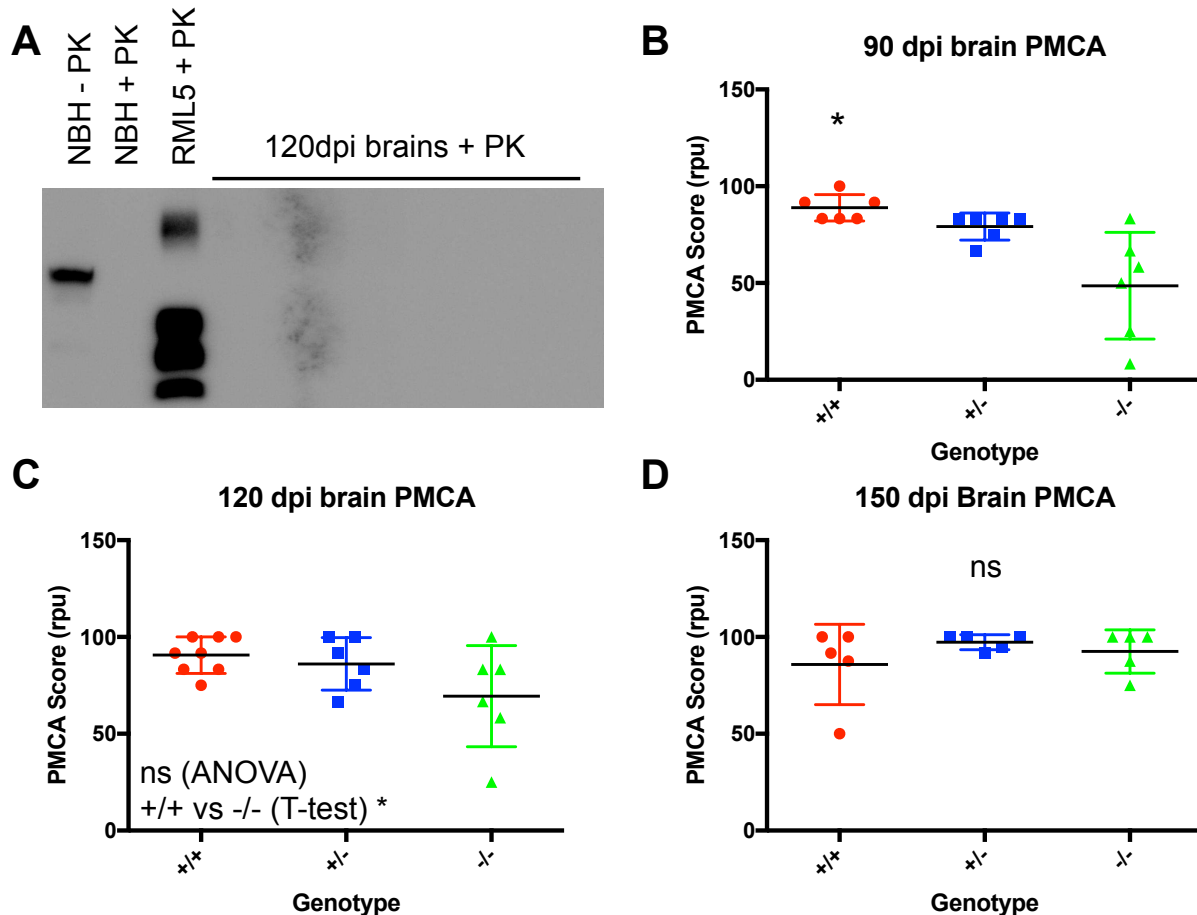


Figure 2.9. Analysis of prion loads in brain at early time points. Mice (n=5+ per genotype) received 100 μ L of 1% RML5 and were sacrificed at the indicated time points. PrP^{RES} was not observable by straight western blotting at 120dpi (A), and tissues from 150dpi underwent several freeze-thaws, so all brains were subjected to sPMCA. ANOVA analyses revealed significant differences among genotypes at 90dpi (p=0.0285) but not 120dpi (p=0.0902) or 150dpi (p=0.4411). However, unpaired T-test (one way) analyses of wild type vs knockout shows a significant difference at 120dpi (p=0.0269).

Temporal characteristics of prion accumulation over time, and its dependence on fH.

Wild type, fH sufficient mice contained increasing splenic prion loads over time until reaching a plateau phase by 90dpi (Figure 2.11). Hemizygous mice displayed a lag phase, yet reached prion loads similar to wild type by 120dpi. Knockout mice did not reach prion loads similar to hemizygous and wild until 150dpi. As observed in spleen, prion accumulation in brain was delayed in knockout mice (Figure 2.11). Knockout mice

reached wild type and hemizygous prion loads by 150dpi (Figure 2.11), and densitometric comparisons did not reveal a statistical difference in PrP^{RES} western blot signal at 180dpi (Figure 2.10).

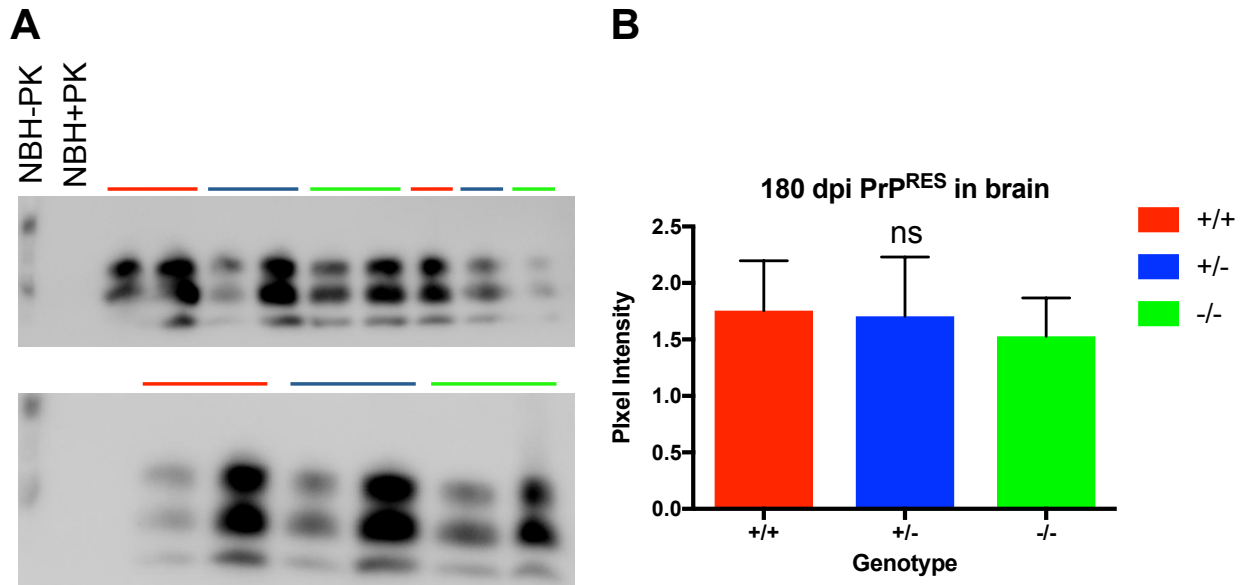


Figure 2.10. Mice of all fH genotypes contain detectable PK-resistant prions in their brain by 180dpi. Mice (n=6+ per genotype) received 100 μ L of 1% RML5 and were sacrificed at 180dpi. Brains (10% w/v) were subjected to PK digestion (50 μ g/mL) and western blotting (A). Densitometric analysis via ImageJ revealed a trend, albeit not statistically different, in the amount of PrP^{RES} in brain at 180dpi.

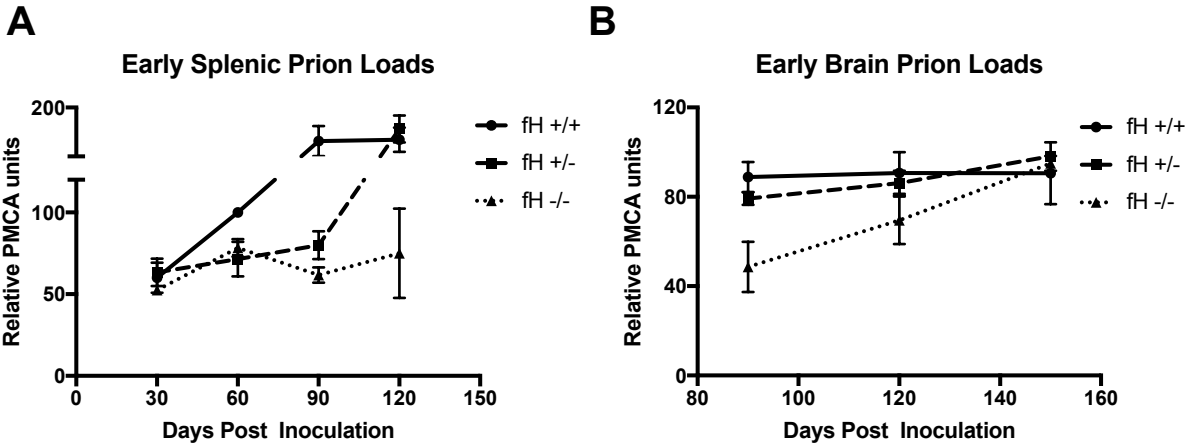
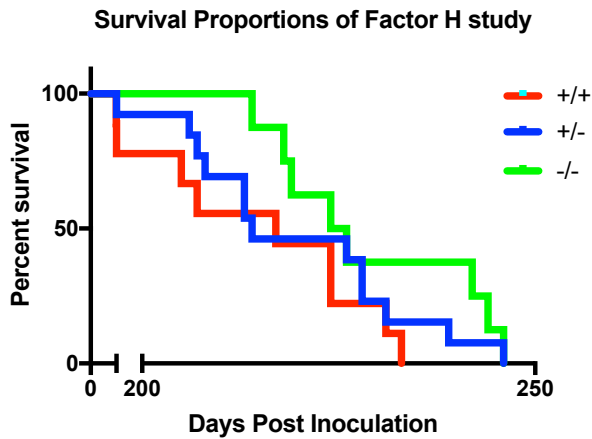


Figure 2.11. Cumulative early time point data. Data from previous figures except spleen at 150dpi were combined in order to visualize the effect of fH in prion loads in brain and spleen over time. Note that samples positive by straight western blotting received a conservative amplification score of 200.

Absence of fH delays clinical manifestations of terminal prion disease. In a blind-to-genotype study, we challenged littermates with a single peritoneal dose of RML5 and monitored mice daily for onset of clinical disease (Figure 2.12). Prion loads were assessed in brain via western blot (data not shown), and histopathological examinations were performed via immunohistochemistry (Figure 2.13). Aligning with early accumulation studies, fH^{-/-} mice resisted the onset of terminal prion disease, perhaps due to the initial delay in splenic and brain propagation.

A**B**

Genotype	Sex	Strain	Attack Rate	Days \pm sd
fH +/+	M	C57/Bl6	5/5	222 \pm 14
	F	C57/Bl6	5/5	207 \pm 7
fH +/-	M	C57/Bl6	9/9	222 \pm 16
	F	C57/Bl6	4/4	215 \pm 8
fH -/-	M	C57/Bl6	4/4	238 \pm 13
	F	C57/Bl6	4/4	221 \pm 6

Figure 2.12. Factor H knockout mice resist the onset of terminal disease longer than wild type or hemizygous littermates. Mice (n=8+ per genotype) received 100 μ L of 1% RML5 and monitored daily for the onset of terminal disease while blinded to genotype. See Materials and Methods for clinical scoring paradigm. Log-rank (Mantel-Cox) statistical test revealed a significant difference in the survival curves (A, $p=0.0018$). Interestingly, we observed significant difference between sexes, although this did not depend on fH status.

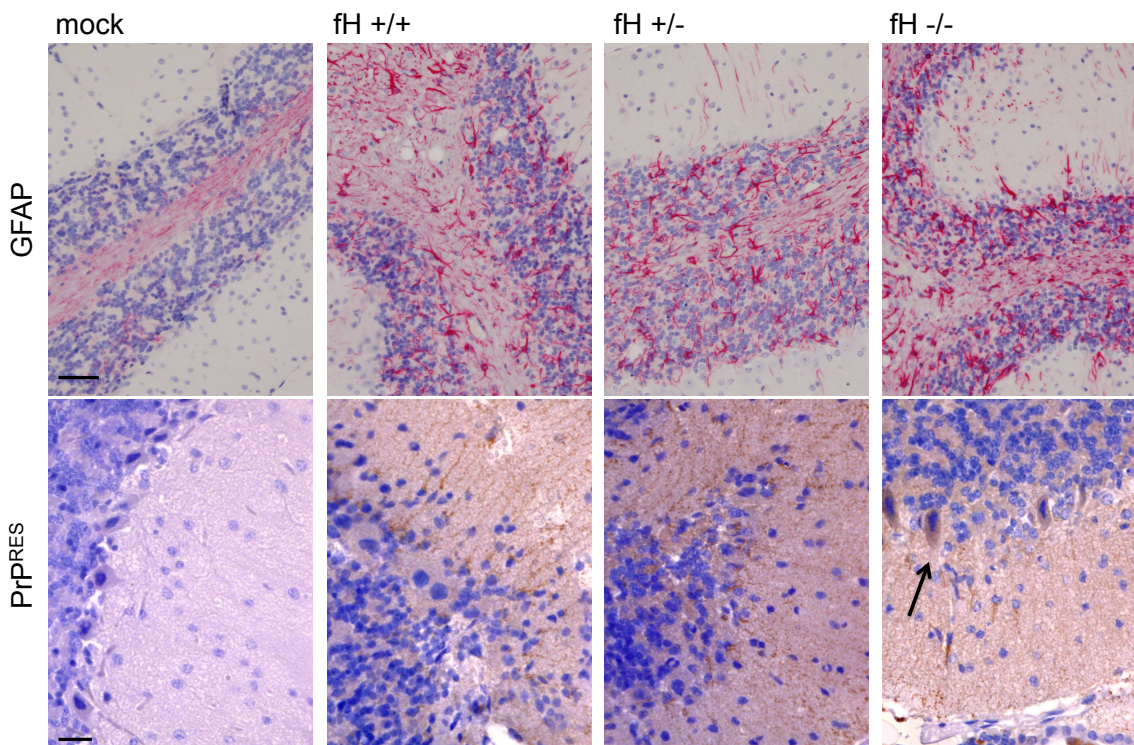


Figure 2.13. Histological brain examination from Factor H terminal disease study. Paraffin-embedded sections were stained for PrP^{RES} (A, top, 40X) and glial fibrillary

acidic protein in hippocampus (B, bottom, 20X). These images reveal prion deposition and neuroinflammation in cerebellum. Interestingly, knockout mice exhibited immunostaining indicative of intracellular inclusion body deposition (arrow). Scale bars indicate 20 μ m (top) and 50 μ m (bottom).

Female mice succumb to prion infection after peripheral inoculation before males. We observed an unexpected sex difference in mice of all fH genotypes, although two-way ANOVA analyses suggest the sex difference does not depend on fH genotype. To ascertain whether the sex difference arose depending on route of inoculation, data generated from previous researchers in the Zabel lab were statistically analyzed. Interestingly, the sex difference was only observed after peripheral (i.p.) exposure, but not after inoculation into the brain (Figure 2.14).

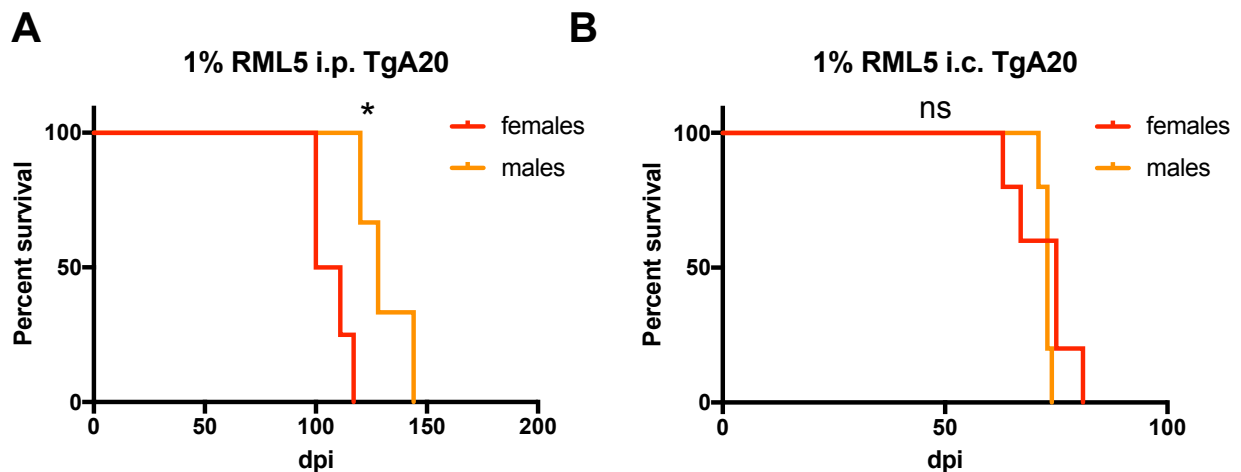


Figure 2.14. The RML5 sex difference depends on route of inoculation. TgA20 mice received 1% RML5 either intraperitoneally (i.p., n=3+ per sex) or intracerebrally (i.c., n=5+ per sex), and were sacrificed at the onset of terminal disease. Log-rank (Mantel-Cox) statistically analyses revealed significant differences between sexes after i.p. inoculation (p=0.0158), but not after i.c. inoculation (p=0.2535). Data from i.p. inoculation data was kindly provided by Dana Hill.

Factor H may select for certain prion strains. In an attempt to develop an *in vitro* assay which assesses whether fH affects prion infection, we pre-incubated RML5-infected

brain homogenate with purified mouse fH containing short consensus repeats (SCRs) 15-20 prior to infecting cells. Intriguingly, western blot analyses reveal a slightly elevated proportion of di-glycosylated PrP^{RES} in cells infected with RML5 pre-treated with fH (Figure 2.15). Furthermore, histological examination show fH^{-/-} mice contained unique PrP^{RES} staining. Nearly all wild type mice infected with RML5 exclusively contain diffuse prion deposits, but fH^{-/-} mice contained both puncta and florid plaques indicative of a perhaps new prion strain (Figure 2.15D).

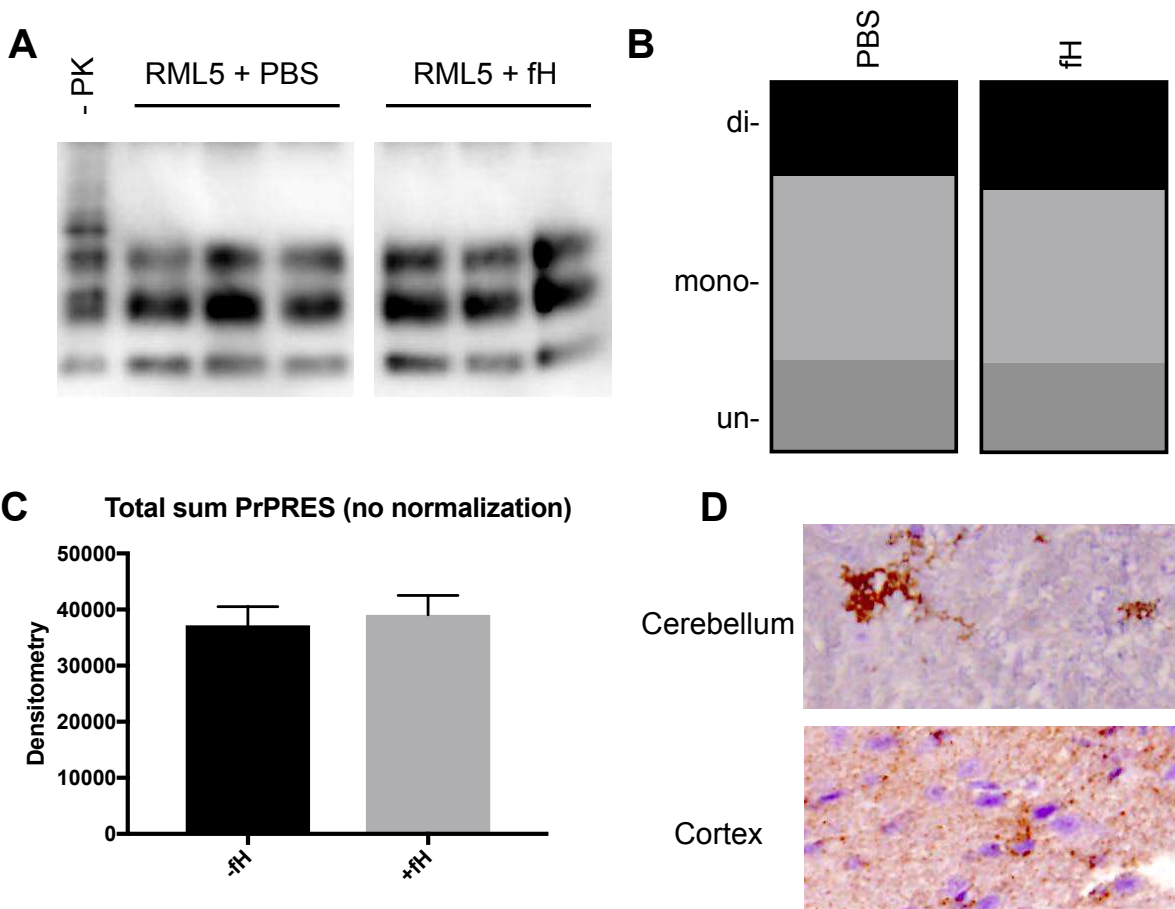


Figure 2.15. Preliminary data: fH may select for certain prion strains. RML5 infected brain homogenate (0.3%) was pre-treated with PBS or fH containing SCRs 15-20 (5 µg/mL final) prior to infecting N2a cells (A-C). Cells were grown for 4 days and analyzed for PrP^{RES} via western blotting. While not statistically significant, a slight trend was observed consistent with previous findings: fH promotes prion infection (C) and may select for di-glycosylated prions (B). Furthermore, unique prion deposition was

observed in a subset of knockout mice (D, 20X), which differed from the typically diffuse RML5 deposition seen in wild type mice.

C3 may confound the effects seen in this chapter. Transgenesis leading to Factor H deficiency also renders mice deficient in serum C3 (Pickering et al. 2002). We confirmed these findings (Figure 2.16B,D). Previous reports in our lab among others (Michel et al. 2013; Mabbott et al. 2001) highlight a critical role of C3 in promoting prion disease (Figure 2.16), which necessitated an experimental design which specifically addressed the role of Factor H in prion disease. Klein et al (2001) reported a high dose of RML5 prions causes disease in wild type mice nearly identically to C3 deficient mice. While we attempted to circumvent this issue, we cannot overlook the possibility of C3 as a confounding variable.

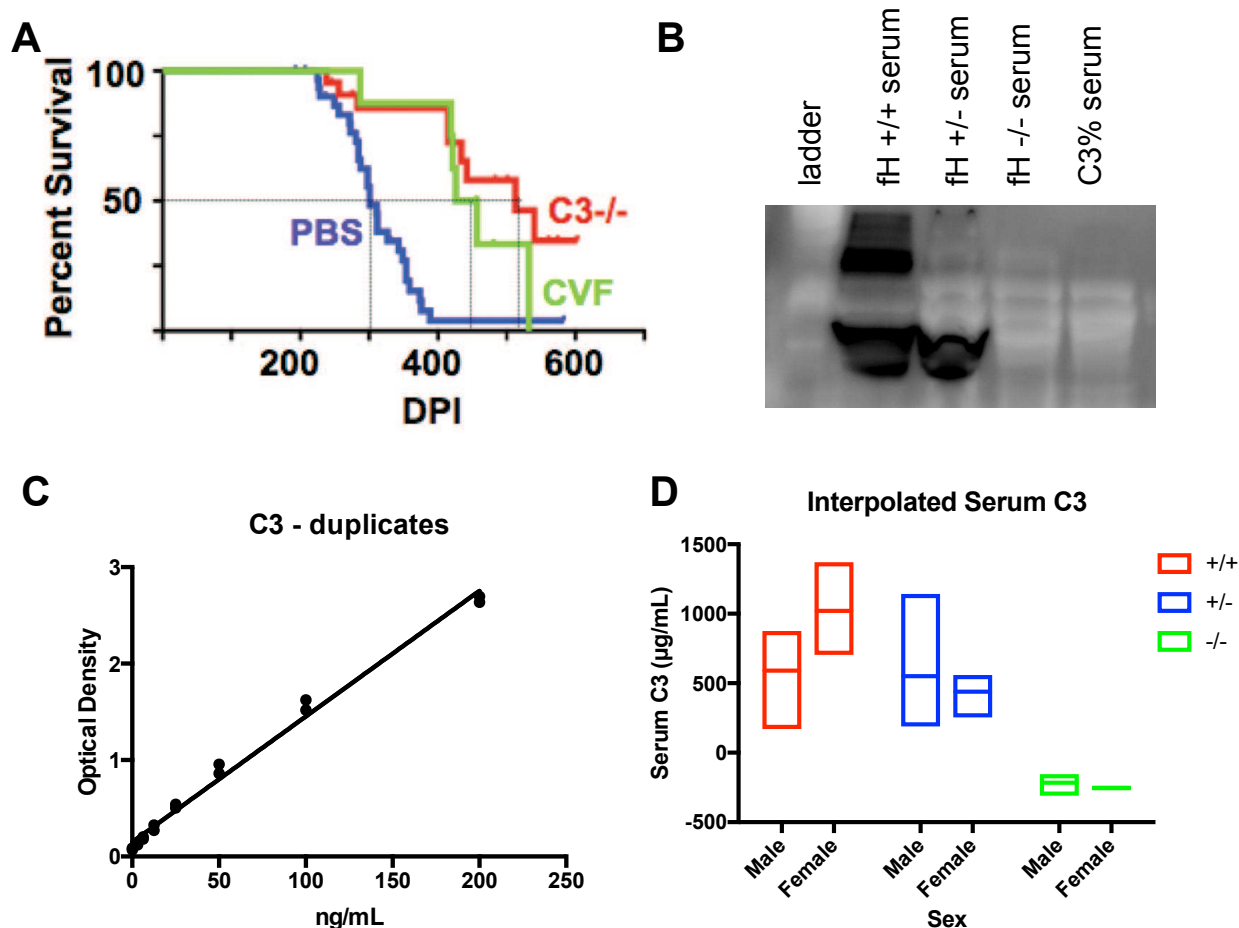


Figure 2.16. C3 may confound the Factor H study. Previous work in the Zabel laboratory (A, Michel et al. 2013) revealed C3 promotes prion disease because mice genetically or pharmacologically deficient in C3 survive longer than their C3-sufficient cohorts. To assess the effect of Factor H deficiency on C3 levels, western blotting (B) and ELISA (C-D) were used to compare levels of C3 in serum of prion-inoculated fH mice. Factor H knockout mice contained undetectable levels of C3 in their serum. However, we inoculated with a high dose of RML5 prions which affected mice regardless of C3 status (Klein et al. 2001).

C3 promotes CWD infection after intracerebral challenge in transgenic mice. In an attempt to assess the role of C3 in brain pathology, and its potential confounding effects in the aforementioned Factor H study, we intracerebrally challenged transgenic mice which overexpress elk PrP^C and are C3 deficient (Tg5037;C3^{-/-}) and monitored signs of clinical disease. Survival rates were compared to data previously generated in our lab by Dr. Brady Michel. As seen in Figure 2.17, C3^{-/-} mice resisted prion disease

significantly longer than C3-sufficient mice. Further, C3 was detected in the brains of infected mice from the above Factor H study via ELISA, but not on prion rods used for SPR experiments (Figure 2.1).

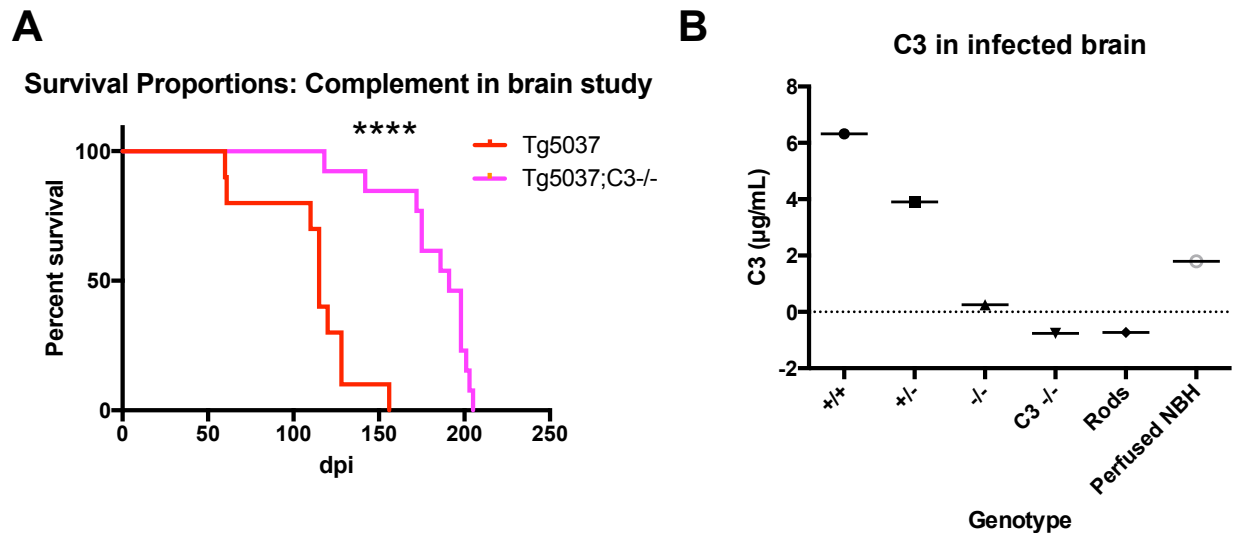


Figure 2.17. C3 promotes prion pathogenesis in the central nervous system. To assess whether C3 promotes prion disease specifically in the brain, transgenic mice expressing cervid PrP with or without C3 were intracerebrally inoculated with 30 µL 1% CWD-infected brain homogenate (E2) and monitored for clinical signs. Mice deficient in C3 survived significantly longer than their C3-sufficient historical controls (A). C3 was detected in brains of prion-infected mice via ELISA (B), although Factor H knockout mice contained significantly less C3 than their hemizygous or wild type cohorts.

Discussion

We investigated the influence of Complement regulatory protein Factor H in establishing prion infection after peripheral insult. We initially hypothesized fH directly binds prions and protects them from Complement recognition and thus impedes subsequent trafficking/propagation in the lymphoreticular system. While we show fH directly binds prions (Figure 2.1), the *in vivo* data show an opposite trend than expected. These

findings may be explained by strain selection, enhanced stability, or enhanced retention due to a direct, biophysical relationship between prions and fH. Our data indeed show fH directly binds prions, yet counter-intuitively promotes splenic propagation, neuroinvasion, and terminal disease onset. While fH^{-/-} mice eventually succumbed to prion disease, lymphotropism and subsequent neuroinvasion were impaired (Summarized in Figure 2.11).

Interestingly, splenic prion burdens did not differ between genotypes at 30dpi. While we cannot conclude whether fH plays a role in the initial trafficking of prions to the LRS, these data suggest fH may stabilize prions or promote propagation once captured in the LRS. We previously showed fluorescent prion rods entering afferent lymphatics both cell- and non-cell- associated (Michel et al. 2012). These findings suggest prions could traffic to lymphoid tissues cell-autonomously, which supports prions trafficking to the lymphoreticular system independent of an intact Complement system and perhaps partially aided by soluble fH acting as a transport chaperone. Thus, we cannot ascertain the effect of fH in the early trafficking stage of disease from the data presented here. Future studies could include fH inoculum pre-treatment and assessing early cell-mediated and cell-autonomous trafficking, as well as degradation.

We can envision a number of roles for fH in directly promoting prion disease. As discussed above, fH could act as a soluble prion receptor and cell-autonomously shuttle prions to extraneural sites of prion replication. Alternatively, or even additionally, fH bound to PrP^C-expressing cells could capture prions, bringing them to the vicinity of

PrP^C molecules, which then misfold and join the growing prion aggregate. Furthermore, fH may bind certain prion conformations or PTM statuses, thereby selecting for certain strains to replicate in the LRS.

Previous studies using mouse models of scrapie (Mabbott et al. 2001) and CWD (Michel et al. 2013) reveal that mice genetically or pharmacologically deficient in C3 accumulate less prions and resist terminal disease longer than their C3-sufficient controls. Prion opsonization likely involves not only local degradation of prions by macrophages, but also trafficking to and subsequent propagation in the LRS, hallmark areas of early prion replication. Factor H deficiency results in increased C3 convertase formation and causes unregulated cleavage of C3 and downstream depletion of serum C3 (Pickering et al. 2002). However, Klein et al. (2001) reported no difference in progression to terminal prion disease in C3 deficient and wild type mice upon a high-dose challenge. Here, we report a significant delayed onset to terminal prion disease upon high dose challenge in mice lacking fH and, therefore C3, compared to wild type mice. Thus, fH deficiency likely plays a more substantial role in prolonging survival than simply eliminating C3. However, C3 deficiency in Factor H deficient mice nevertheless presents a confounding variable which we cannot overlook. Indeed, we present evidence that C3 could promote neuropathological manifestations of prion disease because mice deficient in C3 resist CWD longer than C3-sufficient mice (Figure 2.17).

Complement control proteins contain highly homologous series of 60-70 amino acids termed short consensus repeats (SCRs). SCRs recognize certain C3/C4 cleavage

products, and each Complement control protein elicits distinct downstream functions. For example, Complement receptors 2 (CR2 or CD21) recognize opsonized pathogens via its SCRs and reduce the threshold of B cell activation, whereas Factor H recognizes sialylated host products via its SCRs to prevent autoimmunity. In essence, these proteins stimulate opposing effects using highly homologous SCRs. Domain mapping studies reveal CD21 containing the first two SCRs as sufficient to recognize prion amyloid (data presented in Chapter 3). We therefore conclude CD21 is a cell-surface prion receptor utilized to propagate in lymphoid tissues prior to neuroinvasion. We propose fH is a both a soluble and cell-associated prion receptor and assists in prion disease similarly to CD21. We therefore conclude SCRs on complement control proteins, such as CD21 and fH, bind prions either cell-mediated or cell-autonomously and promote lymphotropism and subsequent neuroinvasion.

Sjoberg et al (2008) reported fH biochemically interacts with various conformers of PrP, but preferentially bound oligomeric species. Amyloid plaques, both in Alzheimer's and prion diseases, appear to be relatively innocuous forms of the misfolded protein, whereas oligomeric species cause the cytotoxic features (Silveira et al. 2005). Perhaps oligomeric species, due to their smaller size and less amyloidogenic status, are more sensitive to protease or cell-mediated degradation. Factor H may bind, thereby protect, and shuttle protease-sensitive oligomers to extraneural sites of prion propagation and amyloid production. We are currently investigating the role of fH in prion stabilization and trafficking.

Baskakov and colleagues convincingly demonstrated that sialylation status differs among prion strains (Katorcha et al. 2015), which could dictate fH binding. Katorcha et al. (2014) reported that PrP^{Sc} sialylation increased prion infectivity. PMCA-generated material derived from de-sialylated substrate did not infect wild type mice, whereas PMCA-generated material from fully sialylated substrate exhibited 100% attack rate. fH may bind sialylated PrP^{Sc} and facilitate disease, albeit through an unknown mechanism. Hepatocarcinoma cells utilize sialic acids to selectively adhere to SLOs (reviewed in Baskakov and Katorcha (2016)). Perhaps sialylated prions infect SLOs via a similar mechanism. Accordingly, de-sialylated PMCA material was undetectable in spleen or brain after serial rounds of PMCA, indicative of either degradation or urinary or fecal secretion. Perhaps fH could explain both of these findings by binding sialic acid on both cancerous cells and prions, causing an evasion of cellular destruction and granting entry to lymphoid tissues.

Factor H could also be involved in selecting different prion strains allowed to propagate in lymphoid organs by preferentially binding sialylated prions. Although we show here that fH binds both lymphotropic and non-lymphotropic strains (Figure 2.1), their sialylation status is unknown. Factor H has also been shown to bind recombinant PrP free of post-translational modifications (Mitchell et al. 2007; Sjoberg et al. 2008), and therefore may dictate prion strain selection and disease outcomes independent of, or in addition to, sialylation status. Qualitative, histological examination revealed a higher proportion of fH^{-/-} mice contained florid or intracellular prion deposition/accumulation

versus the typical, diffuse RML5 deposition in wild type mice (see Figures 2.13 and 2.15), supporting the hypothesis fH is a key host factor in prion strain selection.

Altogether, these data support a role for fH in peripheral prion disease pathogenesis by directly interacting with infectious prions and promoting lymphotropism and subsequent neuroinvasion. We propose Factor H selects for certain prion strains. Whether this selection occurs at the level of prion conformation; sialylation status; evasion of degradation; or a combination therein remains unknown.

REFERENCES

Bartz JC, Dejoia C, Tucker T, Kincaid AE, Bessen RA. Extraneural prion neuroinvasion without lymphoreticular system infection. *J Virol.* 2005 Sep;79(18):11858-63. PubMed PMID: 16140762; PubMed Central PMCID: PMC1212615.

Baskakov IV, Katorcha E. Multifaceted Role of Sialylation in Prion Diseases. *Front Neurosci.* 2016 Aug 8;10:358. doi: 10.3389/fnins.2016.00358. eCollection 2016. Review. PubMed PMID: 27551257; PubMed Central PMCID: PMC4976111.

Beringue V, Demoy M, Lasmézas CI, Gouritin B, Weingarten C, Deslys JP, Andreux JP, Couvreur P, Dormont D. Role of spleen macrophages in the clearance of scrapie agent early in pathogenesis. *J Pathol.* 2000 Mar;190(4):495-502. PubMed PMID: 10700001.

Béringue V, Herzog L, Jaumain E, Reine F, Sibille P, Le Dur A, Vilotte JL, Laude H. Facilitated cross-species transmission of prions in extraneural tissue. *Science.* 2012 Jan 27;335(6067):472-5. doi: 10.1126/science.1215659. PubMed PMID: 22282814. Bessen RA, Marsh RF. Biochemical and physical properties of the prion protein from two strains of the transmissible mink encephalopathy agent. *J Virol.* 1992 Apr;66(4):2096-101. PubMed PMID: 1347795; PubMed Central PMCID: PMC289000.

Brown KL, Stewart K, Ritchie DL, Mabbott NA, Williams A, Fraser H, Morrison WI, Bruce ME. Scrapie replication in lymphoid tissues depends on prion protein-expressing follicular dendritic cells. *Nat Med.* 1999 Nov;5(11):1308-12. PubMed PMID: 10545999.

Carroll MV, Sim RB. Complement in health and disease. *Adv Drug Deliv Rev.* 2011 Sep 16;63(12):965-75. doi: 10.1016/j.addr.2011.06.005. Epub 2011 Jun 16. Review. PubMed PMID: 21704094.

Hageman GS, Anderson DH, Johnson LV, Hancox LS, Taiber AJ, Hardisty LI, Hageman JL, Stockman HA, Borchardt JD, Gehrs KM, Smith RJ, Silvestri G, Russell SR, Klaver CC, Barbazetto I, Chang S, Yannuzzi LA, Barile GR, Merriam JC, Smith RT, Olsh AK, Bergeron J, Zernant J, Merriam JE, Gold B, Dean M, Allikmets R. A common haplotype in the complement regulatory gene factor H (HF1/CFH) predisposes individuals to age-related macular degeneration. *Proc Natl Acad Sci U S A.* 2005 May 17;102(20):7227-32. Epub 2005 May 3. PubMed PMID: 15870199; PubMed Central PMCID: PMC1088171.

Johnson TE, Michel BA, Meyerett C, Duffy A, Avery A, Dow S, Zabel MD. Monitoring immune cells trafficking fluorescent prion rods hours after intraperitoneal infection. *J Vis Exp.* 2010 Nov 19;(45). pii: 2349. doi: 10.3791/2349. PubMed PMID: 21113122; PubMed Central PMCID: PMC3159585.

Katorcha E, Makarava N, Savtchenko R, Baskakov IV. Sialylation of the prion protein glycans controls prion replication rate and glycoform ratio. *Sci Rep*. 2015 Nov 18;5:16912. doi: 10.1038/srep16912. PubMed PMID: 26576925; PubMed Central PMCID: PMC4649626.

Katorcha E, Makarava N, Savtchenko R, D'Azzo A, Baskakov IV. Sialylation of prion protein controls the rate of prion amplification, the cross-species barrier, the ratio of PrP^{Sc} glycoform and prion infectivity. *PLoS Pathog*. 2014 Sep 11;10(9):e1004366. doi: 10.1371/journal.ppat.1004366. eCollection 2014 Sep. PubMed PMID: 25211026; PubMed Central PMCID: PMC4161476.

Klein MA, Frigg R, Raeber AJ, Flechsig E, Hegyi I, Zinkernagel RM, Weissmann C, Aguzzi A. PrP expression in B lymphocytes is not required for prion neuroinvasion. *Nat Med*. 1998 Dec;4(12):1429-33. PubMed PMID: 9846583.

Klein MA, Kaeser PS, Schwarz P, Weyd H, Xenarios I, Zinkernagel RM, Carroll MC, Verbeek JS, Botto M, Walport MJ, Molina H, Kalinke U, Acha-Orbea H, Aguzzi A. Complement facilitates early prion pathogenesis. *Nat Med*. 2001 Apr;7(4):488-92. PubMed PMID: 11283678.

Mabbott NA, Bruce ME, Botto M, Walport MJ, Pepys MB. Temporary depletion of complement component C3 or genetic deficiency of C1q significantly delays onset of scrapie. *Nat Med*. 2001 Apr;7(4):485-7. PubMed PMID: 11283677.

McCulloch L, Brown KL, Bradford BM, Hopkins J, Bailey M, Rajewsky K, Manson JC, Mabbott NA. Follicular dendritic cell-specific prion protein (PrP) expression alone is sufficient to sustain prion infection in the spleen. *PLoS Pathog*. 2011 Dec;7(12):e1002402. doi: 10.1371/journal.ppat.1002402. Epub 2011 Dec 1. PubMed PMID: 22144895; PubMed Central PMCID: PMC3228802.

Michel B, Ferguson A, Johnson T, Bender H, Meyerett-Reid C, Pulford B, von Teichman A, Seelig D, Weis JH, Telling GC, Aguzzi A, Zabel MD. Genetic depletion of complement receptors CD21/35 prevents terminal prion disease in a mouse model of chronic wasting disease. *J Immunol*. 2012 Nov 1;189(9):4520-7. doi: 10.4049/jimmunol.1201579. Epub 2012 Sep 21. PubMed PMID: 23002439; PubMed Central PMCID: PMC3478448.

Michel B, Meyerett-Reid C, Johnson T, Ferguson A, Wyckoff C, Pulford B, Bender H, Avery A, Telling G, Dow S, Zabel MD. Incunabular immunological events in prion trafficking. *Sci Rep*. 2012;2:440. doi: 10.1038/srep00440. Epub 2012 Jun 6. PubMed PMID: 22679554; PubMed Central PMCID: PMC3368226.

Mitchell DA, Kirby L, Paulin SM, Villiers CL, Sim RB. Prion protein activates and fixes complement directly via the classical pathway: implications for the mechanism of scrapie agent propagation in lymphoid tissue. *Mol Immunol*. 2007 Apr;44(11):2997-3004. Epub 2007 Mar 6. PubMed PMID: 17337056.

Montrasio F, Frigg R, Glatzel M, Klein MA, Mackay F, Aguzzi A, Weissmann C. Impaired prion replication in spleens of mice lacking functional follicular dendritic cells. *Science*. 2000 May 19;288(5469):1257-9. PubMed PMID: 10818004.

Pickering MC, Cook HT, Warren J, Bygrave AE, Moss J, Walport MJ, Botto M. Uncontrolled C3 activation causes membranoproliferative glomerulonephritis in mice deficient in complement factor H. *Nat Genet*. 2002 Aug;31(4):424-8. Epub 2002 Jul 1. PubMed PMID: 12091909.

Pulford B, Spraker TR, Wyckoff AC, Meyerett C, Bender H, Ferguson A, Wyatt B, Lockwood K, Powers J, Telling GC, Wild MA, Zabel MD. Detection of PrPCWD in feces from naturally exposed Rocky Mountain elk (*Cervus elaphus nelsoni*) using protein misfolding cyclic amplification. *J Wildl Dis*. 2012 Apr;48(2):425-34. PubMed PMID: 22493117.

Safar J, Wang W, Padgett MP, Ceroni M, Piccardo P, Zopf D, Gajdusek DC, Gibbs CJ Jr. Molecular mass, biochemical composition, and physicochemical behavior of the infectious form of the scrapie precursor protein monomer. *Proc Natl Acad Sci U S A*. 1990 Aug;87(16):6373-7. PubMed PMID: 1974720; PubMed Central PMCID: PMC54536.

Silveira JR, Raymond GJ, Hughson AG, Race RE, Sim VL, Hayes SF, Caughey B. The most infectious prion protein particles. *Nature*. 2005 Sep 8;437(7056):257-61. PubMed PMID: 16148934; PubMed Central PMCID: PMC1513539

Sjöberg AP, Nyström S, Hammarström P, Blom AM. Native, amyloid fibrils and beta-oligomers of the C-terminal domain of human prion protein display differential activation of complement and bind C1q, factor H and C4b-binding protein directly. *Mol Immunol*. 2008 Jun;45(11):3213-21. doi: 10.1016/j.molimm.2008.02.023. Epub 2008 Apr 11. PubMed PMID: 18406463.

Somerville RA, Birkett CR, Farquhar CF, Hunter N, Goldmann W, Dornan J, Grover D, Hennion RM, Percy C, Foster J, Jeffrey M. Immunodetection of PrPSc in spleens of some scrapie-infected sheep but not BSE-infected cows. *J Gen Virol*. 1997 Sep;78 (Pt 9):2389-96. PubMed PMID: 9292029.

Srivastava S, Makarava N, Katorcha E, Savtchenko R, Brossmer R, Baskakov IV. Post-conversion sialylation of prions in lymphoid tissues. *Proc Natl Acad Sci U S A*. 2015 Dec 1;112(48):E6654-62. doi: 10.1073/pnas.1517993112. Epub 2015 Nov 16. PubMed PMID: 26627256; PubMed Central PMCID: PMC4672809.

Zabel MD, Heikenwalder M, Prinz M, Arrighi I, Schwarz P, Kranich J, von Teichman A, Haas KM, Zeller N, Tedder TF, Weis JH, Aguzzi A. Stromal complement receptor CD21/35 facilitates lymphoid prion colonization and pathogenesis. *J Immunol*. 2007 Nov 1;179(9):6144-52. PubMed PMID: 17947689.

Zipfel PF, Edey M, Heinen S, Józsi M, Richter H, Misselwitz J, Hoppe B, Routledge D, Strain L, Hughes AE, Goodship JA, Licht C, Goodship TH, Skerka C. Deletion of complement factor H-related genes CFHR1 and CFHR3 is associated with atypical hemolytic uremic syndrome. *PLoS Genet.* 2007 Mar 16;3(3):e41. Epub 2007 Feb 1. PubMed PMID: 17367211; PubMed Central PMCID: PMC1828695.

CHAPTER 3 – RELATIVE IMPORTANCE OF COMPLEMENT RECEPTORS CD21/35 (CR2/1) IN SCRAPIE PATHOGENESIS²

Summary

Complement Receptors 1 and 2 (CR1/2 or CD35/CD21) recognize opsonized antigens and stimulate phagocytosis and humoral immunity, respectively. Transcripts from the mouse *Cr2* gene undergo differential splicing to generate proteins with both shared and unique Complement binding capacities and cell-type expression. In mouse models, genetic depletion of *Cr2* causes either a delay or complete prevention² of prion disease. However, the relative importance of CD35 vs CD21 in promoting prion disease remains unknown. Data from this chapter suggest both proteins can biochemically serve as cell-surface prion receptors. However, mice lacking CD21 resist prion disease, whereas mice lacking CD35 succumb to prion disease at the same rate as wild type and hemizygous mice. Further, CD21 knockout mice contained lower splenic prion loads than CD35 knockout mice at 30dpi. FACS analysis of PrP^C and CD19, cell-surface proteins known to impact prion disease, revealed a drastic increase of splenic CD19 in mice lacking CD21. Accordingly, previous studies reveal accelerated prion disease in mice lacking CD19, suggesting CD19 may exert protective effects against prion disease. Altogether, data from this chapter suggest CD21 promotes prion disease more-so than splice variant CD35.

² A version of this manuscript will be published in *mSphere* (under Editorial review): Kane, SJ *et al.* (2017). Relative Impact of Complement Receptors CD21/35 (Cr2/1) On Scrapie Pathogenesis in Mice.

Introduction

The Complement system consists of >30 serine proteases which serves three main functions: 1) create the membrane attack complex (MAC) on pathogen cell surfaces to provoke osmotic pressure-induced cell-lysis; 2) opsonize pathogens to trigger phagocytosis; and 3) reduce the threshold for B cell activation upon simultaneous engagement of B cell receptor and Complement receptor 2. While Complement activation involves a largely nonspecific recognition of proteins and lipids, it links the fast-acting innate immune system with the long-term, memory-producing, adaptive immune system.

As mentioned in previous chapters, Complement facilitates the early spread and propagation of prions to and within the lymphoreticular system (LRS). Specifically, transgenesis leading to deficiency in Complement proteins C3, C4, C1q, or CD21/35 causes a delay or complete prevention of prion accumulation and disease onset (Mabbott et al. 2001; Zabel et al. 2007; Michel et al. 2012; Michel et al. 2013).

Interestingly, in a mouse model of CWD, genetic depletion of Complement Receptors CD21/35 (Michel et al. 2012) completely protected mice from infection, whereas depletion of the receptors' ligand, C3, delayed, but did not entirely prevent, disease (Michel et al. 2013). These data strongly suggest CD21/35 impacts disease independently of its natural ligand, C3.

Murine CD21/35 (AKA CR2/1) arise from differentially splicing *Cr2* transcripts (Molina et al. 1990), whereas the human genome encodes for CD21 and CD35 in separate genes

(Kurtz et al. 1990). In mice, *Cr2* on chromosome 1 encodes 26 exons (NCBI gene, Figure 3.1A). Both transcripts share the first exon encoding for the signal sequence, and splicing to exon 7 and 2 encodes for CD21 and CD35, respectively. As discussed in Chapter 1, Complement control proteins bind ligand via their short-consensus repeats (SCRs) which elicit various, sometimes opposing, downstream functions. CD21 contains 15 SCRs and recognizes C3 cleavage products. CD35 contains an additional 6 N-terminal SCRs (Figure 3.1B) which recognize C4 cleavage products (Molina et al. 1990; Fingerroth et al. 1989; Kurtz et al. 1990).

CD21 binds to all its known ligands, iC3b, C3d, C3dg, CD23, and Epstein Barr gp350/220 using the first two SCRs (Kovacs et al. 2010, reviewed in Hannan 2016), whereas CD35 binds C4b cleavage products in addition to CD21 ligands (Reilly et al. 1994). Thus, any interaction with CD21 also occurs with CD35, yet CD35 uniquely binds certain ligands. Some cell-types express both Complement receptors, whereas certain cell types express only one or the other. Considering murine *Cr2* encodes both CD21 and CD35, it is difficult to ascertain cell-type specific expression. However, humans encode CD21 and CD35 on separate genes and exhibit cell-type specific expression. In human, CD35 expression serves to clear immune complex by providing a phagocytic signal for macrophages (Newman et al. 1985) and neutrophils (Changelian et al. 1985). CD21 expression on B cells provides a co-stimulatory signal to reduce the activation threshold upon engagement of B cell receptor with its specific antigen (Cherukuri et al. 2001; Del Nagro et al. 2005; Barrington et al. 2009). Mice deficient in both CD21 and CD35 exhibit impairment in combatting bacteremia (Cunnion et al. 2004) and eliciting a

humoral immune response (Haas et al. 2002). However, whether these findings arise from CD35 or CD21 remain unknown. Considering the highly homologous nature between mouse and human Complement proteins, we hypothesize mouse CD21 and CD35 serve similar functions as human CD21 and CD35.

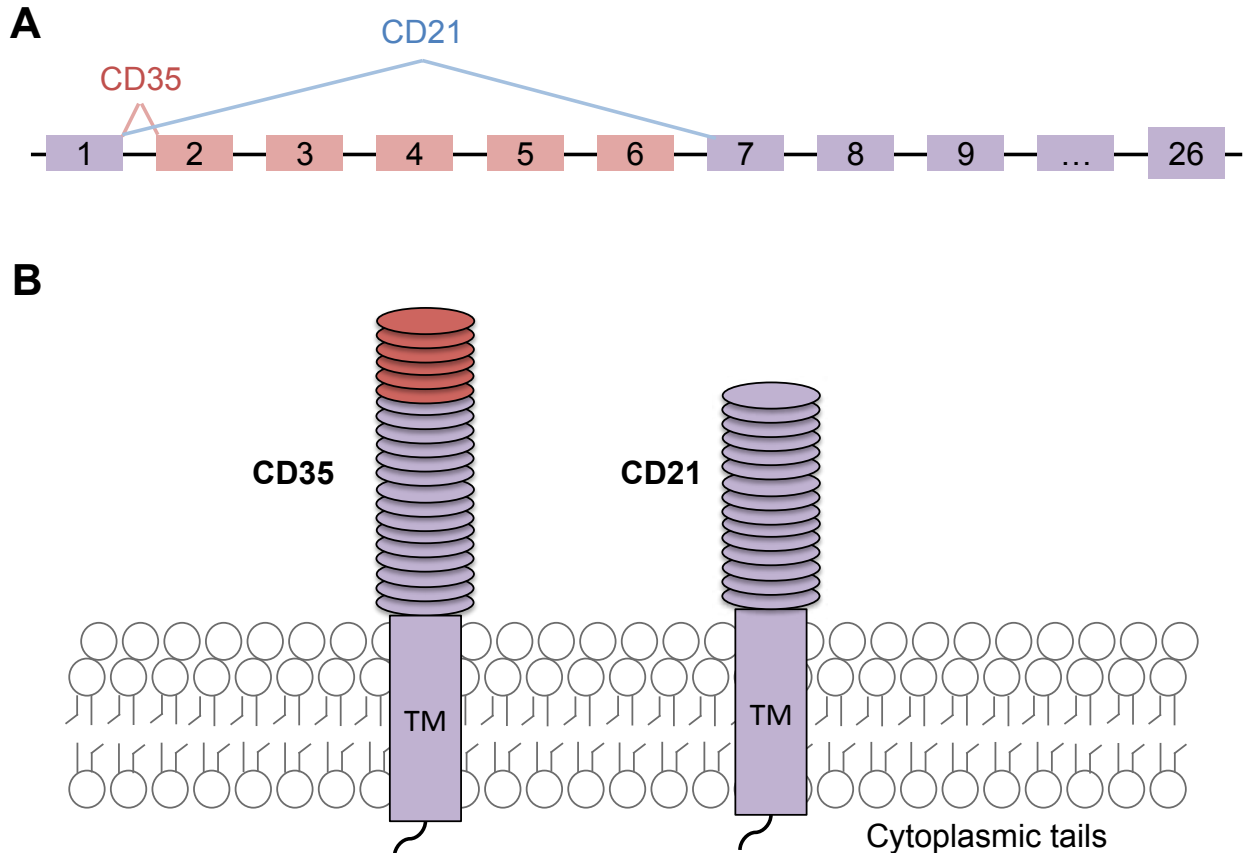


Figure 3.1. Illustration of murine splice variants CD35 and CD21. Murine *Cr2* encodes 26 exons, and CD21 and CD35 share exon 1 (A). Transcripts encoding for CD21 splice exon 1 to exon 7, whereas CD35 contains intervening sequences (A). CD21 and CD35 both contain extracellular short consensus repeats, a transmembrane (TM) domain, and a short cytoplasmic tail (B). However, CD35 contains an additional 6 N-terminal SCRs (B). Shared sequences and structures are indicated in purple, and red indicates components unique to CD35.

Considering murine CD21 and CD35 arise from the same gene, the relative functions of each isoform remains largely unknown. However, Donius et al. (2013a,b) generated mice which specifically express only one isoform (termed CD21 KO or CD35 KO here).

Therefore, these mice provide valuable tools to ascertain specific isoform and cell type specific functions. We aimed to address the relative importance of CD21 and CD35 in prion accumulation and disease onset.

The interaction between the host's immune system and prions may initially seem counter-intuitive. Prions require expression of a host protein, PrP^C (Bueler et al. 1993; Pruisner et al. 1993), to cause disease. However, immunomodulatory mechanisms during development ensure auto-reactive lymphocyte (B and T cell) quiescence. These mechanisms certainly evolved to prevent self-antigen recognition and downstream auto-immunity. Therefore, questions in the field include: how could a host elicit an adaptive immune response to prions without causing autoimmunity, and if prions bypass adaptive immunity, what components of the host's immune system do they use to spread and cause disease? Data presented in this chapter aim to address the latter.

Materials and Methods

Mice. All mice were bred and maintained at Lab Animal Resources, accredited by the Association for Assessment and Accreditation of Lab Animal Care International and approved on January 14, 2016 by the Institutional Animal Care and Use Committee at Colorado State University (Protocol ID: 09-1580A). CD21 (CR2) or CD35 (CR1) specific knockout mice on the C57/Bl6 background were kindly provided by the Weis laboratory (University of Utah School of Medicine). We crossed the individual knockout mice to achieve hemizyosity.

Mouse inoculations and clinical sign scoring. Age- and sex- matched mice ($n \geq 6$ per genotype) ranging from 6 weeks to 1 year intraperitoneally received 100 μ L of approximately 10^6 lethal dose₅₀ units of mouse-adapted scrapie strain RML5 prions. Mice were monitored daily and sacrificed at the onset of terminal disease or specified timepoints. We employed a scoring system to assess the severity of disease, including: tail rigidity (0-2), akinesia (0-4), ataxia (0-4), tremors (0-4), and weight loss (0-2). Mice scored above 10 (total) or with a 4 or above in one category were euthanized via CO₂ inhalation replacing 20% of air per minute to effect.

Tissue collection and analysis. After euthanasia, the following samples were collected and frozen or fixed in 4% formaldehyde in 1X PBS: serum, spleen (half fixed, half frozen), kidneys (one fixed, one frozen), tail clip, and brain (half fixed, half frozen). We assessed the presence of protease-resistant prions (PrP^{RES}) in 10% (w/v) homogenate after proteinase K (Roche) digestion (10 μ g/mL for spleen and 50 μ g/mL for brain) and western blotting using anti-PrP monoclonal antibody BAR224 (Cayman) conjugated to horseradish peroxidase (HRP). Blots were developed using chemiluminescent substrates hydrogen peroxide and luminol for 5 minutes at room temperature and visualized using a GE digital imager and ImageQuant software. Tissues negative for PrP^{RES} on western blots were subjected to serial protein misfolding cyclic amplification (PMCA; Saborio and Soto, 2001). Briefly, PMCA uses 10% normal brain homogenate in PMCA buffer (1X PBS, 1% Triton X-100, 4 mM EDTA and 150 mM NaCl) from PrP^C over-expressing transgenic mice, strain TgA20, as substrate for amplification of previously undetectable prions. Twenty-five microliters of normal brain homogenate

(NBH) and 25 μ L 10% sample homogenate, underwent a 40 second pulse of sonication at ~150 watts, followed by a 30 minute incubation, and repeated for 24 hours (one round). Serial rounds were set up similarly, transferring 25 μ L of the previous round's sample to 25 μ L of fresh NBH. Each biological sample was run in at least technical duplicates, and round-to-positivity was determined by PK digestion and western blotting. Relative PMCA units were assigned as previously described (Pulford et al. 2012).

Prion rod preparation and surface plasmon resonance. Prion rods were enriched from infected brain as previously described (Michel et al. 2012, Safar et al. 1990). Briefly, brains from animals infected with chronic wasting disease (E2), hyper- or drowsy-transmissible spongiform encephalopathies (HY- or DY-TME) were homogenized in 1X PBS to 10% (w/v) concentration. Sucrose (1.2 M) was added to 10 mL of clarified tissue to a final concentration of 165.5 mM, and samples were ultracentrifuged (100,000 x g) for one hour at 4°C. Pellets were resuspended to a final protein concentration of 5.0 mg/mL in 1X TBS containing 2.0% Triton X-100 (TBST) and incubated on ice for 30 minutes. Samples were subjected to another round of ultracentrifugation for 20 minutes at 0°C, washed twice in 1X TBST, and twice with 1X TBS. The pellets were then resuspended in 1X PBS containing 1% sarcosyl and protease inhibitor cocktail (Roche). Vortexed samples were incubated on a heated shaker at 37°C for two hours at 800 rpm. Samples were then gently overlaid on a 0.32 M sucrose in PMCA buffer 1 (PMCA buffer without Triton-X 100) cushion, ultracentrifuged for one hour at 4°C, and supernatants removed. Pellets were resuspended in 2.3 M NaCl, 5% sarcosyl in 1X PBS, centrifuges at 13,000 x g, washed three times in 50 mM Tris 150 mM NaCl, and

were either stored dry or suspended in PBS at -80°C. Presence of PK resistant prion rods were confirmed by western blot.

Highly enriched prion rods were coupled to CM-5 sensor chips outside of the instrument after generating the reference flow cells within the instrument by activating with EDC/NHS and deactivating with ethanolamine three to five times. The chip was then removed from the instrument and the gold chip disassembled from the cassette. The entire surface was activated with 100 µL of EDC/NHS for 12 minutes. A pellet of rods was resuspended in 100 µL of 10 mM sodium acetate pH 5.4, sonicated at 37°C for 40 seconds, and incubated on the gold chip at room temperature for one hour. The chip was then briefly rinsed with 1X PBS, and remaining active groups were deactivated with ethanolamine for 7 minutes. Prior to use in interaction analyses, a startup cycle of 50 mM sodium hydroxide served to remove any nonspecifically bound prion rods from the surface.

All SPR experiments involved recombinant PrP (rPrP) or prion rod enriched from infected brain as the ligand coated to a CM5 Series S sensor chip, and purified CD21 containing SCR1-2 or SCR1-6 was kindly provided by Dr. Hannan from University of Colorado (Denver) School of Medicine. CD21 was buffer exchanged in Amicon filter devices into 1X Running Buffer (50 mM Tris HCl, 150 mM NaCl, pH 7.42). The rPrP-coated chip was kindly provided by Dr. Hae-Eun Kang in the Telling lab. Briefly, flow cells were first activated with 0.2 M 1-ethyl-3-(3-dimethylaminopropyl) carbodiimide hydrochloride (EDC) and 0.05 M N-hydroxysuccinimide (NHS) for seven minutes at 10

$\mu\text{L}/\text{min}$. Amine coupling recombinant cervid or murine PrP^C in 10 mM sodium acetate pH 5.5 was accomplished by flowing 20 $\mu\text{g}/\text{mL}$ of ligand over the activated chip for seven minutes at 10 $\mu\text{L}/\text{min}$. Excess activated groups were deactivated with 1 M ethanolamine HCl pH 8.5 for seven minutes at 10 $\mu\text{L}/\text{min}$. Reference flow cells, built-in negative controls for this system, underwent rounds of activation and deactivation without the addition of protein ligand.

Cell culture prion infection. N2a mouse neuroblastoma cells were grown in RPMI medium containing 10% fetal bovine serum and 1% penicillin/streptomycin. RML5 infected brain homogenate was UV-sterilized prior to infecting cells. RML5 was pre-incubated with PBS or CD21 (SCR1-2; 5 $\mu\text{g}/\text{mL}$ final) for 10-20 minutes prior to infecting cells. N2a cells were seeded at 100,000 cells per well in a 12 well plate and infected with 0.3% RML5 containing PBS or fH. Cells were grown at 37°C and 5% CO₂ for 4 days. Wells were rinsed 2X in 1X PBS, and cells were detached from the plate using 5 mM EDTA in 1X PBS for 10 minutes. Cell pellets were resuspended in 100 μL PMCA buffer containing 1% Triton X-100 and lysed on ice for 30 minutes. Lysates were assessed for PrP^{RES} using traditional PK digestion and western blotting techniques.

Flow Cytometry (FACS). Fresh brain and spleens were harvested and processed to single-cell suspensions in 3 mL PBS. Briefly, tissues were passed through 40 μm mesh filters using sterile plungers and cold PBS washes. Cells were pelleted at 250 x g for 5 minutes at 4°C, and the supernatant was discarded. Red blood cells (RBCs) were lysed in lysis buffer for 5 minutes, cells were pelleted as previous, and washed in FACS buffer

(1X PBS, 1% FBS, and 1 mM EDTA). Primary splenocytes or brain suspensions were blocked in 7% mouse serum and 1:50 F_c block (BD Pharmagin) for 20-60 minutes on ice. Antibody solutions (1:100 final) were added to cells and incubated in the dark for one hour on ice. Cells were washed by adding 1 mL FACS buffer to existing antibody solution. Cells were pelleted, supernatant removed, and resuspended in 1 mL FACS buffer for a total of 3 washes. 792 μ L cell suspension was added to 8 μ L of Propidium Iodide (SIGMA) immediately prior to data acquisition in a Cyan flow cytometer. Cells were analyzed 500-1500 events per second. Unstained samples were analyzed first in order to set parameters to achieve a well-defined peak in the first fluorescent decade.

FACS analysis in Flow-Jo. Cellular debris was gated off the Y- axis of forward and side scatter plots. PI-positive (dead) cells were also gated off. Fluorochrome-positive gates were set by setting a threshold of 1% in the unstained population. In other words, stained cells were considered positive if their fluorescent intensity was greater than 99% of the unstained population. Mean fluorescent intensity (MFI), as well as frequency of parent gate, values were imported into Excel and/or GraphPad Prism for analysis.

Statistical analyses. All statistical analyses were performed using GraphPad Prism software. One-way ANOVAs were run to compare genotypes. P-values < 0.05 were considered significantly different.

Results

CD21 and CD35 both bind prion amyloid. Previous reports indicate a crucial role for CD21/35 in prion disease, but whether due to a direct interaction remained unknown. We performed a previously published protocol which removes soluble PrP^C and highly enriches insoluble prion rods (Safar et al. 1990; Michel et al. 2012; Johnson et al. 2010). We then coupled these prion rods to a CM5 sensor chip and tested an interaction with purified CD21 protein containing either SCR1-2 or SCR1-6. We also test interactions between CD21 and HY- or DY- TME and observed interactions with both (data not shown). We then tested whether inhibitory monoclonal antibody 171 (imAb 171), which binds and blocks interactions at SCR 1-2 (Kulik et al. 2011), inhibits the interaction between CD21 and prion rods. imAb 171 reduced, but did not completely eliminate, the interaction. These data suggest CD21/35 bind prion rods at least partially using the first two SCRs on CD21. It is important to note, however, that the first two SCRs on the CD21 molecular correspond to SCRs 7-8 on CD35. Whether additional binding occurs on the first six SCRs on CD35, corresponding to C4 binding sites, remains unknown.

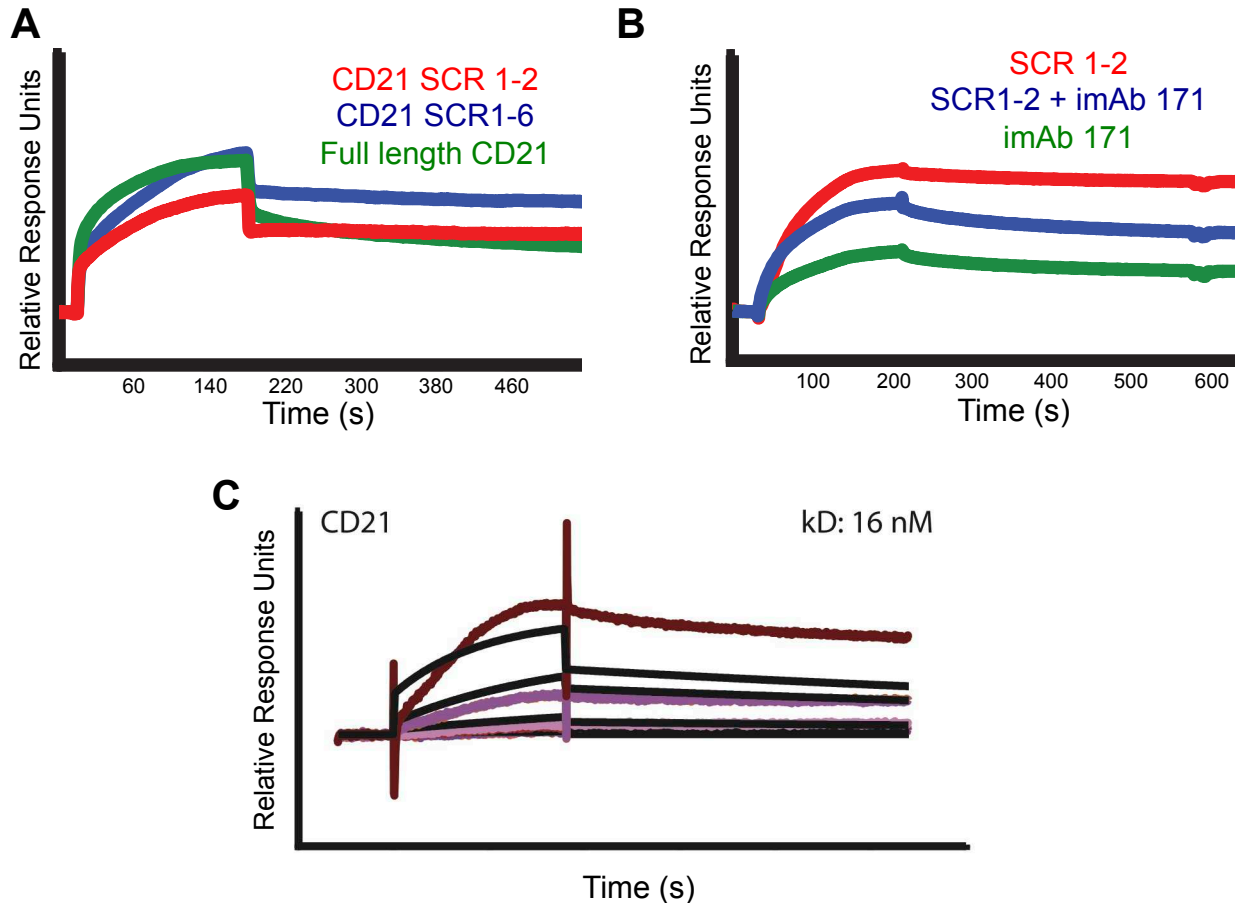


Figure 3.2. CD21 and CD35 both bind prion rods. Prion rods were enriched from elk brain infected with chronic wasting disease as previously described. Equimolar full length CD21, or protein containing the first two or first six SCRs on CD21, all bound prion rods (A). Addition of inhibitory monoclonal antibody 171 (imAb 171) at least partially reduced the interaction, although we also observed some nonspecific binding with imAb 171 alone (B). Kinetic analysis reveal a 16 nM dissociation constant (kD) between full-length CD21 and prion rods (C). Concentrations of CD21 (C) tested include: 0(bottom), 1, 2, 10, 20, 100, and 200 nM(top). These data suggest the prion:CD21/35 interaction at least partially occurs using the first two SCRs on CD21/35.

Early splenic accumulation partially relies on CD21. We inoculated mice with RML5 prions and assessed prion loads in spleen at 30dpi. Mice deficient in CD21 accumulated slightly fewer prions in their spleen than CD35 deficient mice ($p=0.0459$). However, when C57/BI6 wild type 30dpi PMCA data (Chapter 2) was included in the analysis, ANOVA analysis revealed no significant differences between genotypes. However, wild

type mice were not inoculated on the same day as CD21 or CD35 deficient mice, so this data was excluded from Figure 3.3.

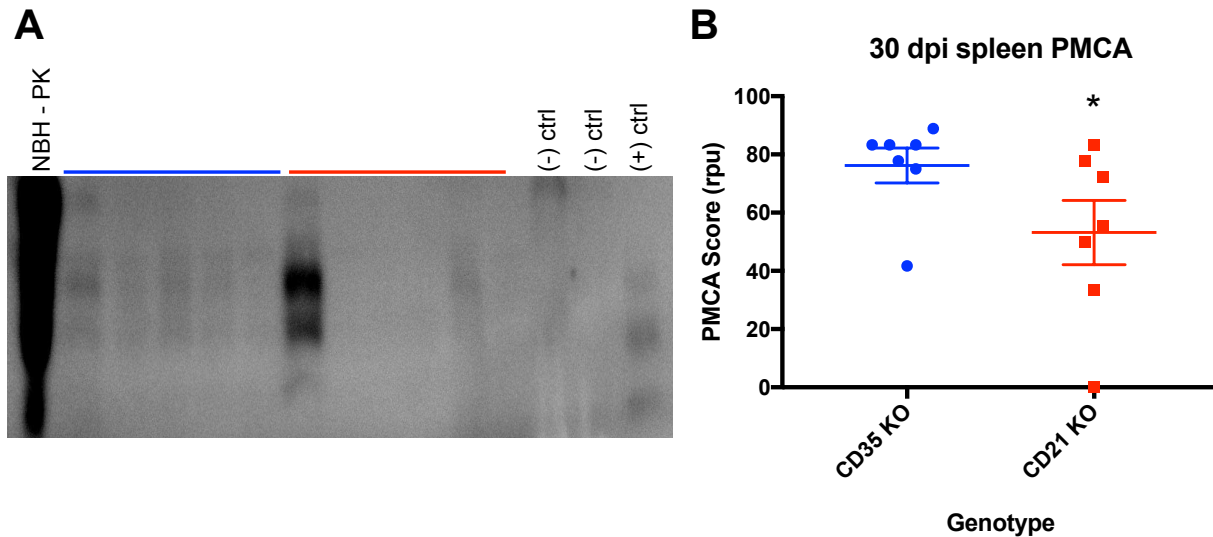


Figure 3.3. CD21 promotes splenic accumulation at 30dpi. Mice deficient in either CD35 or CD21 (n=7/genotype) were inoculated with RML5 prions and sacrificed at 30dpi. Spleens (10% w/v) were subjected to serial rounds of PMCA and analyzed for PrP^{RES} via western blotting (A). Mice deficient in CD21 scored significantly lower than CD35 deficient mice (B, p=0.0459; one-tailed T-test).

Terminal prion disease onset relies on CD21, not CD35. Previous data suggested CD21 may promote initial trafficking to and propagation in spleen (Figure 3.3). To ascertain whether splice variant CD35 or CD21 promotes the onset of terminal prion disease, we inoculated mice with RML5 prions and monitored the time to disease onset. CD21 deficient mice resisted disease significantly longer than wild type, CD35 deficient, or hemizygous mice (Figure 3.4).

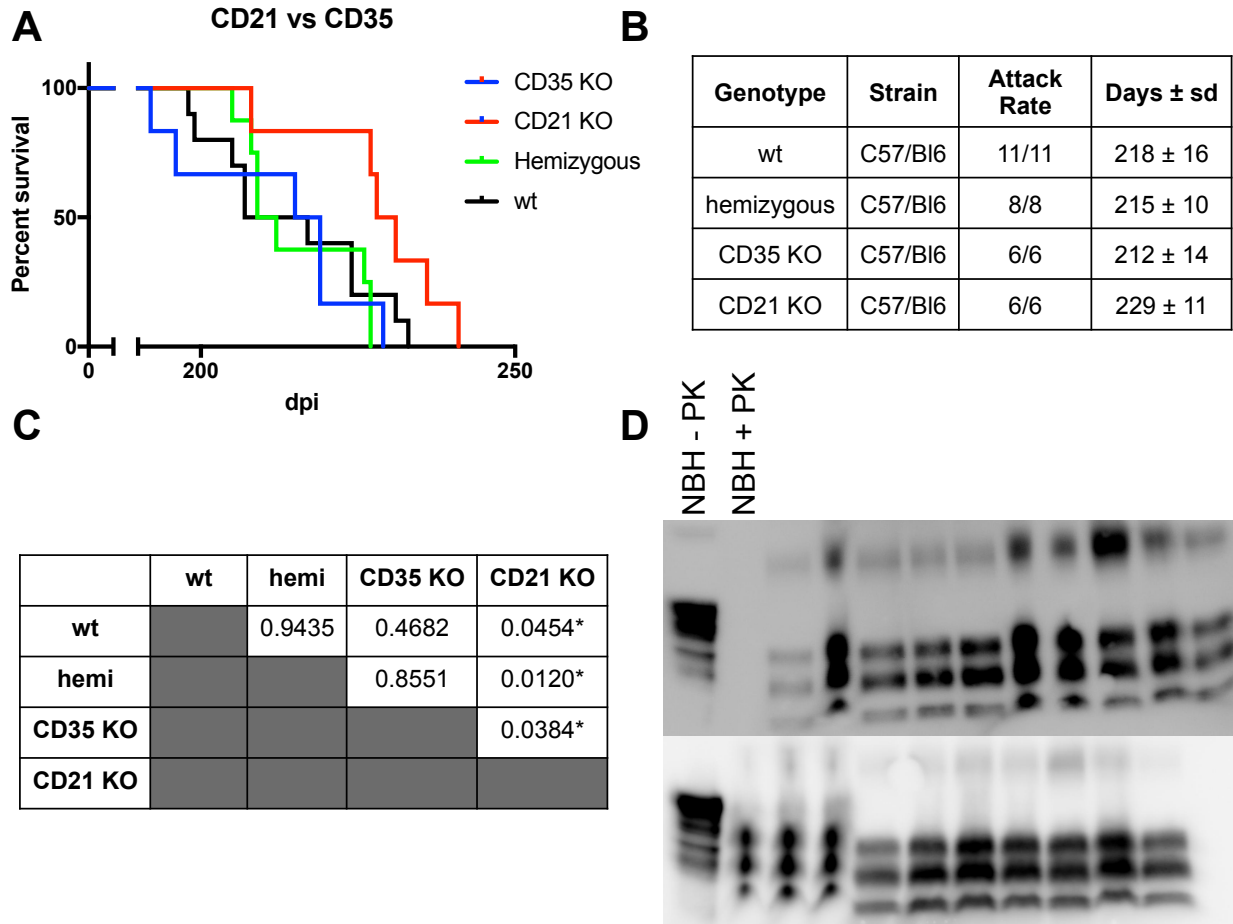


Figure 3.4. CD21-deficient mice resist terminal disease onset longer than wild type, hemizygous, or CD35-deficient mice. Mice ($n > 6$ per genotype) were inoculated with a single dose of RML5 prions and monitored for the onset of terminal disease. Mice deficient in CD21 lived significantly longer than all other genotypes, which did not significantly differ from each other (A-C). Panel B shows mean and standard deviation, and C shows p-value comparisons per group (Log-rank Mantel-Cox). Western blotting analysis revealed all mice contained PrP^{RES} at the onset of terminal disease (D).

CD21 pre-treatment inhibits prion replication in vitro. Cell-surface CD21 promotes prion disease, leading us to question whether pre-incubating prions with soluble CD21 could serve to block the prion:CD21 interaction and thus infection. Pre-treating RML5-infected brain homogenate with CD21 led to decreased PrP^{RES} signal compared to PBS-treated control (Figure 3.5). Interestingly, non-digested, CD21 pre-treated samples contained less total PrP signal (-PK) than PBS treated controls. However, we cannot conclude

whether CD21 caused a reduction of PrP^C, or whether increased PrP^{RES} contributed to the higher total PrP signal in PBS-treated samples. These data suggest soluble CD21 could serve as a therapeutic, and future directions include testing whether these findings are translatable *in vivo*.

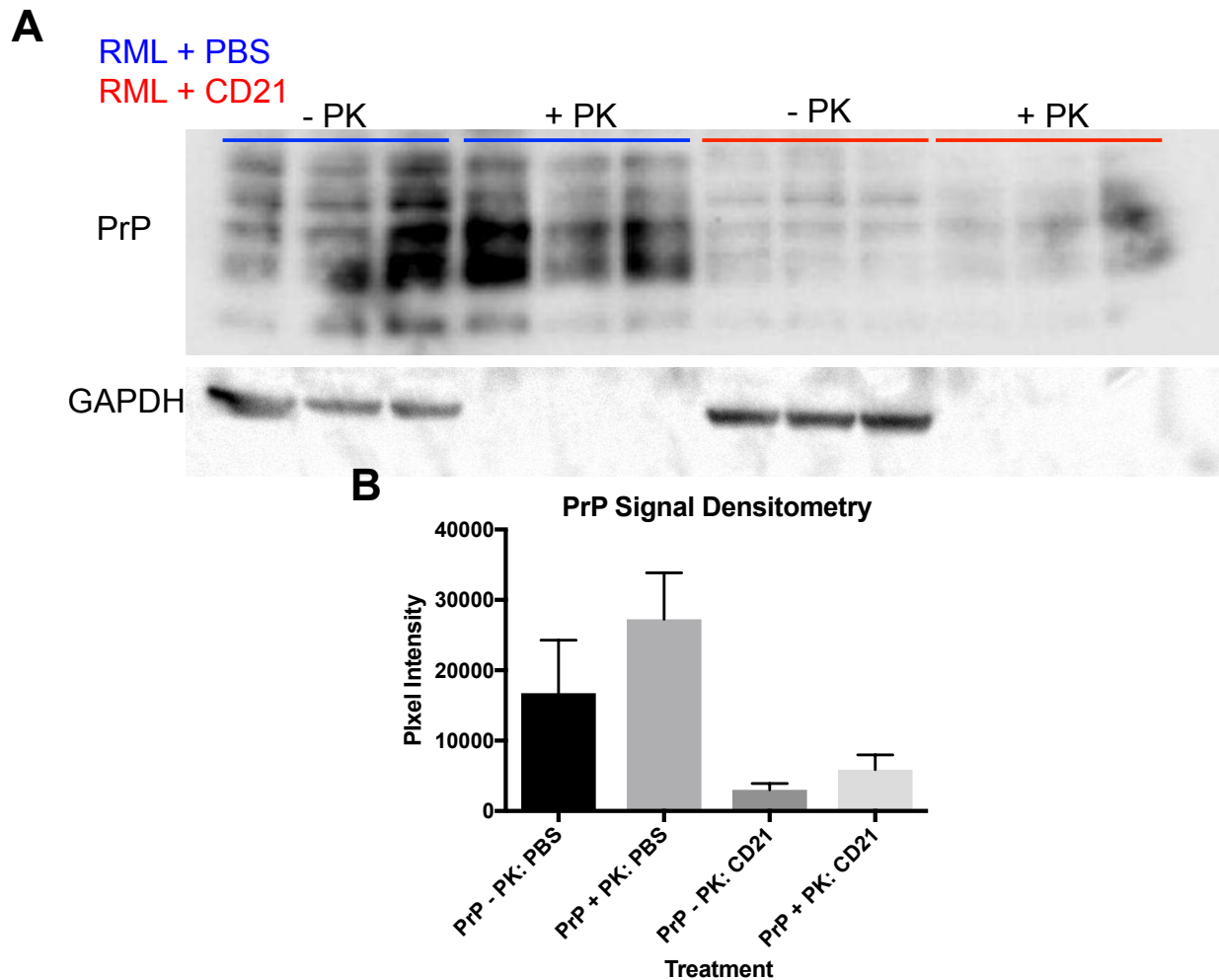


Figure 3.5. Soluble CD21 may serve as a therapeutic. RML5-infected brain homogenate (0.33%) was pre-treated with either PBS or CD21 (5 µg/mL final) prior to infecting N2a cells. After culturing cells with treatment for 4 days, cells were harvested and analyzed for PrP^{RES} and GAPDH as a loading control (A). Cells infected with CD21 pre-treated inoculum contained significantly lower PrP^{RES} densitometric signal than PBS-treated controls (B, unpaired one-way T-test, p=0.0182).

CD21/35 double knockout phenotype depends on CD21. Previous reports indicate lack of CD21/35 causes an increase in another member of the BCR, CD19 (Hasegawa et al. 2001). As shown in Figure 3.6, FACS analysis of CD19 cell-surface levels reveal a ~35% increase of CD19 in CD21 knockout mice when compared to wild type or CD35 knockout mice. Importantly, CD35 KO mice did not significantly differ from wild type mice. CD19 deficiency is known to promote prion disease (von Poster-Klein et al. 2008). However, CD19 deficiency did not impact splenic prion titers, but rather juxtaposed sympathetic neurons to FDC networks and thus facilitated more rapid neuroinvasion. Other members of the Zabel laboratory analyzed nerve fiber positioning and showed CD21 deficiency perplexingly also juxtaposes sympathetic nerve fibers to FDC networks (data not shown).

CD21 or CD35 deficiency does not alter PrP^C levels in brain. Data from other chapters suggests PrP^C and CD21/35 may be co-regulated. CD21 deficiency leading to PrP^C deficiency could explain the increased survival time and reduced prion loads in CD21 knockout mice. To ensure this putative co-regulation did not confound the effects described here, we analyzed PrP MFI, as well as relative proportion of PrP^C+ cells in brain. CD21 or CD35 deficient mice did not differ in the percentage of PrP^C+ cells, nor MFI compared to wild type (Figure 3.7). These data suggest the CD21 effect cannot be explained by altering PrP^C levels.

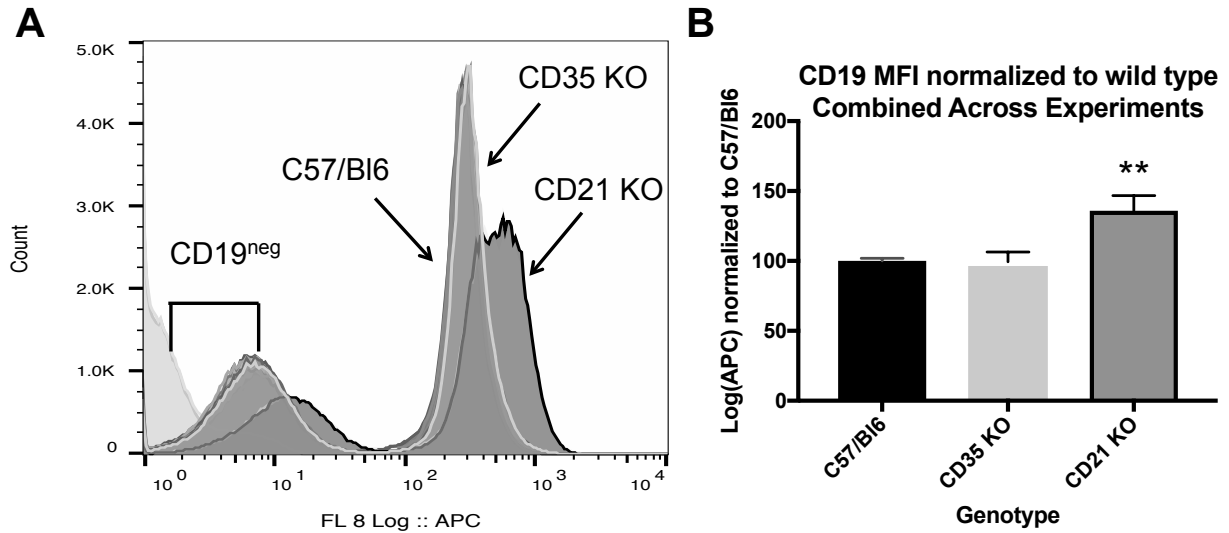


Figure 3.6. CD19 alterations depend on CD21. Previous reports show ~30% increase in surface CD19 in CD21/35 double knockouts (Hasegawa et al. 2001 and Haas et al. 2002), as well as exacerbated disease onset in CD19 knockout mice (von Poster-Klein et al. 2008). We aimed to determine whether this phenotype depended on CD21 or CD35 via FACS. Histograms of live cells show CD21 KO mice have higher fluorescent intensity values than CD35 KO or wild type (A,B ** p=0.0083).

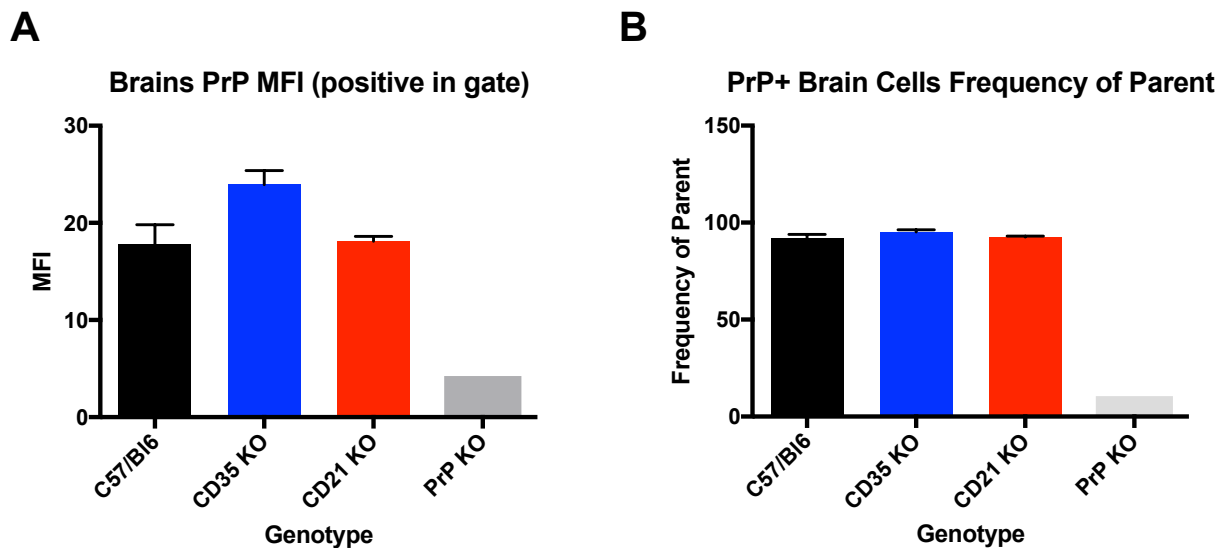


Figure 3.7. PrP^C is not a confounding variable. We tested whether PrP^C levels in brain depended on the presence of CD21 or CD35, and our results suggest no statistical difference in CD21 or CD35 knockout mice (B) when compared to wild type mice.

Discussion

Attempts to ascertain CD21/35 functions previously relied on *Cr2* genetic manipulations which render mice deficient in both CD21 and CD35. However, Donius et al. (2013a,b) generated mice which express one splice variant or the other, allowing researchers to determine the relative importance of cell-types which uniquely express each splice variant. Therefore, these mice provide a powerful tool to ascertain not only splice variant roles, but also specific cell type roles. For example, CD35 on macrophages and neutrophils is generally thought to promote phagocytosis and immune complex clearance, whereas CD21 on follicular dendritic (FDC) and B cells is thought to help link the innate and adaptive immune systems. These mice offer the ability to challenge or confirm these proposed roles.

The role of Complement Receptors in prion disease is well established. Mice deficient in CD21/35 exhibit delayed clinical disease when challenged with mouse-adapted scrapie prions (Zabel et al. 2007). Interestingly, transgenic mice expressing cervid PrP^C concomitant with CD21/35 deficiency completely resist terminal disease when challenged with elk chronic wasting disease prions (Michel et al. 2012). These seminal papers highlight a crucial role in CD21/35 in prion disease, although the relative importance of each splice variant remained unknown.

Data presented in this chapter suggest both variants derived from *Cr2* transcripts can biochemically interact with prion amyloid (Figure 3.2). This finding supports the previous *in vivo* data and suggests CD21/35 are cell-surface prion receptors. Interestingly, in the

mouse model of chronic wasting disease, C3 deficient mice eventually succumbed to prion disease, whereas CD21/35 deficient mice entirely resisted disease (Michel et al. 2013 and 2012). These findings highlight Complement Receptors CD21/35 as more critical than their endogenous ligand, C3. These data, along with the biochemical data presented in this chapter, suggest CD21/35 impacts prion disease by directly interacting with prions. CD21/35 likely exerts its effects along with C3 opsonization, although perhaps not crucially.

CD21/35-expressing B cells and FDCs are known to impact prion disease. Interestingly, B cells likely promote prion trafficking, not replication, because deleting *Prnp* specifically in B cells did not inhibit prion disease (Klein et al. 1998). In other words, B cells promote prion disease independent of PrP^C expression. We believe data presented here could explain these findings. Perhaps CD21, not PrP^C, is the cellular factor on B cells which aids prion pathogenesis. Future directions to test this hypothesis could involve silencing CD21/35 specifically in B cells and assessing the impact on prion accumulation and disease onset.

To date, known CD35 functions include inducing immune complex phagocytosis on neutrophils and macrophages (Newman et al. 1985; Changelian et al. 1985) and immune complex clearance. CD21, however, engages C3d/g opsonized pathogens and provides a co-stimulatory signal when a mature, naïve B cell encounters its specific antigen. Therefore, in conjunction with previous reports, our data confirm B cells' importance in prion disease, which likely arise from the interaction of CD21:prions.

However, CD35 can also biochemically react with prions, but likely promote phagocytosis and destruction with macrophages, the only cell-type known to help resolve prion infection (Beringue et al. 2000).

Alternatively, or perhaps additionally, CD19 on B cells may dictate prion pathogenesis. Previous reports indicate CD21/35 deficiency causes a 36% increase in splenic CD19 (Hasegawa et al. 2001; Haas et al. 2002), and we found this effect to mostly rely on the lack of CD21 (Figure 3.6A). CD19 deficiency causes prion disease exacerbation (von Poser-Klein et al. 2008). Reason would serve to suggest CD19 over-expression may inhibit disease, although this prediction has not yet been tested. However, CD19 deficiency promoted neuroinvasion, not splenic accumulation or replication because splenic prion titers did not differ in wild type vs CD19 deficient mice at 90dpi. Rather, histological examination revealed CD19 deficiency led to dopaminergic nerve fiber positioning closer to FDC networks. This data suggests CD19 deficiency promotes neuroinvasion, not splenic accumulation or replication, by positioning nerve fibers closer to prion-replicating germinal centers. In contrast, data presented in this chapter suggest CD21 promotes splenic accumulation and/or replication (Figure 3.3), suggesting CD21 promotes prion disease independently of CD19 alterations. In fact, other members in the Zabel laboratory showed increased nerve fiber juxtaposition in CD21 KO mice. Thus, CD21 deficiency impacts prion disease despite CD19 upregulation and hyperinnervation.

Collectively, data presented in this chapter highlight a crucial role for CD21, not CD35, in prion disease. While CD21 and CD35 arise from the same gene in mice, and genetic deficiency in both isoforms protects or entirely prevents prion disease in mice (Zabel et al. 2007; Michel et al. 2012), the relative importance of each splice variant remained unknown. CD21 and CD35 exhibit cell-type specific expression, some of which promote prion disease (B cells), and some of which help resolve prion disease (Macrophages). While our SPR data suggests shared SCRs on both proteins can directly bind prions (Figure 3.1), we propose CD21-expressing cell types promote prion trafficking and replication more so than CD35-expressing cell types because CD21 deficient mice contained less prion burden in spleen at 30dpi and resist the onset of terminal disease (Figure 3.3 and 3.4). Further, soluble CD21 may serve as a prion disease therapeutic (Figure 3.5), likely by preventing the prion:PrP^C interaction. Future directions include translating these findings *in vivo*.

REFERENCES

Barrington RA, Schneider TJ, Pitcher LA, Mempel TR, Ma M, Barteneva NS, Carroll MC. Uncoupling CD21 and CD19 of the B-cell coreceptor. *Proc Natl Acad Sci U S A*. 2009 Aug 25;106(34):14490-5. doi: 10.1073/pnas.0903477106. Epub 2009 Aug 12. PubMed PMID: 19706534; PubMed Central PMCID: PMC2732852.

Beringue V, Demoy M, Lasmézas CI, Gouritin B, Weingarten C, Deslys JP, Andreux JP, Couvreur P, Dormont D. Role of spleen macrophages in the clearance of scrapie agent early in pathogenesis. *J Pathol*. 2000 Mar;190(4):495-502. PubMed PMID: 10700001.

Büeler H, Aguzzi A, Sailer A, Greiner RA, Autenried P, Aguet M, Weissmann C. Mice devoid of PrP are resistant to scrapie. *Cell*. 1993 Jul 2;73(7):1339-47. PubMed PMID: 8100741.

Changelian PS, Jack RM, Collins LA, Fearon DT. PMA induces the ligand-independent internalization of CR1 on human neutrophils. *J Immunol*. 1985 Mar;134(3):1851-8. PubMed PMID: 3155775.

Cherukuri A, Cheng PC, Pierce SK. The role of the CD19/CD21 complex in B cell processing and presentation of complement-tagged antigens. *J Immunol*. 2001 Jul 1;167(1):163-72. PubMed PMID: 11418645.

Cunnion KM, Benjamin DK Jr, Hester CG, Frank MM. Role of complement receptors 1 and 2 (CD35 and CD21), C3, C4, and C5 in survival by mice of *Staphylococcus aureus* bacteremia. *J Lab Clin Med*. 2004 Jun;143(6):358-65. PubMed PMID: 15192652.

Del Nagro CJ, Kolla RV, Rickert RC. A critical role for complement C3d and the B cell coreceptor (CD19/CD21) complex in the initiation of inflammatory arthritis. *J Immunol*. 2005 Oct 15;175(8):5379-89. PubMed PMID: 16210644.

Donius LR, Handy JM, Weis JJ, Weis JH. Optimal germinal center B cell activation and T-dependent antibody responses require expression of the mouse complement receptor Cr1. *J Immunol*. 2013 Jul 1;191(1):434-47. doi: 10.4049/jimmunol.1203176. Epub 2013 Jun 3. PubMed PMID: 23733878; PubMed Central PMCID: PMC3707406.

Donius LR, Orlando CM, Weis JJ, Weis JH. Generation of a novel Cr2 gene allele by homologous recombination that abrogates production of Cr2 but is sufficient for expression of Cr1. *Immunobiology*. 2014 Jan;219(1):53-63. doi: 10.1016/j.imbio.2013.08.003. Epub 2013 Aug 21. PubMed PMID: 24012440; PubMed Central PMCID: PMC4133946.

Fingerroth JD, Heath ME, Ambrosino DM. Proliferation of resting B cells is modulated by CR2 and CR1. *Immunol Lett*. 1989 Jun 15;21(4):291-301. PubMed PMID: 2527816.

Haas KM, Hasegawa M, Steeber DA, Poe JC, Zabel MD, Bock CB, Karp DR, Briles DE, Weis JH, Tedder TF. Complement receptors CD21/35 link innate and protective immunity during *Streptococcus pneumoniae* infection by regulating IgG3 antibody responses. *Immunity*. 2002 Dec;17(6):713-23. PubMed PMID: 12479818.

Hannan JP. The Structure-Function Relationships of Complement Receptor Type 2 (CR2; CD21). *Curr Protein Pept Sci*. 2016;17(5):463-87. Review. PubMed PMID: 26916158.

Hasegawa M, Fujimoto M, Poe JC, Steeber DA, Tedder TF. CD19 can regulate B lymphocyte signal transduction independent of complement activation. *J Immunol*. 2001 Sep 15;167(6):3190-200. PubMed PMID: 11544305.

Johnson TE, Michel BA, Meyerett C, Duffy A, Avery A, Dow S, Zabel MD. Monitoring immune cells trafficking fluorescent prion rods hours after intraperitoneal infection. *J Vis Exp*. 2010 Nov 19;(45). pii: 2349. doi: 10.3791/2349. PubMed PMID: 21113122; PubMed Central PMCID: PMC3159585.

Klein MA, Frigg R, Raeber AJ, Flechsig E, Hegyi I, Zinkernagel RM, Weissmann C, Aguzzi A. PrP expression in B lymphocytes is not required for prion neuroinvasion. *Nat Med*. 1998 Dec;4(12):1429-33. PubMed PMID: 9846583.

Kovacs JM, Hannan JP, Eisenmesser EZ, Holers VM. Biophysical investigations of complement receptor 2 (CD21 and CR2)-ligand interactions reveal amino acid contacts unique to each receptor-ligand pair. *J Biol Chem*. 2010 Aug 27;285(35):27251-8. doi: 10.1074/jbc.M110.106617. Epub 2010 Jun 17. PubMed PMID: 20558730; PubMed Central PMCID: PMC2930724.

Kulik L, Chen K, Huber BT, Holers VM. Human complement receptor type 2 (CR2/CD21) transgenic mice provide an in vivo model to study immunoregulatory effects of receptor antagonists. *Mol Immunol*. 2011 Mar;48(6-7):883-94. doi: 10.1016/j.molimm.2010.12.019. Epub 2011 Jan 26. PubMed PMID: 21269698.

Kurtz CB, O'Toole E, Christensen SM, Weis JH. The murine complement receptor gene family. IV. Alternative splicing of Cr2 gene transcripts predicts two distinct gene products that share homologous domains with both human CR2 and CR1. *J Immunol*. 1990 May 1;144(9):3581-91. PubMed PMID: 2139460.

Mabbott NA, Bruce ME, Botto M, Walport MJ, Pepys MB. Temporary depletion of complement component C3 or genetic deficiency of C1q significantly delays onset of scrapie. *Nat Med*. 2001 Apr;7(4):485-7. PubMed PMID: 11283677.

Michel B, Ferguson A, Johnson T, Bender H, Meyerett-Reid C, Pulford B, von Teichman A, Seelig D, Weis JH, Telling GC, Aguzzi A, Zabel MD. Genetic depletion of complement receptors CD21/35 prevents terminal prion disease in a mouse model of chronic wasting disease. *J Immunol*. 2012 Nov 1;189(9):4520-7. doi:

10.4049/jimmunol.1201579. Epub 2012 Sep 21. PubMed PMID: 23002439; PubMed Central PMCID: PMC3478448.

Michel B, Ferguson A, Johnson T, Bender H, Meyerett-Reid C, Wyckoff AC, Pulford B, Telling GC, Zabel MD. Complement protein C3 exacerbates prion disease in a mouse model of chronic wasting disease. *Int Immunol*. 2013 Dec;25(12):697-702. doi: 10.1093/intimm/dxt034. Epub 2013 Sep 13. PubMed PMID: 24038599; PubMed Central PMCID: PMC3900863.

Michel B, Meyerett-Reid C, Johnson T, Ferguson A, Wyckoff C, Pulford B, Bender H, Avery A, Telling G, Dow S, Zabel MD. Incunabular immunological events in prion trafficking. *Sci Rep*. 2012;2:440. doi: 10.1038/srep00440. Epub 2012 Jun 6. PubMed PMID: 22679554; PubMed Central PMCID: PMC3368226.

Molina H, Kinoshita T, Inoue K, Carel JC, Holers VM. A molecular and immunochemical characterization of mouse CR2. Evidence for a single gene model of mouse complement receptors 1 and 2. *J Immunol*. 1990 Nov 1;145(9):2974-83. PubMed PMID: 2145366.

Newman SL, Becker S, Halme J. Phagocytosis by receptors for C3b (CR1), iC3b (CR3), and IgG (Fc) on human peritoneal macrophages. *J Leukoc Biol*. 1985 Aug;38(2):267-78. PubMed PMID: 2993460.

Prusiner SB, Groth D, Serban A, Koehler R, Foster D, Torchia M, Burton D, Yang SL, DeArmond SJ. Ablation of the prion protein (PrP) gene in mice prevents scrapie and facilitates production of anti-PrP antibodies. *Proc Natl Acad Sci U S A*. 1993 Nov 15;90(22):10608-12. PubMed PMID: 7902565; PubMed Central PMCID: PMC47826.

Pulford B, Spraker TR, Wyckoff AC, Meyerett C, Bender H, Ferguson A, Wyatt B, Lockwood K, Powers J, Telling GC, Wild MA, Zabel MD. Detection of PrPCWD in feces from naturally exposed Rocky Mountain elk (*Cervus elaphus nelsoni*) using protein misfolding cyclic amplification. *J Wildl Dis*. 2012 Apr;48(2):425-34. PubMed PMID: 22493117.

Reilly BD, Makrides SC, Ford PJ, Marsh HC Jr, Mold C. Quantitative analysis of C4b dimer binding to distinct sites on the C3b/C4b receptor (CR1). *J Biol Chem*. 1994 Mar 11;269(10):7696-701. PubMed PMID: 8125996.

Safar J, Wang W, Padgett MP, Ceroni M, Piccardo P, Zopf D, Gajdusek DC, Gibbs CJ Jr. Molecular mass, biochemical composition, and physicochemical behavior of the infectious form of the scrapie precursor protein monomer. *Proc Natl Acad Sci U S A*. 1990 Aug;87(16):6373-7. PubMed PMID: 1974720; PubMed Central PMCID: PMC54536.

von Poser-Klein C, Flechsig E, Hoffmann T, Schwarz P, Harms H, Bujdoso R, Aguzzi A, Klein MA. Alteration of B-cell subsets enhances neuroinvasion in mouse scrapie

infection. *J Virol.* 2008 Apr;82(7):3791-5. doi: 10.1128/JVI.02036-07. Epub 2008 Jan 16. PubMed PMID: 18199638; PubMed Central PMCID: PMC2268467.

Zabel MD, Heikenwalder M, Prinz M, Arrighi I, Schwarz P, Kranich J, von Teichman A, Haas KM, Zeller N, Tedder TF, Weis JH, Aguzzi A. Stromal complement receptor CD21/35 facilitates lymphoid prion colonization and pathogenesis. *J Immunol.* 2007 Nov 1;179(9):6144-52. PubMed PMID: 17947689.

CHAPTER 4 – CLASSICAL COMPLEMENT ACTIVATOR C1Q MAY IMPACT PRION DISEASES IN A STRAIN-SPECIFIC MANNER

Summary

As discussed in previous chapters, Complement exacerbates prion disease. Previous reports illustrate C1q, a potent Classical Complement cascade activator, promotes scrapie pathogenesis. However, whether C1q impacts chronic wasting disease (CWD) remains unknown. In a CWD transgenic mouse model, we report mice which express elk PrP^C and lack C1q paradoxically accumulate more prions and succumb to prion disease at a faster rate than C1q-sufficient mice. These findings are in direct opposition to expected outcomes based on previous literature. However, we conclude C1q does directly impact prion disease because we observe a biophysical interaction between C1q and prion amyloid rods enriched from infected brain. Perplexingly, we found C1q to bind multiple strains of prion rods, suggesting C1q does not exert strain selection via simply binding or not. Future directions could include testing whether C1q causes differential Complement opsonization on certain prion strains or whether C1q preferentially binds certain PrP^{Sc} conformers. We conclude C1q impacts prion disease via strain selection mechanisms, although the precise mechanism remains unknown. Further, we propose repeating all experiments presented in this chapter due to a combination of human error and comparing new data to previously generated data. Caveats of this study's experimental design, as well as interpretation limits, are addressed.

Introduction

The Complement cascade involves a proteolytic cascade which functions to help the host clear cellular debris and microorganisms. The three main Complement functions include: opsonize (“tag”) structures for destruction via phagocytes; form the membrane attack complex to promote cell-lysis; and promote humoral immunity. While Complement consists of mostly nonspecific, fast-acting cascades, it plays a crucial role in eliciting a long-term, memory-producing, antibody response. For example, when a mature, naïve B cell encounters its antigen via membrane-bound IgM, simultaneous Complement recognition and CD21 engagement reduces the activation threshold.

While the immune system generally clears the body from foreign invaders and aberrant cells (ie cancer), certain pathogens use the immune system in order cause disease. For example, human immunodeficiency virus (HIV) infects certain cells of the immune system in order to replicate and spread disease. Many prion strains also hijack the normal, physiological function of the immune system in order to spread and propagate. Various Complement proteins and receptors promote prion disease because transgenic mice lacking C3, C1q, or CD21/35 exhibit delayed or entire prevention of prion disease (Mabbott et al. 2001; Michel et al. 2013; Michel et al. 2012).

The C1q complex consists of 18 polypeptides arising from 3 subunits: C1qa, C1qb, and C1qc. Each subunit is encoded from a separate gene on chromosome 1, and six peptides of each subunit come together to form the 400 kD C1q complex. Each peptide contains collagen-like stalk near the N-terminus and a globular C-terminal domain. Bally

et al. (2013) likens the C1q complex to a bouquet of flowers. The collagen stalk domains associate to form the stem bundle, and the globular domains extend outward like the flowers. C1q recognizes IgM or dimeric IgG bound to pathogen using the globular domains.

C1q is both a pattern recognition receptor (Jiang et al. 2015) and a potent classical Complement cascade activator. C1q recognizes immune complexes and stimulates the classical Complement pathway. C1q bound to immunoglobulin recruits calcium-dependent C1s and C1r tetramer. This 790,000 kD multimolecular, complex, termed C1, recruits a series of proteins to form the C3 convertase, C4bC2a. Cleaved C3b joins the convertase to form the C5 convertase. This stimulates the terminal phase to form the membrane attack complex. The downstream effects of C1q recognizing immune complex includes phagocytic cell recruitment, as well as pathogen cell lysis.

Several lines of evidence suggest C1q promotes synapse loss seen in neurodegenerative conditions. Silverman et al. (2016) showed C1q upregulation in wild type mice brain after CNS insult. Interestingly, C1q promotes neuronal loss because C1qa mice were protected against retinal ganglion cell loss and microglia activation. Further, Hong et al. (2016) showed C1q upregulation prior to synapse loss and plaque deposits in transgenic J20 brains which over-express human APP associated with familial Alzheimer's Disease (Mucke et al. 2000). Hong et al. (2016) provide evidence that C1q directly responds to amyloid beta oligomers in early stages of AD. Oligomers led to C1q elevation and subsequent microglia activation in wild type mice, whereas

C1qa knockout mice exhibited less microglia activation and synapse loss after amyloid beta treatment. Therefore, C1q appears to promote neurodegeneration after injury and during disease.

Previous reports highlight a role for C1q in scrapie pathogenesis (Mabbott et al. 2001). Whether C1q impacts other prion diseases such as chronic wasting disease (CWD), bovine spongiform encephalopathy, transmissible mink encephalopathy (TME), etc, remains unknown. Previous reports suggest C1q binds a conformationally modified form of recombinant PrP (Blanquet-Grossard et al. 2005). Therefore, we hypothesize C1q directly binds prions (and other plaque-forming proteins) and promotes initial trafficking, retention, and propagation of prions. Data presented in this chapter aimed to address the role of C1q in CWD. However, a combination of human error and comparisons between different studies limit the interpretation of findings presented in this chapter.

Materials and Methods

Mice. Protocol ID: 09-1580A. All mice were bred and maintained at Lab Animal Resources, accredited by the Association for Assessment and Accreditation of Lab Animal Care International and approved on January 14, 2016 by the Institutional Animal Care and Use Committee at Colorado State University. We bred mice of various *C1q* genotypes to knockout or hemizyosity status. We determined *C1q* and *Prnp* genotype from extracted tail clip DNA (Qiagen 69504) using previously published primers and PCR conditions. Transgenic mice expressing elk PrP^C (Tg5037) were kindly provided by the Telling lab.

Mouse inoculations and clinical sign scoring. Age- and sex- matched mice ($n \geq 5$ per genotype) received 100 μL of 1% (w/v) CWD elk isolate (E2) brain homogenate in the peritoneal cavity. Mice were sacrificed at specific time points or prior terminal prion disease onset. Mice were monitored daily and sacrificed at the onset of terminal disease or specified timepoints. We employed a scoring system to assess the severity of disease, including: tail rigidity (0-2), akinesia (0-4), ataxia (0-4), tremors (0-4), and weight loss (0-2). Mice scored above 10 (total) or with a 4 or above in one category were euthanized via CO_2 inhalation replacing 20% of air per minute to effect.

Tissue collection and analysis. After euthanasia, the following samples were collected and frozen or fixed in 4% formaldehyde in 1X PBS: serum, spleen (half fixed, half frozen), kidneys (one fixed, one frozen), tail clip, and brain (half fixed, half frozen). We assessed the presence of protease-resistant prions (PrP^{RES}) in 10% (w/v) homogenate after proteinase K (Roche) digestion (10 $\mu\text{g}/\text{mL}$ for spleen and 50 $\mu\text{g}/\text{mL}$ for brain) and western blotting using anti-PrP monoclonal antibody BAR224 (Cayman) conjugated to horseradish peroxidase (HRP). Blots were developed using chemiluminescent substrates hydrogen peroxide and luminol for 5 minutes at room temperature and visualized using a GE digital imager and ImageQuant software. Tissues negative for PrP^{RES} on western blots were subjected to serial protein misfolding cyclic amplification (PMCA; Saborio and Soto, 2001). Briefly, PMCA uses 10% normal brain homogenate in PMCA buffer (1X PBS, 1% Triton X-100, 4 mM EDTA and 150 mM NaCl) from PrP^{C} over-expressing transgenic mice, strain Tg5037 (Telling laboratory), as substrate for amplification of previously undetectable prions. Twenty-five microliters of normal brain

homogenate (NBH) and 25 μ L 10% sample homogenate, underwent a 40 second pulse of sonication at ~150 watts, followed by a 30 minute incubation, and repeated for 24 hours (one round). Serial rounds were set up similarly, transferring 25 μ L of the previous round's sample to 25 μ L of fresh NBH. Each biological sample was run in at least technical duplicates, and round-to-positivity was determined by PK digestion and western blotting. Relative PMCA units were assigned as previously described (Pulford et al. 2012).

Prion rod preparation and surface plasmon resonance. Prion rods were enriched from infected brain as previously described (Safar et al. 1990; Michel et al. 2012). Briefly, brains from animals infected with chronic wasting disease (E2), hyper- or drowsy-transmissible spongiform encephalopathies (HY- or DY-TME) were homogenized in 1X PBS to 10% (w/v) concentration. Sucrose (1.2 M) was added to 10 mL of clarified tissue to a final concentration of 165.5 mM, and samples were ultracentrifuged (100,000 x g) for one hour at 4°C. Pellets were resuspended to a final protein concentration of 5.0 mg/mL in 1X TBS containing 2.0% Triton X-100 (TBST) and incubated on ice for 30 minutes. Samples were subjected to another round of ultracentrifugation for 20 minutes at 0°C, washed twice in 1X TBST, and twice with 1X TBS. The pellets were then resuspended in 1X PBS containing 1% sarcosyl and protease inhibitor cocktail (Roche). Vortexed samples were incubated on a heated shaker at 37°C for two hours at 800 rpm. Samples were then gently overlayed on a 0.32 M sucrose in PMCA buffer 1 (PMCA buffer without Triton-X 100) cushion, ultracentrifuged for one hour at 4°C, and supernatants removed. Pellets were resuspended in 2.3 M NaCl, 5% sarcosyl in 1X

PBS, centrifuges at 13,000 x g, washed three times in 50 mM Tris 150 mM NaCl, and were either stored dry or suspended in PBS at -80°C. Presence of PK resistant prion rods were confirmed by western blot.

Highly enriched prion rods were coupled to CM-5 sensor chips outside of the instrument after generating the reference flow cells within the instrument by activating with EDC/NHS and deactivating with ethanolamine three to five times. The chip was then removed from the instrument and the gold chip disassembled from the cassette. The entire surface was activated with 100 µL of EDC/NHS for 12 minutes. A pellet of rods was resuspended in 100 µL of 10 mM sodium acetate pH 5.4, sonicated at 37°C for 40 seconds, and incubated on the gold chip at room temperature for one hour. The chip was then briefly rinsed with 1X PBS, and remaining active groups were deactivated with ethanolamine for 7 minutes. Prior to use in interaction analyses, a startup cycle of 50 mM sodium hydroxide served to remove any nonspecifically bound prion rods from the surface.

All SPR experiments involved recombinant PrP (rPrP) or prion rod enriched from infected brain as the ligand coated to a CM5 Series S sensor chip, and commercially-available C1q (CompTech) as the analyte. C1q was buffer exchanged in Amicon filter devices into 1X Running Buffer (50 mM Tris HCl, 150 mM NaCl, pH 7.42). The rPrP-coated chip was kindly provided by Dr. Hae-Eun Kang in the Telling lab. Briefly, flow cells were first activated with 0.2 M 1-ethyl-3-(3-dimethylaminopropyl) carbodiimide hydrochloride (EDC) and 0.05 M N-hydroxysuccinimide (NHS) for seven minutes at 10

$\mu\text{L}/\text{min}$. Amine coupling recombinant cervid or murine PrP^C in 10 mM sodium acetate pH 5.5 was accomplished by flowing 20 $\mu\text{g}/\text{mL}$ of ligand over the activated chip for seven minutes at 10 $\mu\text{L}/\text{min}$. Excess activated groups were deactivated with 1 M ethanolamine HCl pH 8.5 for seven minutes at 10 $\mu\text{L}/\text{min}$. Reference flow cells, built-in negative controls for this system, underwent rounds of activation and deactivation without the addition of protein ligand.

Cell culture prion infection. N2a mouse neuroblastoma or rabbit kidney epithelial cells stably transfected with murine or elk *Prnp*-encoding plasmids were grown in RPMI medium containing 10% fetal bovine serum and 1% penicillin/streptomycin. RML5 or E2 infected brain homogenate was UV-sterilized prior to infecting cells. Infected brain homogenate was pre-incubated with PBS or C1q (5 $\mu\text{g}/\text{mL}$ final) for at least 15 minutes prior to infecting cells. Cells were seeded at 100,000 cells per well in a 12 well plate and infected with 0.3% brain homogenates containing equal volume glycerol or C1q. Cells were grown at 37°C and 5% CO₂ for 4 days. Wells were rinsed 2X in 1X PBS, and cells were detached from the plate using 5 mM EDTA in 1X PBS for 10 minutes. Cell pellets were resuspended in 100 μL PMCA buffer containing 1% Triton X-100 and lysed on ice for 30 minutes. Lysates were assessed for PrP^{RES} using traditional PK digestion and western blotting techniques.

Statistical analyses. All statistical analyses were performed using GraphPad Prism software. One- or two- way ANOVAs were run to compare genotype, sex, or the interaction between these two variables. P-values < 0.05 were considered significantly

different. In the terminal disease study, we observed one male outlier and subsequently removed this data point. Technical duplicates were averaged, and the mean value of each biological replicate was considered an n of 1.

Results

C1q directly interacts with prion amyloid. Previous reports indicate C1q binds conformationally-modified recombinant PrP. Specifically, C1q interacts with PrP, but only when coated at a high density (Mitchell et al. 2007). We followed up this finding and showed that C1q preferentially bound coated PrP, whereas coated C1q minimally bound soluble PrP analyte (data not shown; previously published by others). We and Mitchell et al. (2007) conclude recombinant PrP on a Biacore sensor chip mimics aggregated PrP, and C1q only binds aggregated PrP. To test this hypothesis, we coated prion rods enriched from prion-infected hamster and elk brain and assayed for binding with C1q as an analyte (Figure 4.1). We report C1q binding hyper (HY) and drowsy (DY) transmissible mink encephalopathy (TME, Figure 4.1A), as well as elk chronic wasting disease (CWD) prion amyloid (Figure 4.1B).

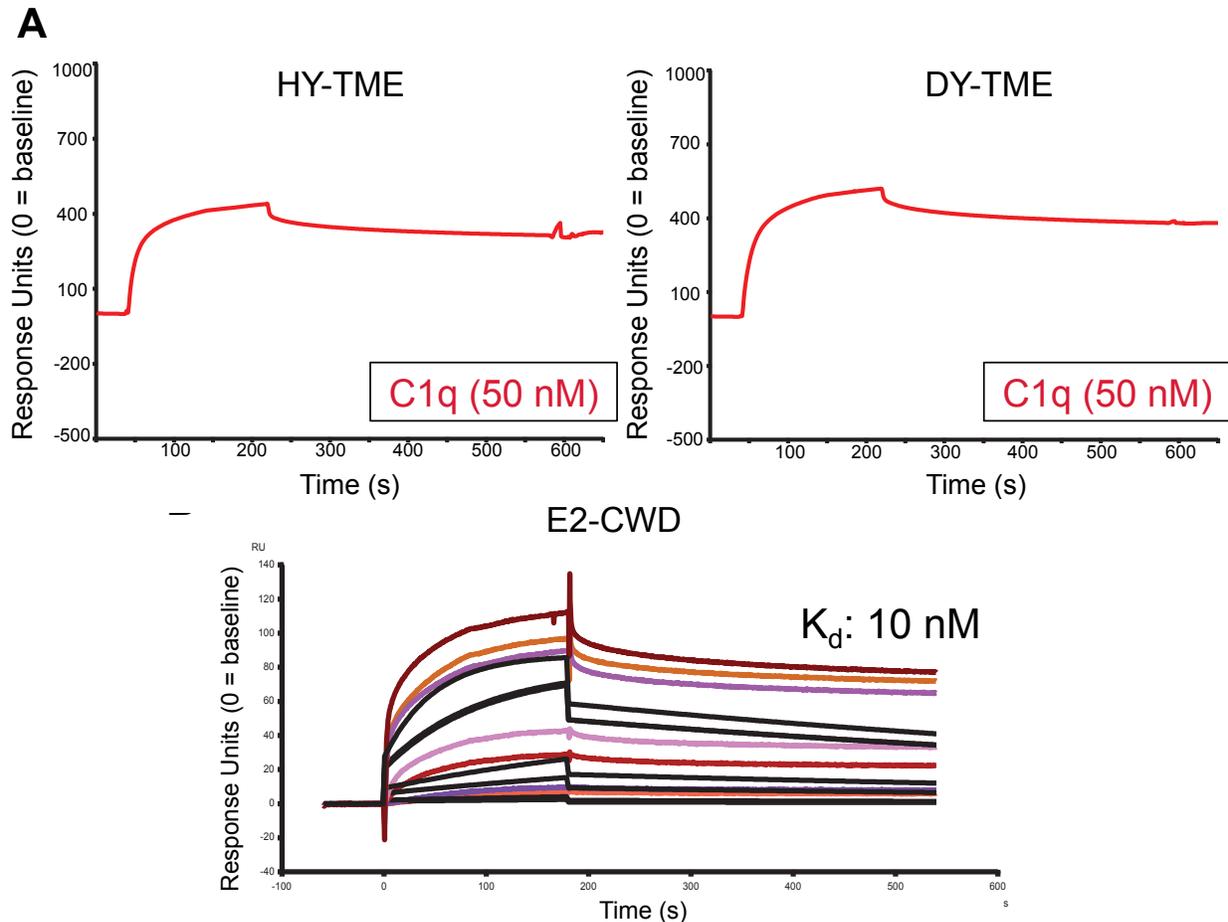


Figure 4.1. C1q directly interacts with prion amyloid. Prion amyloid was enriched from infected brain homogenate as previously described (Safar et al. 1990) and manually coupled to a CM5 series S sensor chip. Surface plasmon resonance (SPR) analyses reveal that Complement component C1q binds prion amyloid. Concentrations of C1q for affinity analyses (bottom) included: 0, 1, 2, 10, 20, 100, and 200 nM.

C1q paradoxically impedes CWD lymphotropism in transgenic mice. Previous reports highlight a crucial role for C1q in scrapie pathogenesis because C1q knockout mice resisted prion accumulation and clinical prion disease onset (Mabbott et al. 2001). However, the role C1q plays in CWD pathogenesis remained unknown. To test whether C1q impacts early events in CWD pathogenesis, ie lymphotropism, we inoculated Tg5037;C1q^{-/-} mice with E2 prions and analyzed prion loads at various time points using PMCA. In contrast to previous reports on the role of C1q in scrapie, C1q knockout

mice paradoxically accumulated more prions at early time points than C1q sufficient Tg5037 mice. However, this experiment contains a number of confounding variables, including: C1q^{+/+} data was obtained from previous experiments and performed by different researchers (Michel et al. 2012); C1q^{-/-} mice were generated on a 129 mixed background, whereas Tg5037 mice from Michel et al. (2012) were generated on an FVB background; and lastly, the researcher who collected the samples from this experiment mislabeled tubes which suggested the same mouse was taken at different time points.

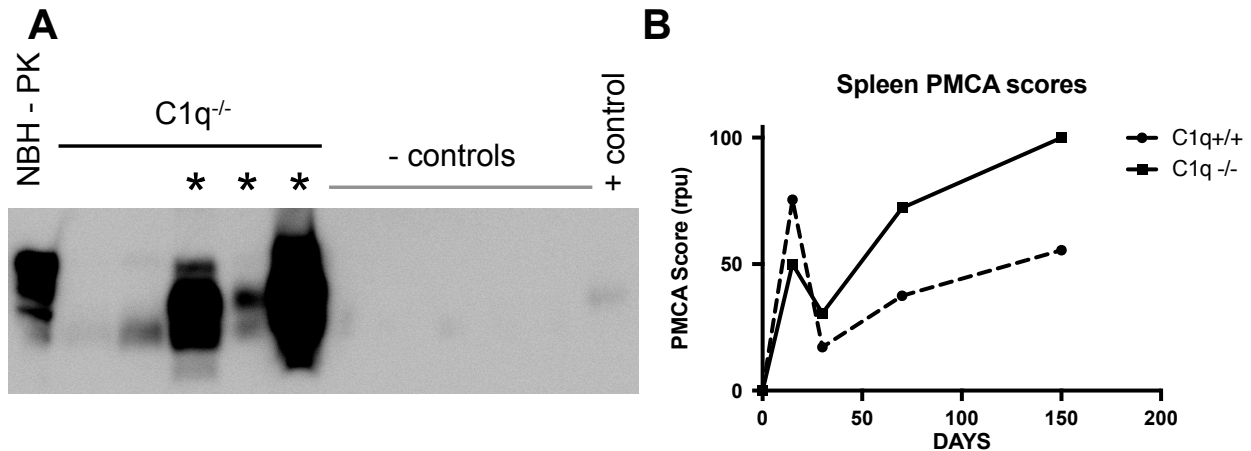


Figure 4.2. C1q paradoxically limits CWD splenic accumulation, yet promotes RML accumulation. C1q knockout (C1q^{-/-}, solid line) mice received E2 CWD prions, were sacrificed at various time points, and prion loads were analyzed via PMCA (A). Comparing C1q^{-/-} relative PMCA units (rpu) scores versus Tg5037 (dashed line) scores from Michel et al. (2012) reveal C1q knockout mice contained higher prion loads than Tg5037 mice by 30dpi. However, criticisms to this experiment include: no Tg5037 mice inoculated at the same time as C1q^{-/-} mice; different mouse background strains; and mislabeling tubes suggesting the same mouse was taken at different time points.

An attempt to control for caveats in Figure 4.2. As mentioned in Figure 4.2, early prion accumulation in spleen data were perplexing. We predicted CWD prions would, similarly to RML prions (Mabbott et al. 2001), utilize C1q to spread and propagate in spleen. However, when compared to historical controls (Michel et al. 2012), we did not observe

this trend. This could be due to: inoculating animals on different days; different mouse background strains; or human error. In attempt to control for the aforementioned caveats, we pre-treated E2 inoculum with 11 μ g purified C1q and compared splenic prion load at 30dpi. If C1q indeed limits CWD accumulation, we would expect C1q pre-treatment to reduce prion load in comparison to controls. Although not statistically significant, we observed the opposite trend. C1q pre-treatment slightly enhanced splenic PMCA scores (Figure 4.3B).

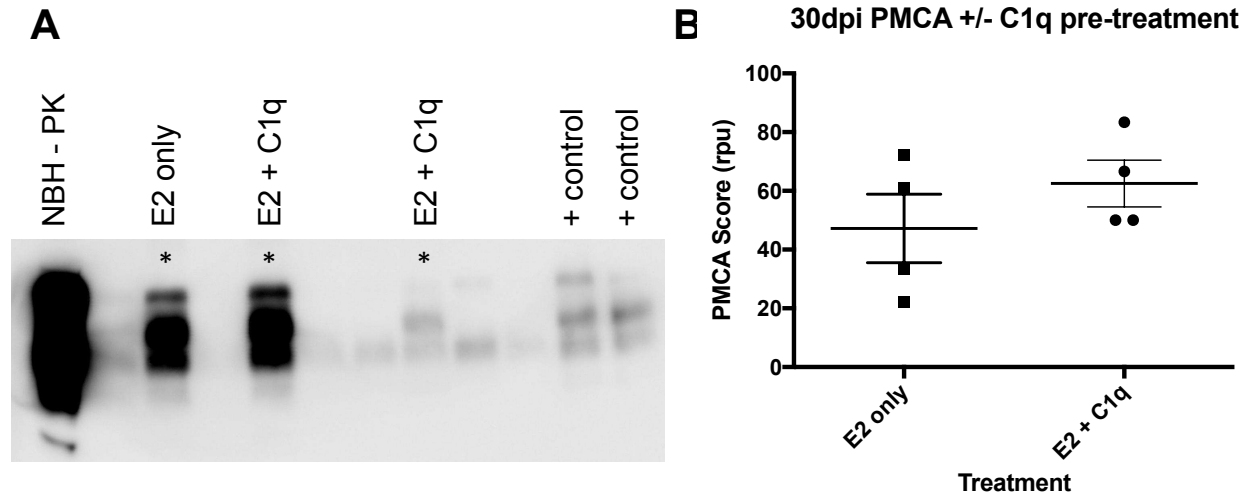


Figure 4.3. C1q slightly enhances splenic CWD accumulation and early propagation in Tg5037;C1q^{+/+} mice. To compare the effect of C1q pre-treatment in mice of the same background strain that were inoculated on the same day, E2 inoculum was pre-treated with 11 μ g C1q per mouse. Mice were sacrificed at 30dpi, and prion loads in spleen were analyzed via PMCA (A). In contrast to Figure 4.2, C1q appeared to promote CWD accumulation, although this effect was not statistically significant.

Cell culture systems may not parse out CWD vs RML reliance on C1q. In order to determine whether the discrepancy between Figure 4.2 and Mabbott et al. (2001) could be confirmed in cell culture systems, we infected rabbit kidney (RK) epithelial cells stably transfected with mouse or elk *Prnp*-expression plasmids. While we confirmed

C1q exacerbates RML5 prion replication in N2a mouse neuroblastoma cells (Figure 4.4C,D), we did not observe a difference in murine RK cells (data not shown). One experimental replicate showed C1q slightly reduced prion burden in elk PrP^C-expressing RK cells. However, this finding was not repeatable (data not shown). Therefore, we cannot conclude the effect of C1q in prion propagation *in vitro*.

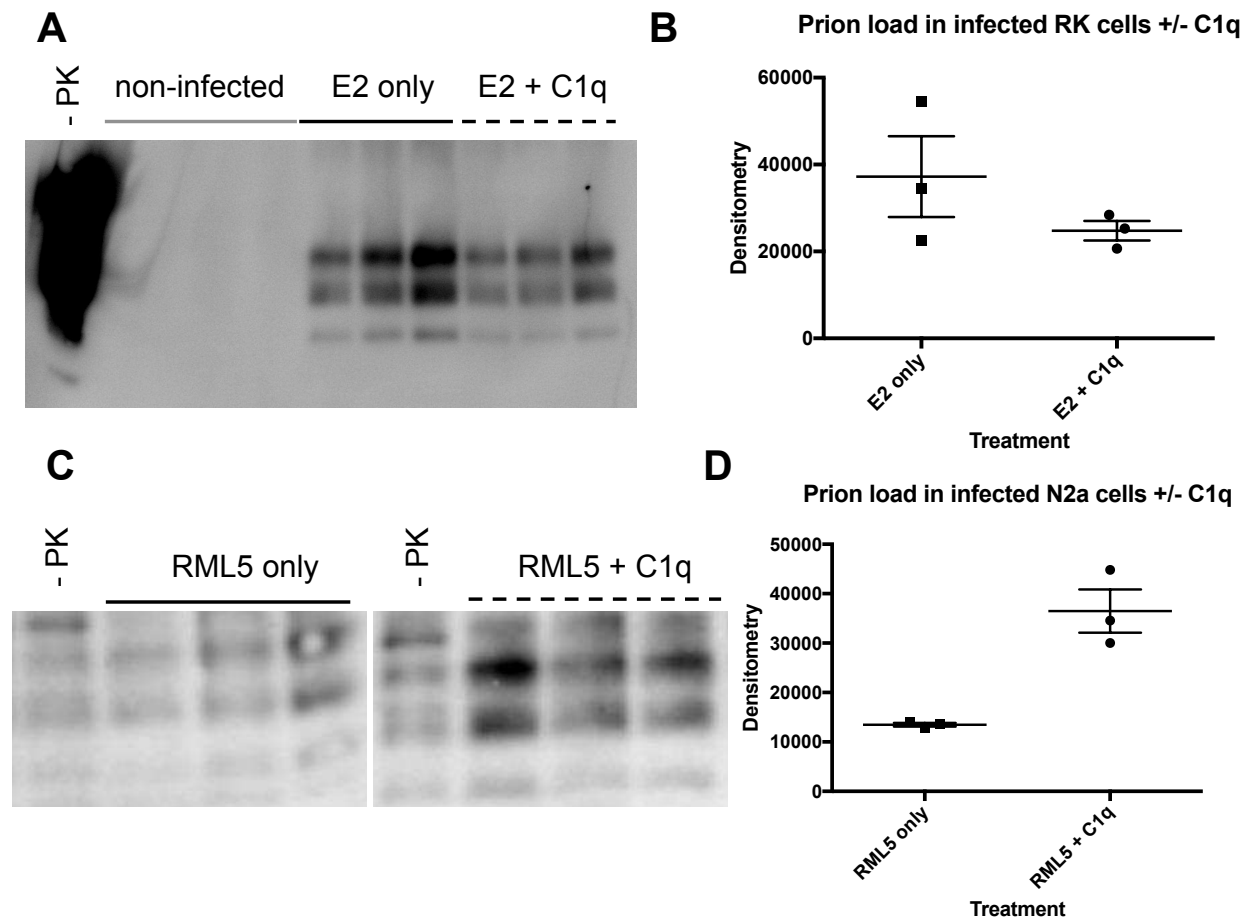


Figure 4.4. *In vitro* prion infection assays +/- C1q pre-treatment. Rabbit kidney (RK) cells stably transfected with elk *Prnp* expression plasmid were infected with E2 +/- 5 µg/mL C1q and analyzed for PK-resistant material via western blotting (A,B). Murine N2a cells were infected with RML5 +/- 5 µg/mL C1q and analyzed for PK-resistant material (C,D). While these non-representative images support *in vivo* findings on the role of C1q in CWD vs RML5, the results were not repeatable nor translatable to other cell lines.

C1q impedes the onset to clinical disease in a CWD transgenic model. To determine whether C1q status dictates the time to clinical disease onset, we inoculated C1q knockout and hemizygous (C1q^{+/-}) mice and monitored signs of clinical disease. We used historical Tg5037 controls (Michel et al. 2012) as discussed above. C1q knockout and hemizygous mice succumbed to prion disease at a significantly faster rate than historical Tg5037 controls (Figure 4.5). Further, C1q knockout mice appeared to contain increased prion amyloid deposition in cerebellum and cortex at terminal disease (Figure 4.5C). However, this experiment contains the same aforementioned confounding variables.

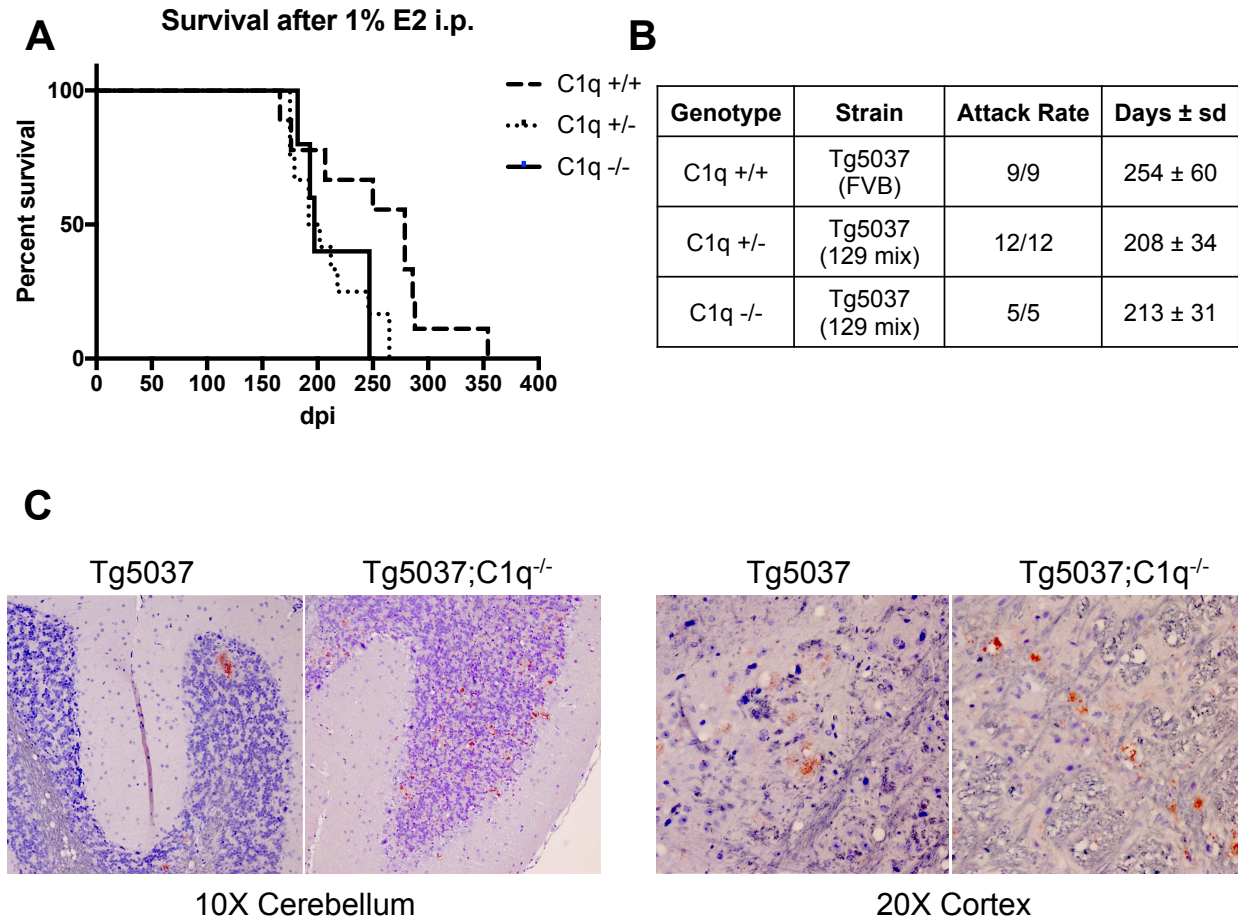


Figure 4.5. C1q delays the onset of terminal CWD in a transgenic mouse model. Time to clinical disease was assessed using a gene-dose transgenic mouse model and compared to historical controls. In alignment with early prion accumulation (Figure 4.2), C1q deficient mice succumbed to prion disease at a faster rate than C1q sufficient controls (A,B). Further, C1q^{-/-} mice contained greater numbers of prion amyloid as seen via immunohistochemistry (C). However, the limitations to this study are similar to those mentioned in previous figures.

Discussion

Previous reports highlight a role for C1q in scrapie pathogenesis (Mabbott et al. 2001). However, whether C1q directly or indirectly impacts lymphotropism and/or neuropathological manifestations remains unclear. For example, perhaps C1q aids in prion opsonization and thus retention on CD21- and PrP^C- expressing follicular dendritic

and B cells. Perhaps this retention increases the probability of contact between infectious prions and PrP^C. However, as discussed in Chapter 3, prion opsonization could lead to increase phagocytosis and destruction by macrophages. The interplay between prions and the Complement system likely involves a delicate balance between both outcomes.

We report C1q directly binds prion amyloid derived from CWD and TME infected elk and hamster brain, respectively. We hypothesize C1q promotes prion trafficking, retention, and propagation in the lymphoreticular system prior to neuroinvasion. Interestingly, we report C1q interacts with both lymphotropic (HY-TME and CWD) and non-lymphotropic (DY-TME) prion strains. Thus, we do not believe C1q dictates whether prion strains are lymphotropic. In fact, these data are quite perplexing because previous reports suggest C1q promotes lymphotropism. Perhaps C1q exerts its effects on prion propagation outside of the lymphoreticular system.

The Complement system plays a larger role in the central nervous system than previously thought. Complement proteins C1q and C3 aid in synapse pruning during development (Stevens et al. 2007), and aberrant Complement-mediated synaptic pruning perhaps contributes to schizophrenia, autism, and early stages of neurodegeneration (Sekar et al. 2016). Further, Complement proteins are detected after brain injury (Bellander et al. 2000), and likely function to clear damaged tissue. Thus, Complement promotes normal physiology during development and in response to injury. However, the Complement system also leads to inflammation, and neuroinflammation is

thought to cause the ultimate death of prion-infected animals. Thus, ensuring the balance of normal physiology, yet preventing over-activation, may prove beneficial in the outcome of neurodegenerative diseases.

Perhaps the enclosed findings are reproducible. If so, C1q poses opposite effects depending on prion strain. If this is indeed the case, perhaps C1q differentially binds scrapie prions. Future directions could involve enriching scrapie prion rods and assessing for interactions via SPR similarly to Figure 4.1. If C1q differentially binds scrapie prions, this could dictate downstream effects. Perhaps C1q binds scrapie prions with higher affinity than CWD prions. If so, C1q could more robustly activate the Complement cascade and thus promote neuroinflammation and ultimate death. This could explain why C1q knockout mice resist scrapie infection. However, future experiments are required to address this hypothesis.

In summary, data presented in this chapter suggest C1q may impact CWD outcomes, yet confounding variables limit the interpretation of presented data. For example, *in vitro* experiments outlined in this chapter were not reproducible between researchers.

Perhaps increasing technical replicates and/or titrating the concentration of C1q needed to observe a statistical difference are necessary. Further, *in vivo* experiments compared data generated from two researchers (myself and an undergraduate) to data generated from a former graduate student (Michel et al. 2012). We propose these findings need to be repeated with the proper controls.

REFERENCES

Bally I, Ancelet S, Moriscot C, Gonnet F, Mantovani A, Daniel R, Schoehn G, Arlaud GJ, Thielens NM. Expression of recombinant human complement C1q allows identification of the C1r/C1s-binding sites. *Proc Natl Acad Sci U S A*. 2013 May 21;110(21):8650-5. doi: 10.1073/pnas.1304894110. Epub 2013 May 6. PubMed PMID: 23650384; PubMed Central PMCID: PMC3666734.

Bellander BM, Singhrao SK, Ohlsson M, Mattsson P, Svensson M. Complement activation in the human brain after traumatic head injury. *J Neurotrauma*. 2001 Dec;18(12):1295-311. PubMed PMID: 11780861.

Blanquet-Grossard F, Thielens NM, Vendrely C, Jamin M, Arlaud GJ. Complement protein C1q recognizes a conformationally modified form of the prion protein. *Biochemistry*. 2005 Mar 22;44(11):4349-56. PubMed PMID: 15766264.

Hong S, Beja-Glasser VF, Nfonoyim BM, Frouin A, Li S, Ramakrishnan S, Merry KM, Shi Q, Rosenthal A, Barres BA, Lemere CA, Selkoe DJ, Stevens B. Complement and microglia mediate early synapse loss in Alzheimer mouse models. *Science*. 2016 May 6;352(6286):712-716. doi: 10.1126/science.aad8373. Epub 2016 Mar 31. PubMed PMID: 27033548; PubMed Central PMCID: PMC5094372.

Jiang S, Li H, Zhang D, Zhang H, Wang L, Sun J, Song L. A C1q domain containing protein from *Crassostrea gigas* serves as pattern recognition receptor and opsonin with high binding affinity to LPS. *Fish Shellfish Immunol*. 2015 Aug;45(2):583-91. doi: 10.1016/j.fsi.2015.05.021. Epub 2015 May 19. PubMed PMID: 26002640.

Mabbott NA, Bruce ME, Botto M, Walport MJ, Pepys MB. Temporary depletion of complement component C3 or genetic deficiency of C1q significantly delays onset of scrapie. *Nat Med*. 2001 Apr;7(4):485-7. PubMed PMID: 11283677.

Michel B, Ferguson A, Johnson T, Bender H, Meyerett-Reid C, Pulford B, von Teichman A, Seelig D, Weis JH, Telling GC, Aguzzi A, Zabel MD. Genetic depletion of complement receptors CD21/35 prevents terminal prion disease in a mouse model of chronic wasting disease. *J Immunol*. 2012 Nov 1;189(9):4520-7. doi: 10.4049/jimmunol.1201579. Epub 2012 Sep 21. PubMed PMID: 23002439; PubMed Central PMCID: PMC3478448.

Michel B, Ferguson A, Johnson T, Bender H, Meyerett-Reid C, Wyckoff AC, Pulford B, Telling GC, Zabel MD. Complement protein C3 exacerbates prion disease in a mouse model of chronic wasting disease. *Int Immunol*. 2013 Dec;25(12):697-702. doi: 10.1093/intimm/dxt034. Epub 2013 Sep 13. PubMed PMID: 24038599; PubMed Central PMCID: PMC3900863.

Mitchell DA, Kirby L, Paulin SM, Villiers CL, Sim RB. Prion protein activates and fixes complement directly via the classical pathway: implications for the mechanism of scrapie agent propagation in lymphoid tissue. *Mol Immunol*. 2007 Apr;44(11):2997-3004. Epub 2007 Mar 6. PubMed PMID: 17337056.

Mucke L, Masliah E, Yu GQ, Mallory M, Rockenstein EM, Tatsuno G, Hu K, Kholodenko D, Johnson-Wood K, McConlogue L. High-level neuronal expression of abeta 1-42 in wild-type human amyloid protein precursor transgenic mice: synaptotoxicity without plaque formation. *J Neurosci*. 2000 Jun 1;20(11):4050-8. PubMed PMID: 10818140.

Pulford B, Spraker TR, Wyckoff AC, Meyerett C, Bender H, Ferguson A, Wyatt B, Lockwood K, Powers J, Telling GC, Wild MA, Zabel MD. Detection of PrPCWD in feces from naturally exposed Rocky Mountain elk (*Cervus elaphus nelsoni*) using protein misfolding cyclic amplification. *J Wildl Dis*. 2012 Apr;48(2):425-34. PubMed PMID: 22493117.

Saborio GP, Permanne B, Soto C. Sensitive detection of pathological prion protein by cyclic amplification of protein misfolding. *Nature*. 2001 Jun 14;411(6839):810-3. PubMed PMID: 11459061.

Safar J, Wang W, Padgett MP, Ceroni M, Piccardo P, Zopf D, Gajdusek DC, Gibbs CJ Jr. Molecular mass, biochemical composition, and physicochemical behavior of the infectious form of the scrapie precursor protein monomer. *Proc Natl Acad Sci U S A*. 1990 Aug;87(16):6373-7. PubMed PMID: 1974720; PubMed Central PMCID: PMC54536.

Sekar A, Bialas AR, de Rivera H, Davis A, Hammond TR, Kamitaki N, Tooley K, Presumey J, Baum M, Van Doren V, Genovese G, Rose SA, Handsaker RE; Schizophrenia Working Group of the Psychiatric Genomics Consortium., Daly MJ, Carroll MC, Stevens B, McCarroll SA. Schizophrenia risk from complex variation of complement component 4. *Nature*. 2016 Feb 11;530(7589):177-83. doi: 10.1038/nature16549. Epub 2016 Jan 27. PubMed PMID: 26814963; PubMed Central PMCID: PMC4752392.

Silverman SM, Kim BJ, Howell GR, Miller J, John SW, Wordinger RJ, Clark AF. C1q propagates microglial activation and neurodegeneration in the visual axis following retinal ischemia/reperfusion injury. *Mol Neurodegener*. 2016 Mar 24;11:24. doi: 10.1186/s13024-016-0089-0. PubMed PMID: 27008854; PubMed Central PMCID: PMC4806521.

Stevens B, Allen NJ, Vazquez LE, Howell GR, Christopherson KS, Nouri N, Micheva KD, Mehalow AK, Huberman AD, Stafford B, Sher A, Litke AM, Lambris JD, Smith SJ, John SW, Barres BA. The classical complement cascade mediates CNS synapse elimination. *Cell*. 2007 Dec 14;131(6):1164-78. PubMed PMID: 18083105.

CHAPTER 5 – PrP^C, LIKELY IN COOPERATION WITH CD21/35, PROMOTES HUMORAL IMMUNITY

Summary

Prion diseases require host expression of the cellular prion protein, PrP^C. However, the precise function of PrP^C remains elusive. Putative functions involving PrP^C include: synaptic signaling in the hippocampus, cell adhesion, and T cell proliferation. PrP^C signals via Src family kinase member, Fyn, and B cells activate via similar signaling molecules. PrP^C expression is largely limited to cells of the immune and nervous systems, leading us to question whether PrP^C provides a co-stimulatory signal to stimulate immune responses. We aimed to address three main questions: is PrP^C regulated during an immune response? Are *Prnp* knockout mice immunocompromised? Does PrP^C interact and signal with B cell co-receptor members? Upon stimulation with various immunological stimuli, cell-surface levels of PrP^C reduce. However, whether this response promotes PrP^C degradation, or perhaps intracellular signaling, remains unknown. We report no impairments of total B or T cell proportions in *Prnp* knockout (PrP KO) mice, although PrP KO mice exhibit impaired immune responses. *In vitro* analyses reveal malfunctions in key signaling molecules downstream of B cell receptor engagement, as well as altered B cell receptor protein expression in PrP^C deficient mice. PrP KO mice also reveal humoral impairments when vaccinated and challenged with *Escherichia coli*. Further, we report a direct interaction and co-localization between PrP^C and B cell co-receptor member CD21. CD21 on B cells translocates to lipid rafts after engagement with complement-tagged antigens and reduces the activation

threshold. Altogether, data presented in this chapter reveal a pivotal role for PrP^C in B cell activation signaling. Future directions include assessing the role of PrP^C in the response to intracellular or gram positive pathogens, as well as testing whether PrP^C aggregation could serve an immunological signal similarly to mitochondrial antiviral-signaling (MAVS) protein.

Introduction

Mature, naïve B lymphocytes express surface immunoglobulin and various co-receptor proteins which coalesce in lipid rafts upon B cell receptor (BCR) engagement. When the BCR recognizes its specific antigen, subsequent events lead to B cell activation and antibody secretion, culminating in humoral immunity and host protection. However, prior to antibody production and secretion, several cell biological events must occur to activate a B cell. Upon antigen recognition, BCR and co-receptor proteins translocate into lipid rafts (Cherukuri et al. 2004; Sohn et al. 2008). Upon lipid raft coalescence, Src family tyrosine kinases phosphorylate Ig α and Ig β cytoplasmic tails, leading to PLC γ 2 activation and calcium mobilization. These event precede antibody production and thus provide opportunities to monitor early events of B cell activation.

The cellular prion protein, PrP^C, is a 35 kD (human) glycoprotein permanently anchored to through GPI attachment to lipids which accumulate in cholesterol-rich membrane domains termed “lipid rafts.” PrP^C consists of an unstructured N-terminal domain and contains heavy metal-binding octapeptide repeats. The C-terminal, structured domain becomes anchored to the plasma membrane after glycosylphosphatidylinositol (GPI)

addition. While previous research primarily focused on its requisite in prion diseases, the precise physiological function of PrP^C remains elusive because *Prnp*^{-/-} transgenic (PrP KO) mice appear to develop normally (Prusiner et al. 1993). However, work from the Strittmatter group reports synaptic signaling via the metabotropic glutamate receptor involves PrP^C (Haas et al. 2016). Further, PrP^C promotes neurite outgrowth via interactions with neural cell adhesion molecule (NCAM) and Fyn kinase (Santuccione et al. 2005).

Most previous research on the role of PrP^C in the immune system suggests a role in T cell proliferation and/or the immunological synapse between antigen presenting cells (APCs) and T cells. Specifically, Mabbott et al (1997) showed primary mouse lymphocyte proliferation in response to Con-A partially depended on PrP^C because anti-PrP antibodies abrogated proliferation. However, antibody treatment could potentially disrupt cell:cell interactions necessary for stimulation, and a brief literature search revealed rebuttals and debates regarding this study. Interestingly, however, PrP^{-/-} dendritic cells (DCs) exhibited impaired PrP^{+/+} T cell stimulation, suggesting PrP^C may exert its effect via APCs at the level of the immunological synapse (Ballerini et al. 2006).

Several lines of evidence suggest PrP^C may play a role in cell stress/immunological responses. For example, Shyu et al. (2002) reported *Prnp* mRNA upregulation in response to heat shock. Further, T cell mitogen PHA caused an upregulation in human T cells, and T cell proliferation in response to anti-CD3 was abrogated by anti-PrP antibody 8H4 (Li et al. 2001). Cashman et al. (1990) also reported cell-activation

increased surface levels of PrP^C, and anti-PrP antibodies suppressed proliferation. Interestingly, Lotscher et al. (2003) also reported increased PrP^C immunodetection in germinal centers and follicular dendritic cell networks after vesicular stomatitis viral infection. Collectively, these results suggest PrP^C participates in immunological events leading to lymphocyte activation.

While both B and T lymphocytes express PrP^C to varying degrees, human CD8+ T cells express slightly higher levels than CD4+ positive T cells (Politopoulou et al. 2000 and Durig et al. 2000). CD8+ T cells help to provide protection against intracellular pathogens such as viruses, whereas CD4+ T cells aid in the protection against extracellular pathogens such as certain bacteria and helminths. Logic therefore serves to suggest PrP^C plays a role in CD8+ cell signaling in response to an intracellular pathogen. However, Genoud et al. (2004) reported no deficiency in CD8+ T cell responses against cytotoxic lymphocytic choriomeningitis virus (LCMV) or vesicular stomatitis virus (VSV) in mice deficient in PrP^C and its homolog Doppel. This was observed by LCMV-specific cytotoxic T lymphocyte numbers in blood, as well as antibody responses after vaccination.

B cells can generate humoral (antibody) responses both dependent and independent of T cell help. Lipopolysaccharide (LPS) is an example of a T-independent antigen due to repeating structures capable of activating B cells even without cognate T cell help. Interestingly, PrP KO mice show increased susceptibility to LPS-induced septic shock (Liu et al. 2014). Furthermore, PrP^C cross-linking induced calcium flux and ERK

phosphorylation in Jurkat T cells (Stuermer et al. 2004). ERK phosphorylation and calcium flux also occur in the process of B cell activation. Lastly, PrP^C was found to co-precipitate with Fyn kinase (Shi et al. 2013), another known member involved in B cell activation downstream of antigen recognition. Collectively, PrP^C appears to augment T cell proliferation, yet T-dependent immunological responses to viral infection do not appear to depend on the expression PrP^C (Genoud et al. 2004). Thus, the role of PrP^C in an adaptive immune response remains unclear. Data provided in this chapter suggest PrP^C promotes events leading to B cell activation and antibody production.

Materials and Methods

Mice. All mice were bred and maintained at Lab Animal Resources, accredited by the Association for Assessment and Accreditation of Lab Animal Care International and approved on January 14, 2016 by the Institutional Animal Care and Use Committee at Colorado State University (Protocol ID: 09-1580A). *Prnp* TALEN knockout mice on the C57/Bl6 background were kindly provided by Dr. Adriano Aguzzi (University Hospital - Zurich). *Prnp* knockout mice on the FVB background were kindly provided by Dr. Glenn Telling (Colorado State University). Blood and sera were collected from tail vein or cardiac punctures. Mice were vaccinated and boosted with weekly injections of 10⁵ heat-killed (HK) *E. coli*.

Tissue collection and analysis. After euthanasia, cardiac punctures and spleens were collected. Blood was allowed to clot at room temperature for 10 minutes, centrifuged at 1,000 x g for 10 minutes at 4°C, and serum was transferred to a fresh tube and frozen.

Spleens were processed to single-cell suspensions, and red blood cells were lysed as discussed below.

In vitro activation. Splenocyte single-cell suspension cell density was determined by Bio-Rad cell counter, and 5×10^6 primary splenocytes were transferred to a separate tube and pelleted. Pellets were resuspended in 100 μ L of RPMI media containing 10 μ g/mL anti-IgM (μ -specific, Invitrogen) or 10 μ g/mL anti-CD40 (FGK45, Enzo Life Sciences) with cross-linking anti-rat secondary and incubated at 37°C for 5 minutes. Cells were pelleted and lysed in 90 μ L ice-cold TNE buffer containing protease inhibitors (Roche, complete mini). Samples were run via western blot and probed for activated, phosphorylated Src (Y416, Cell Signaling 2101) via manufacturer guidelines. Blots were stripped and re-probed for GAPDH, and data was analyzed using ImageJ software and presented as percentage or fold change of GAPDH.

ELISAs. *E. coli*-specific antibody responses were determined by ELISA. Heat-killed (HK) *E. coli* (4×10^6 CFUs) was coated in 100 μ L solution carbonate/bicarbonate buffer (SIGMA) overnight at 4°C. Plates were washed multiple times and blocked in 300 μ L 5% nonfat dry milk (NFD) in PBS containing 0.1% Tween 20 for one hour at room temperature. Sera (n=4 mice/genotype) was pooled prior to dilution. Trial experiments carried out two-fold sera dilutions ranging between 1:25 to 1:3200. Subsequent experiments carried out two-fold dilutions ranging between 1:25 to 1:400. Total IgG and IgG3 specific to HK *E. coli* were determined using HRP-conjugated secondary antibodies. Absorbance values from wells containing no sera were subtracted from all

wells. Thresholds per genotype were determined using pre-vaccination absorbance values. The average pre-vaccination absorbance value obtained from the lowest (1:25) sera dilution was added to the standard deviation multiplied by 3, and any post-vaccination dilution above this value was considered a positive titer. Positive titers were imported into Graphpad Prism for statistical analysis. To compare total serum levels of IgG and IgG3, sera was diluted 1:25 to 1:200 and coated on a microtiter plate in carbonate/bicarbonate buffer and processed as discussed above.

Surface plasmon resonance. All SPR experiments involved recombinant PrP (rPrP) as the ligand coated to a CM5 Series S sensor chip, and CD21 (commercially available or kindly provided by Dr. Johnny Hannan) were buffer exchanged in Amicon filter devices into 1X Running Buffer (50 mM Tris HCl, 150 mM NaCl, pH 7.42). The rPrP-coated chip was kindly provided by Dr. Hae-Eun Kang in the Telling lab. Briefly, flow cells were first activated with 0.2 M 1-ethyl-3-(3-dimethylaminopropyl) carbodiimide hydrochloride (EDC) and 0.05 M N-hydroxysuccinimide (NHS) for seven minutes at 10 μ L/min. Amine coupling recombinant cervid or murine PrP^C in 10 mM sodium acetate pH 5.5 was accomplished by flowing 20 μ g/mL of ligand over the activated chip for seven minutes at 10 μ L/min. Excess activated groups were deactivated with 1 M ethanolamine HCl pH 8.5 for seven minutes at 10 μ L/min. Reference flow cells, built-in negative controls for this system, underwent rounds of activation and deactivation without the addition of protein ligand.

P3 cell culture. P3 myeloma cells were kindly provided by the Telling laboratory. Cells were grown in RPMI media containing 10% FBS and 1% penicillin/streptomycin. For immunocytochemistry, cells were grown on sterile glass coverslips placed in 3 mm culture dishes and were stained for CD21/35 (eFluor450), PrP^C (Alexa Fluor 647), and lipid rafts (cholera toxin conjugated to Alexa Fluor 488). Some cells were treated with mouse complement containing HK E. coli to assess CD21/35 translocation into lipid rafts. However, we observed basal levels of CD21/35 in lipid rafts. Images were collected on an Olympus confocal microscope using 40X and 100X objective lenses.

siRNA treatment. siRNA specific for *Prnp* transcripts were kindly provided by Heather Bender (Pulford et al. 2010). Splenocytes were treated with 40 nmole siRNA in OptiMEM for four hours.

Direct Binding Assay. Recombinant human prion protein (rPrP) was kindly provided by the Hoover laboratory. Wells of a 96 well microtiter plate (Nunc) were coated with 1 µg rPrP or BSA in 100 µL carbonate/bicarbonate (SIGMA) buffer at 4°C overnight. Wells were washed and blocked in 300 µL 2% BSA in PBS. Wells were incubated for 24-48 hours at 4°C with 1 µg CD21 kindly provided by Dr. Johnny Hannan. Samples were probed for CD21 using anti-CD21/35 (Santa Cruz) and anti-goat conjugated to horseradish peroxidase (HRP) secondary antibody. Wells were washed several times prior to incubation with 100 µL tetramethylbenzidine (TMB) at room temperature. Reactions were stopped using 0.5 M H₂SO₄, and O.D.₄₅₀ was measured on a spectrophotometer.

Flow Cytometry (FACS). Fresh brain and spleens were harvested and processed to single-cell suspensions in 3 mL PBS. Briefly, tissues were passed through 40 µm mesh filters using sterile plungers and cold PBS washes. Cells were pelleted at 250 x g for 5 minutes at 4°C, and the supernatant was discarded. Red blood cells (RBCs) were lysed in lysis buffer for 5 minutes, cells were pelleted as previous, and washed in FACS buffer (1X PBS, 1% FBS, and 1 mM EDTA). Primary splenocytes or brain suspensions were blocked in 7% mouse serum and 1:50 F_c block (BD Pharmagin) for 20-60 minutes on ice. Antibody solutions (1:100 final) were added to cells and incubated in the dark for one hour on ice. Cells were washed by adding 1 mL FACS buffer to existing antibody solution. Cells were pelleted, supernatant removed, and resuspended in 1 mL FACS buffer for a total of 3 washes. 792 µL cell suspension was added to 8 µL of Propidium Iodide (SIGMA) immediately prior to data acquisition in a Cyan flow cytometer. Cells were analyzed 500-1500 events per second. Unstained samples were analyzed first in order to set parameters to achieve a well-defined peak in the first fluorescent decade.

Escherichia coli culture. Laboratory strain E. coli was kindly provided by Pete Justice (Colorado State University). Single, well-isolated colonies were inoculated into Luria Broth (LB) and allowed to grow in a shaking water bath for 16-20 hours at 35 – 37°C. Culture titer was determined by plating various dilutions (100 µL) onto LB agar plates and counting colonies >16 hrs after growth at 37°C or through obtaining O.D.₆₀₀ value on spectrophotometer and calculated cell/mL using a Agilent Genomics calculator. For vaccinations and boosts, various concentrations of E. coli were heat-killed at 95°C for 5 minutes at 800 rpm.

Calcium Signaling. Primary splenocyte single-cell suspensions were obtained as described above. Primary splenocytes (5×10^6) were loaded with 2 μ M Fluo-4 at 37°C for 30-45 minutes and washed three times in HBSS with 1 mg/mL BSA (HBSS/A). Baseline fluorescence (FITC) was obtained for one minute. Anti-IgM or anti-CD40 cross-linking antibodies (10X) were added to cells, pipetted to mix 3 times, and recorded for 5 minutes.

Lipid raft floatation. Naïve, non-vaccinated mice were inoculated with E. coli and their spleens harvested. Spleens were passed through 40 μ m mesh filters, and approximately 20 million splenocytes were transferred to a fresh tube. Cells were lysed in ice cold TNE buffer (Michel et al. 2012) and passed through syringe and needle 22 times while on ice. Lipid rafts were isolated using sucrose density gradients (9) and ultracentrifugation at 180,000 x g for 18 hours at 4°C.

FACS analysis in Flow-Jo. Cellular debris was gated off the Y- axis of forward and side scatter plots. PI-positive (dead) cells were also gated off. Fluorochrome-positive gates were set by setting a threshold of 1% in the unstained population. In other words, stained cells were considered positive if their fluorescent intensity was greater than 99% of the unstained population. For calcium signaling experiments, calcium responders were determined by setting a gate above 1% of baseline fluorescence. Mean fluorescent intensity (MFI), as well as frequency of parent gate, values were imported into Excel and/or GraphPad Prism for analysis.

Statistical analyses. All statistical analyses were performed using GraphPad Prism software. P-values < 0.05 were considered significantly different. Technical duplicates were averaged, and the mean value of each biological replicate was considered an n of 1.

Results

In vitro stimulation causes reduction in cell-surface PrP^C. To determine whether PrP^C protein levels alter during the course of an immune response, we treated primary splenocytes with multiple immunological stimuli for various time points. FACS analysis revealed PrP^C cell-surface levels were reduced when compared to untreated controls (Figure 5.1). However, these treatments may cause B cells to aggregate, so future directions should also include a B220+ B cell gate. In an attempt to confirm these findings, we treated PrP-expressing rabbit kidney cells (moPrP RK) with LPS and observed similar results, although with different magnitudes and kinetics. These data suggest PrP^C internalization succeeds stimulation. However, whether PrP^C destruction, or perhaps intracellular signaling, occur remains unknown. Therefore, we asked whether *Prnp*^{-/-} (PrP KO) mice exhibit impaired immunological responses.

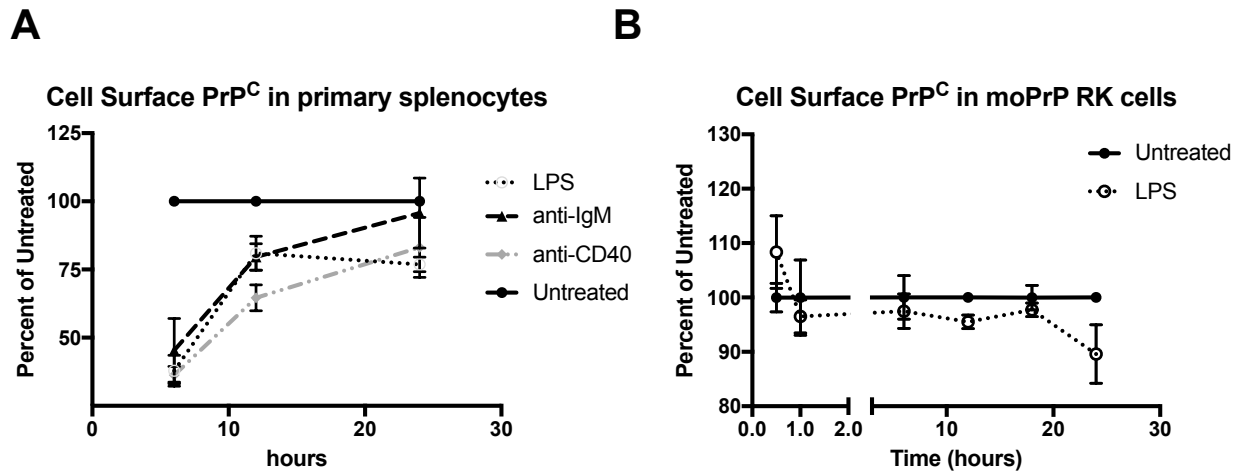


Figure 5.1. Cell-surface PrP^C levels reduce after *in vitro* stimulation. To determine whether PrP^C levels alter during the course of an immune response, primary splenocytes were treated with various immunological stimuli for various time points and analyzed for PrP^C levels via FACS (n=4 FVB mice). Compared to untreated controls, splenocytes treated with various immunological stimuli (LPS or cross-linking antibodies against IgM or CD40) appear to contain less surface levels of PrP^C (A). Although with differing kinetics and magnitudes, similar results were obtained after treating stably transfected rabbit kidney epithelial cells (moPrP RK cells) with LPS (B).

Prnp deficient (*PrP* KO) mice develop normal splenic lymphocyte proportions and fare equal to wild type when naively challenged with *E. coli*. Prior to testing B cell

impairments, we tested whether *PrP* KO mice contain normal lymphocyte frequencies in spleen. FACS analysis revealed no impairments in total B220+, CD19+, or CD21/35+ B cells, nor their relative proportions (Figure 5.2A and data not shown). Previous reports indicate T-cell impairments in *PrP* KO mice, although this does not appear to be due to an impairment in total T cell numbers or proportions. Considering the putative role of PrP^C in cell adhesion (Mange et al. 2002; Santuccione et al. 2005), we assessed whether *PrP* KO mice exhibited normal innate immune responses. Innate immune responses rely on white blood cell extravasation into infected tissue. Therefore, if PrP^C regulates infiltration, we would have expected *PrP* KO mice to succumb to infection with

lower doses of live *E. coli*. However, 500,000 live *E. coli* cells, a modest dose, equally caused disease in wild type and knockout mice (Figure 5.2B,C). Inoculating mice with decreasing doses of *E. coli* may reveal subtle differences, although we do not believe this to be an appropriate use of live animals. Further, we observed a slight trend indicating PrP KO mice may have contained less bacterial burden than wild type (Figure 5.2B). Importantly, C57/Bl6 mice resisted disease with a 20-fold higher doses of *E. coli* than FVB mice (Figure 5.2D), highlighting the importance of matching background strains. We therefore decided to test if fast-acting, cell-biological events in B cell activation rely on PrP^C.

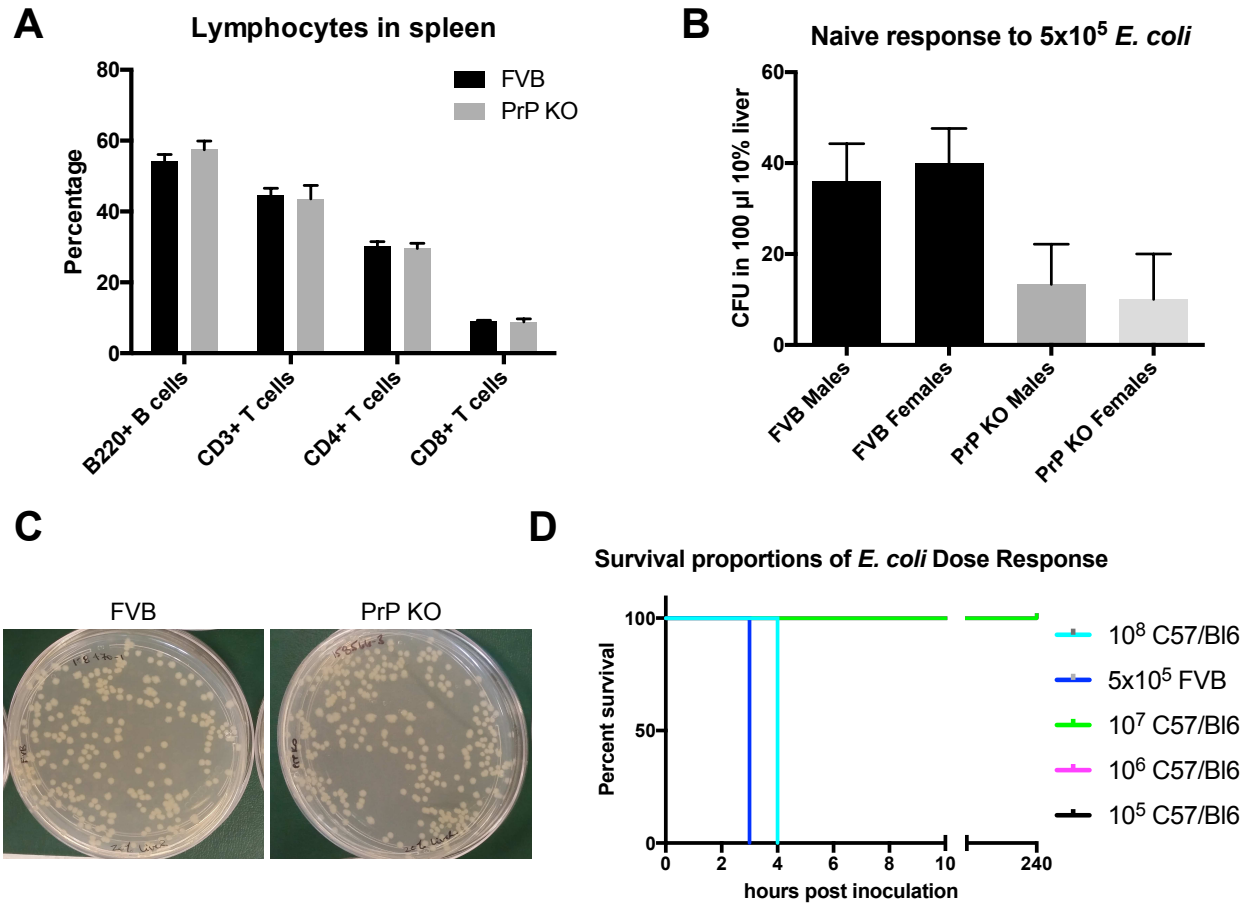


Figure 5.2. Splenic lymphocyte proportions and naive, non-vaccinated survival against *E. coli* infection depends on mouse background, not *Prnp* status. To determine whether PrP KO mice contain normal levels of B and T cells in spleen, we analyzed B220+ B cells, CD3+ T cells, CD4+ T cells, and CD8+ T cells proportions via flow cytometry and did not observe any deficits (A, n=3 mice/genotype). PrP KO mice succumbed to infection without vaccination similarly to wild type mice after a single dose of live *E. coli* (B,C ANOVA p=0.0952). However, survival without vaccination depended on mouse background strain. C57/Bl6 mice survived after receiving 10^7 live bacteria, whereas FVB mice succumbed to infection with 5×10^5 live bacteria (n=1 mouse/dose, D), indicating a necessity to match background strains.

PrP^C promotes calcium signaling and Src family kinase (SFK) phosphorylation. B cell receptor engagement and CD40 ligation precede B cell activation and/or isotype switching. To monitor events downstream of BCR engagement or CD40 ligation, and their dependence on PrP^C, we treated primary splenocytes with cross-linking antibodies

against IgM or CD40 and monitored calcium mobilization via FACS and SRC phosphorylation via western blotting. After cross-linking IgM, PrP KO mice exhibited significantly reduced calcium indicator dye fluorescence, indicative of less calcium mobilization (Figure 5.3A,B). Furthermore, SRC phosphorylation (Y416) in PrP KO mice did not statistically differ from untreated, whereas FVB wild type mice contained significantly higher SRC phosphorylation after IgM or CD40 cross-linking (Figure 5.3C). Lastly, we observed a significant difference in Lyn phosphorylation after challenging naïve mice with *E. coli* (Figure 5.2). These data highlight the necessity of PrP^C in early events of B cell activation.

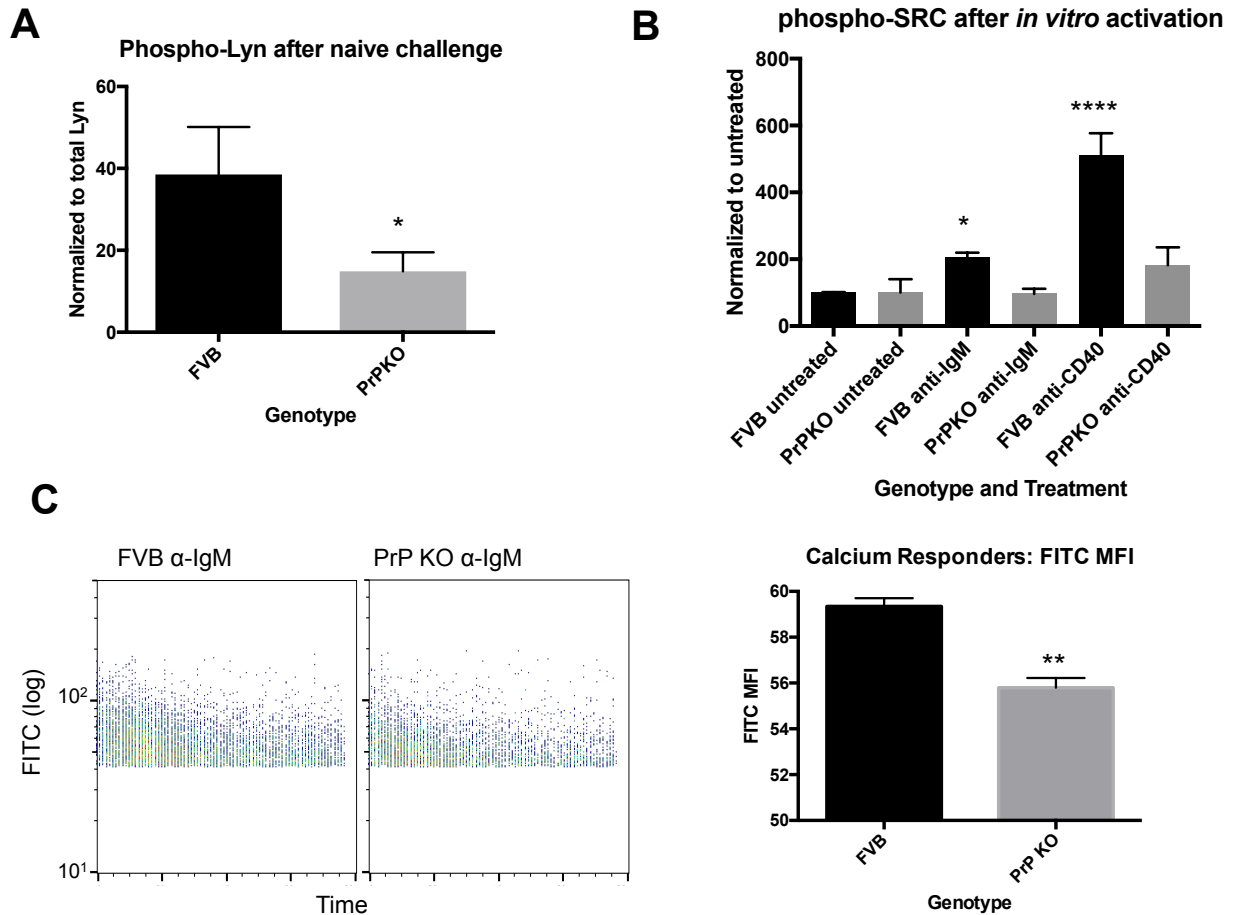


Figure 5.3. PrP^C augments early events in B cell activation. Calcium mobilization and Lyn and SRC phosphorylation precede antibody production and thus provide avenues to monitor early events in B cell activation. Splens from mice in Figure 5.2B (n=6/genotype) were analyzed for phosphorylated Lyn via western blotting (A), and PrP KO mice contained a fewer proportion of phosphorylated Lyn kinase (p=0.0363 one-tailed T test). Further, phosphorylation and activation of SRC kinase was impaired in PrP KO mice after *in vitro* activation (B). IgM (p=0.0242) or CD40 (p<0.0001) cross-linking caused statistically significant increases in SRC phosphorylation (Y416) in FVB mice compared to untreated, whereas treated PrP KO splenocytes did not statistically differ from untreated. FVB and PrP KO primary splenocytes were loaded with calcium indicator dye Fluo-4, and fluorescence after IgM cross-linking was significantly higher in FVB mice compared to PrP KO (C p = 0.0059; data averaged over 5 minutes time course). Data in panels B-D were generated from n=2 mice/genotype, and experiments were repeated twice with 4 additional mice/genotype and showed similar results.

PrP^C bolsters humoral immunity and subsequent protection against extracellular bacteria. The above data suggests PrP^C promotes signaling events in B cell activation,

leading us to question whether PrP KO mice exhibit impairments in humoral immunity. We vaccinated mice with 10^5 HK *E. coli* CFU, boosted twice, and compared total IgG and IgG3 responses in PrP KO and FVB wild type mice via ELISA. PrP KO mice contained significantly less IgG (all subtypes) and IgG3 specific to the coated vaccine (Figure 5.4A,B). We calculated reciprocal IgG titers of >3200 and 400 for FVB and PrP KO mice, respectively.

In a separate experiment, we coated serum on a microtiter plate and compared total levels of IgG and IgG3. We did not observe an impairment in total serum IgG or IgG3, suggesting these animals can indeed produce antibodies (Figure 5.4C,D). In fact, PrP KO mice contained significantly more serum IgG and IgG3 (discussed below). To ascertain whether vaccination protected PrP KO mice despite lower antibody responses to the vaccine, we inoculated mice with live *E. coli* (Figure 5.5). We chose a modest dose of 10^6 live bacteria, corresponding to a two-fold increase over dose known to cause sepsis in naïve, non-vaccinated animals (Figure 5.2). Twenty-five percent (one out of four) of PrP KO mice succumbed to infection despite vaccination, whereas all FVB mice were protected from infection (Figure 5.5). We predict vaccination would protect FVB mice from higher doses of bacteria, while PrP KO mice would succumb to infection. However, we did not believe this titration experiment as justified animal use.

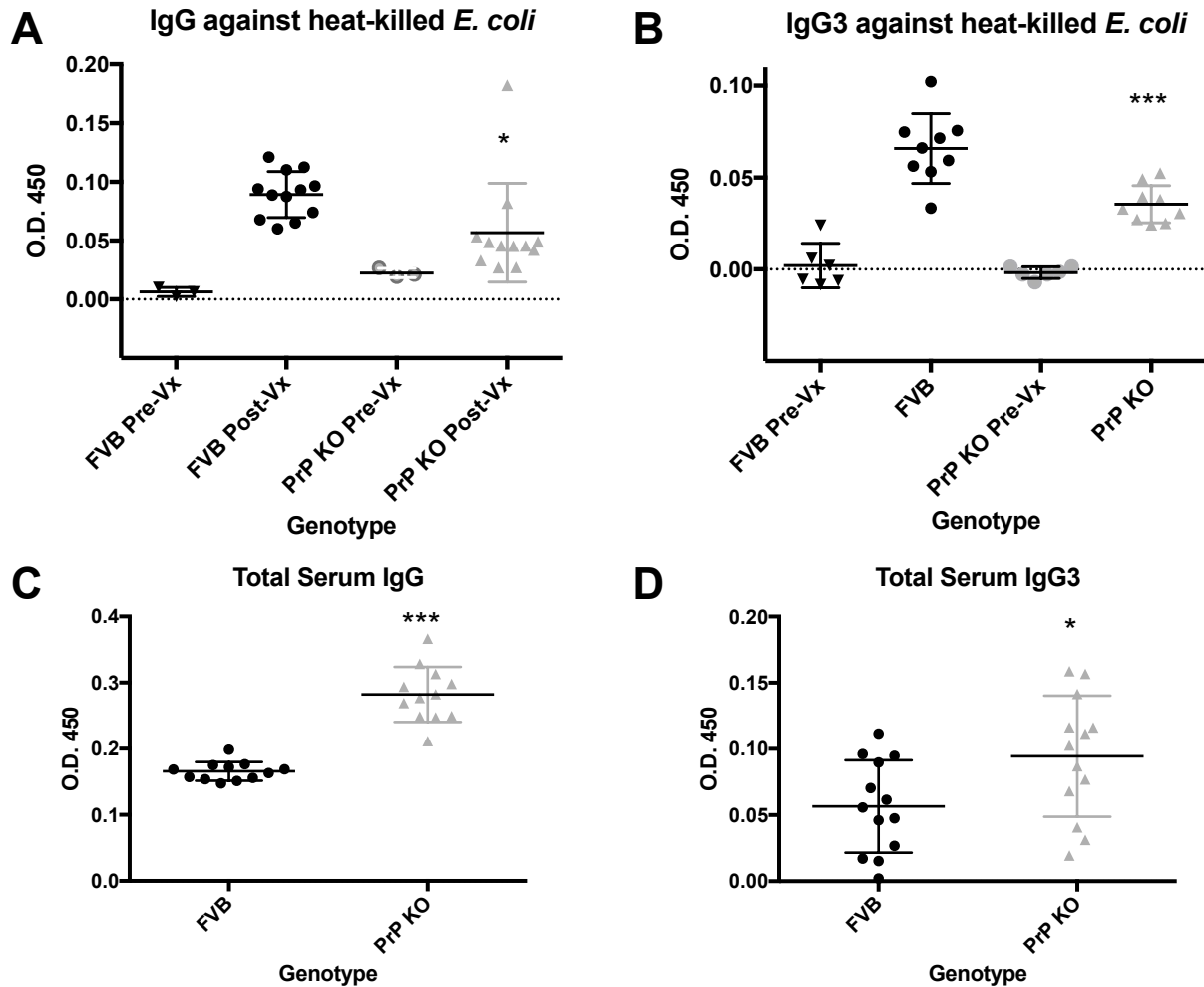
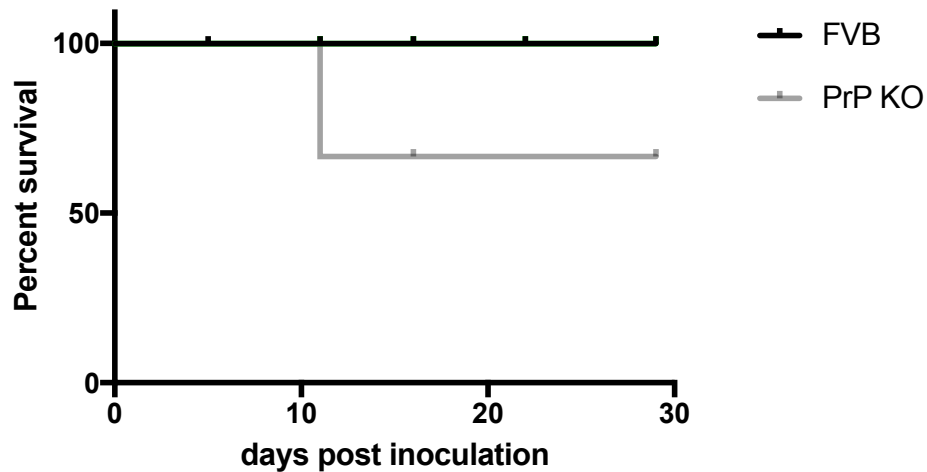


Figure 5.4. PrP^C bolsters humoral immunity after vaccination. To assess B cell function in relation to PrP^C status, we vaccinated PrP KO and FVB mice and boosted weekly for a total of 3 injections. Serum was processed from tail vein blood collection prior to- and post- vaccination. Seroconversion and total serum IgG and IgG3 was assessed via ELISA. Vaccination induced seroconversion in both genotypes, although PrP KO mice contained significantly less total IgG (A, $p=0.0119$, T-test) and IgG3 (B, $p=0.0003$) against coated vaccine. However, comparing total serum levels of IgG and IgG3 did not reveal an impairment in total immunoglobulin (C,D), and in fact showed that PrP KO mice contained significantly higher serum levels of IgG ($p<0.0001$) and IgG3 ($p=0.0250$). Data was generated from pooled serum ($n=4$ mice/genotype).

A Survival After Vaccination, 2 Boosts, and 10^6 live *E. coli*



B



Figure 5.5. Vaccination does not entirely protect PrP KO from infection with live *E. coli*. Vaccinated mice were challenged with 10^6 live *E. coli* and monitored daily. Twenty-five percent (1/4) of PrP KO mice succumbed to infection, whereas vaccination entirely protected wild type FVB mice. Cultures of liver homogenate (B) showed only PrP KO liver contained septic infection.

PrP^C forms a complex with B cell co-receptor member, CD21. The B cell receptor and co-receptor include cell-surface IgM, CD19, CD21, and CD81. When complexed with C3d-tagged antigens, CD21, along with CD19, translocate to lipid rafts. Thus, we hypothesize PrP^C stabilizes members of the B cell co-receptor in lipid rafts. If so, we predicted PrP^C biochemically interacts with CD19, CD21, and/or CD81. We first tested CD21 and indeed observe an interaction. In a direct binding assay, coated recombinant

PrP bound CD21 when compared to a BSA negative control (Figure 5.6B). We also confirmed this finding with surface plasmon resonance (Figure 5.6A). Further, we observe the presence of PrP^C, CD21, and cholera toxin conjugated to Alexa Fluor 488 within lipid raft domains (Figure 5.6C). While we cannot conclude co-localization at this resolution, we provide evidence PrP^C and CD21 form complexes both biochemically and within lipid rafts. Together, these findings suggest PrP^C, a permanent lipid-raft resident, could bind translocated CD21 and perhaps augment signal transduction.

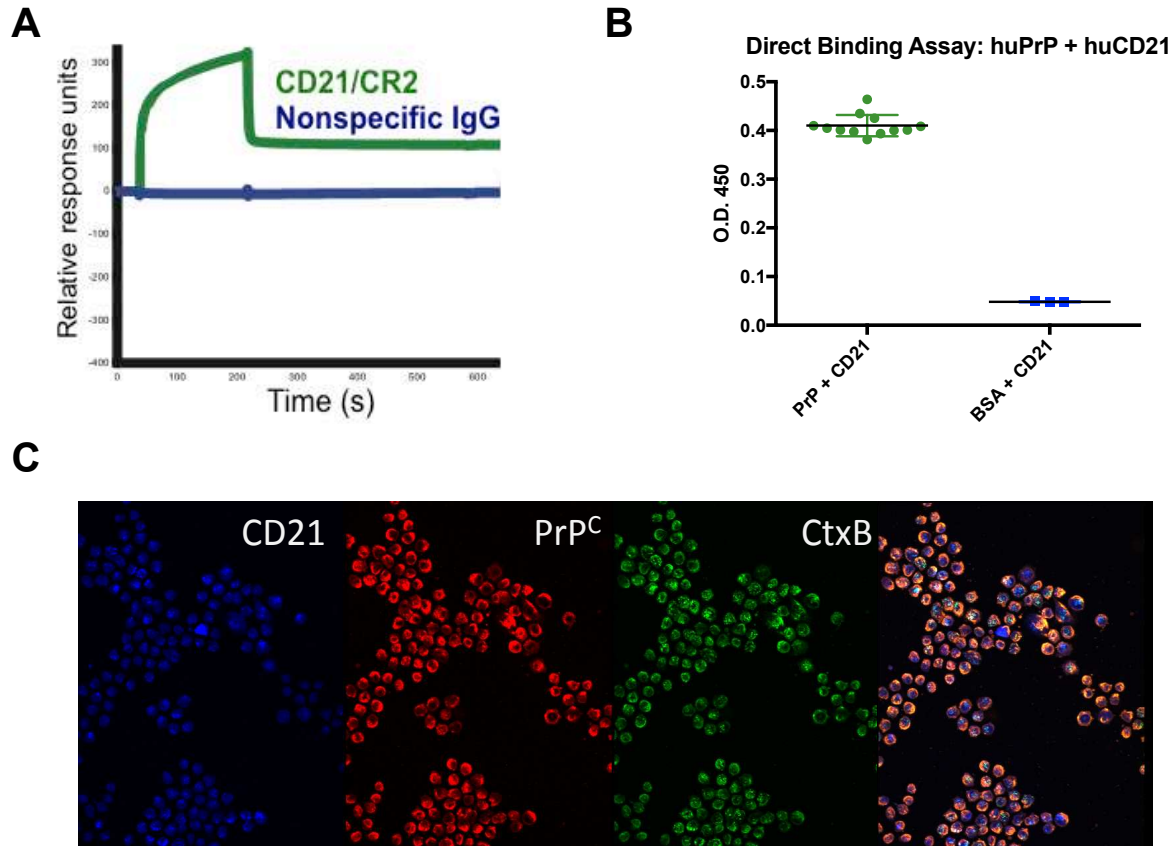


Figure 5.6. PrP^C forms a complex with B cell co-receptor member CD21. Data from previous chapters suggests CD21 impacts prion disease through direct interactions with prions. To determine whether CD21 also binds PrP^C, we coated recombinant PrP on a CM5 sensor chip (A) or microtiter plate (B) and observed an interaction with recombinant CD21 via SPR (A) and direct binding assay (B). CD21 engagement with

opsonized antigen induces translocation into cholesterol-rich signaling domains (lipid rafts). We observe overlapping signal between CD21 (eFluor450), PrP^C (Alexa Fluor 647), and cholera toxin B subunit (lipid raft marker, Alexa Fluor 488 courtesy of the Bamberg lab) in P3 myeloma cells (C). However, we cannot conclude co-localization at this resolution (40X).

PrP^C may promote CD21/35 translocation into lipid rafts. We initially hypothesized PrP^C captures translocated co-receptors proteins and coordinates signaling events. To address this hypothesis, we isolated splenic lipid rafts from mice in Figure 5.2B and probed for CD21/35 (Figure 5.7). Although we detected FVB CD21/35 in lower-density lipid raft fractions than PrP KO mice, densitometric analysis did not reveal a deficit in total lipid raft CD21/35 between genotypes. This experimental paradigm presented a number of difficulties. For example, CD21/35 was invariably present in lower sucrose density fractions than lipid raft marker flotillin. Further, we never achieved concise separation between lipid raft and non- lipid raft fractions. Perhaps a more appropriate, future direction could include CD21/35 detection using microscopic techniques. For example, one could stain lipid rafts with fluorescently-labeled cholera toxin B subunits and analyze for CD21/35 presence (Figure 5.8). We attempted this experiment using P3 myeloma cells treated with or without heat-killed E. coli, although we did not observe a difference between treated and untreated cells. Untreated lipid rafts contained substantial lipid-raft CD21/35, although perhaps other cell types and treatment paradigms could help resolve this issue.

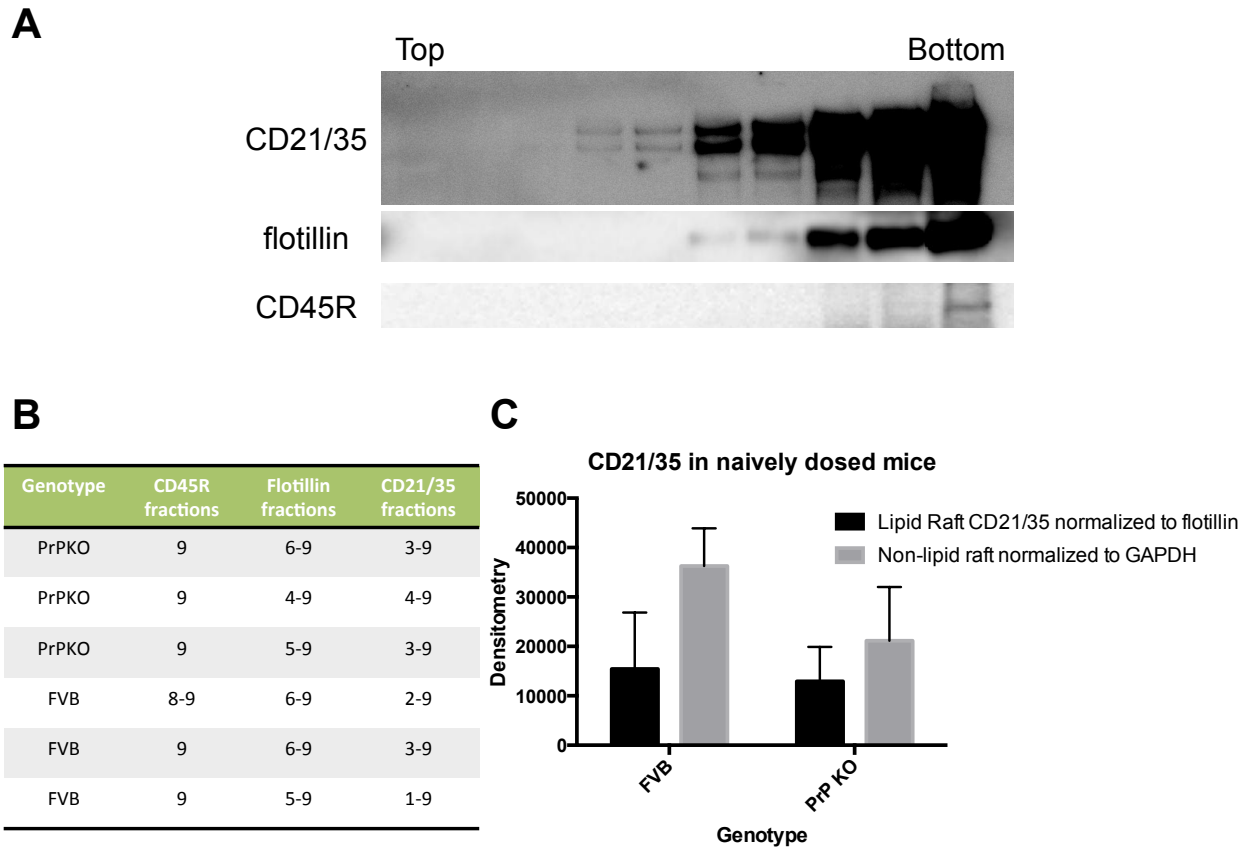


Figure 5.7. PrP^C may regulate CD21 translocation efficiency. Upon engagement with C3d/g-opsonized antigens, CD21 translocates into lipid rafts and cooperatively signals with B cell receptor and co-receptor members. To test whether PrP^C promotes CD21 retention in lipid rafts, we separated lipid raft fractions (9) from non-lipid fractions via sucrose gradient ultracentrifugation from splenic lysates of FVB and PrP KO mice dosed with live *E. coli* (see Figure 5.2B). CD21/35 translocation into lipid rafts was determined by western blotting after probing for lipid raft marker flotillin, non-lipid raft membrane marker CD45R (B220), and CD21/35 (A; Top: fraction 1, Bottom: fraction 9). We observed CD21/35 in lower-density lipid raft fractions in FVB compared to PrP KO mice (B). However, we did not observe densitometric signaling differences in lipid raft or non-lipid raft fractions (C).

PrP^C regulates cell-surface CD19 levels. Considering PrP^C and CD21 form complexes (Figure 5.6) and signal through similar SFKs (Chalupny et al. 1995 and Sempou et al. 2016), we hypothesize PrP^C serves a critical role in signaling with B cell co-receptor members CD21 and CD19. In PrP KO mice, we observed a slight, albeit non-statistically significant, reduction in surface levels of CD21/35 (data not shown), leading

us to question whether PrP^C deficiency impacts CD19 levels. As discussed in Chapter 3, B cell co-receptor members CD21 and CD19 form signaling complexes, and deficiency in one member impacts the other member's cell-surface levels (Hasegawa et al. 2001 and Haas et al. 2002). To test whether PrP^C deficiency impacts CD19 levels, we compared CD19 levels in wild type and PrP KO splenocytes via western blotting and FACS (Figure 5.8). Western blot densitometric analysis revealed higher CD19 levels in whole PrP KO splenocyte lysate (Figure 5.8A,B), and this was confirmed using FACS (Figure 5.8C). Naïve, PrP KO mice contain higher surface CD19 levels (Figure 5.8C), and siRNA treatment against *Prnp* transcripts in wild type splenocytes revealed the same trend (Figure 5.8D).

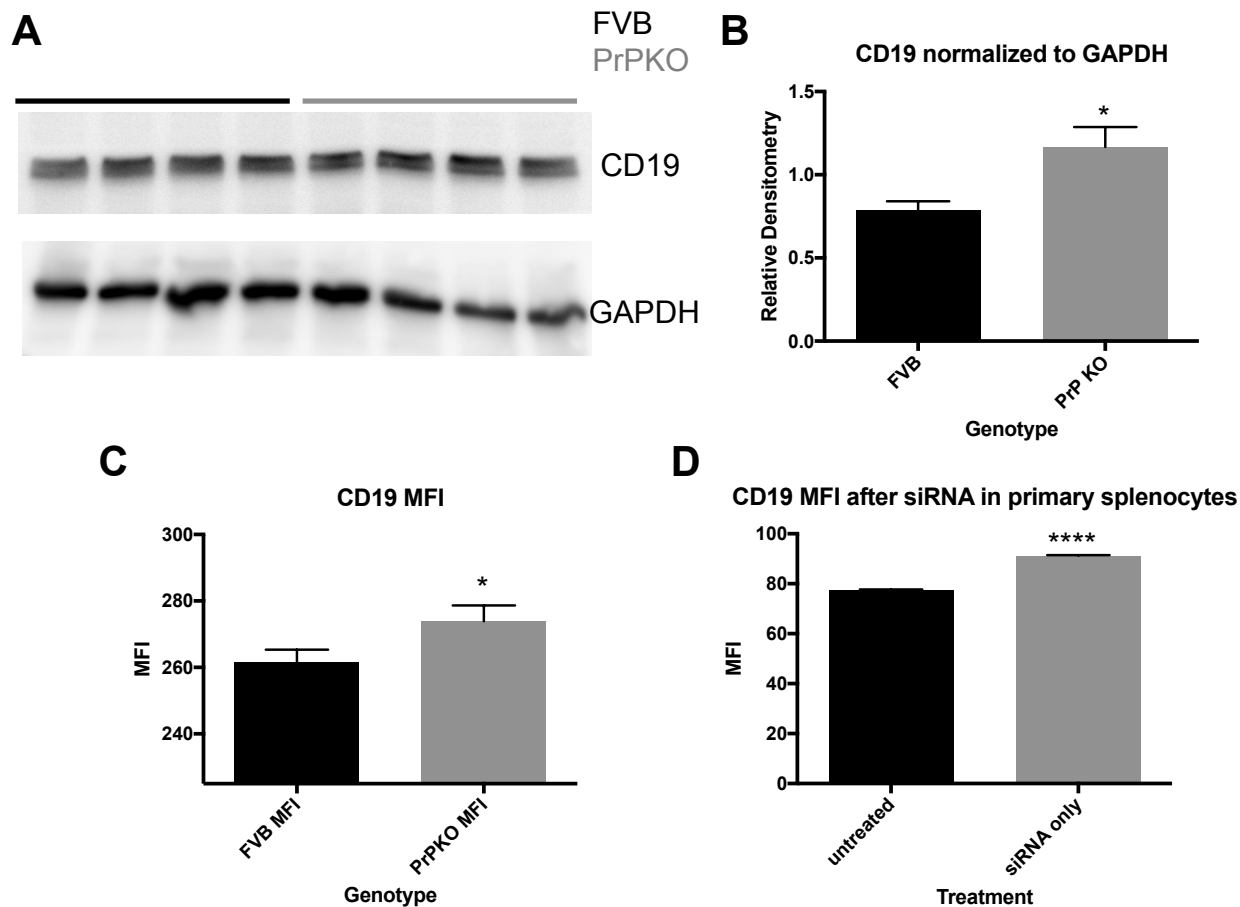


Figure 5.8. PrP^C deficiency increases CD19 protein levels. To assess whether PrP^C deficiency impacts B cell co-receptor member CD19, we analyzed protein levels via western blotting (A, B) and FACS (C, D). We observed statistically significant increase in CD19 normalized to GAPDH via western blot (A, B, $p=0.0276$). This finding was confirmed in naive primary splenocytes (C, $p=0.0331$). To determine whether this effect was due to transgenesis, we treated wild type FVB primary splenocytes with siRNA against *Prnp* transcripts and confirmed PrP^C deficiency causes increase CD19 levels (D, $p<0.0001$).

Discussion

Data presented in this chapter suggest PrP^C augments B cell activation leading to humoral immunity against extracellular, gram-negative bacteria. While neural and certain lymphoid cells express high levels of PrP^C, knockout mice develop normally

without overt phenotypes (Prusiner et al. 1993). However, research animals are kept in specific pathogen free environments, causing the potential to overlook immunodeficiency. While we do not observe an impairment in proportions of splenic lymphocytes (Figure 5.2), steps leading to B cell activation and antibody production appear to partially rely on PrP^C (Figures 5.3 and 5.4).

The B cell receptor and co-receptor include cell-surface IgM, Complement receptor 2 (CD21), CD19, and CD81. Not surprisingly, genetic alterations leading to deficiency in any one of its members causes immunodeficiency. Data presented in this chapter suggest deficiency in PrP^C also cause immunodeficiency. Putative prion disease therapeutics involve down-regulating PrP^C. While these treatments would remove the prion substrate required for disease (Prusiner et al. 1993; White et al. 2008), we propose this treatment paradigm would also render a patient immunosuppressed. However, targeting siRNA treatments specifically to the brain (Pulford et al. 2016; Bender et al. 2016) would presumably circumvent this issue.

Our FACS data suggesting PrP^C becomes internalized after *in vitro* stimulation is in stark contrast with previous reports revealing an upregulation of PrP^C after mitogen stimulus (Mabbott et al. 1997). Possible explanations could include: different cell types, mRNA versus protein, or different time courses. For example, surface PrP^C may upregulate in T cells (Li et al. 2001) but not B cells (Figure 5.1). Further, mRNA changes may not always reflect changes in cell-surface protein levels (Shyu et al. 2002). Lastly, each study analyzed *Prnp* mRNA or protein products using different treatments and

time courses. Our data suggests PrP^C may become internalized, but it's unknown whether that's to signal intracellularly or perhaps signals to stop the pro-inflammatory signal. A broader, longitudinal study with each stimulus and cell type is required to precisely determine *Prnp* regulation in response to immunological stimuli.

B cell activation occurs both dependent and independent of T cell help. T-independent antigens usually contain highly repetitive structures such as lipopolysaccharide (LPS). T-dependent antigens only cause B cell activation when an activated T cell simultaneously recognizes its antigen presented in MHC II peptides on the cognate B cell. CD40 ligation between a B cell and its corresponding helper T cell promotes B cell activation and immunoglobulin isotype switching. Treatments with IgM or CD40 cross-linking antibodies mimic T- independent or dependent activation, respectively, and lead to different B cell phenotypes (Wortis et al. 1995). Interestingly, PrP^C appears to regulate B cell activation in response to T-dependent or -independent antigens because we observed impaired SRC phosphorylation in PrP KO splenocytes after cross-linking IgM or CD40 (Figure 5.3). While heat-killed *E. coli* contains both T- dependent and independent antigens, future studies could include vaccinating mice with purified LPS or protein antigens to parse out differences, if any.

Previous reports indicate a role of PrP^C in T cell proliferation in response to mitogenic stimuli (Mabbott et al. 1997), and cross-linking PrP^C in Jurkat T cells led to increased intracellular calcium mobilization and ERK phosphorylation (Stuermer et al. 2004). The data presented in this chapter suggest PrP^C may also regulate calcium signaling and

SRC phosphorylation in B cells (Figure 5.3). Taken together, these data highlight a crucial role for PrP^C in lymphocyte signaling cascades. However, future studies are required to ascertain the precise roles of PrP^C on B and T cells, as well as the interactions between the two.

Several studies suggest PrP^C serves as an adhesion molecule (reviewed in Petit et al. 2013). For example, PrP^C overexpression caused N2a cells to aggregate in a calcium-independent manner (Mange et al. 2002). This datum suggests PrP^C may promote intercellular adhesion. Future studies could include testing whether PrP^C aids immunological synapse formation between antigen presenting cells and T cells. Whether PrP^C promotes cell:cell contact, brings together signaling molecules to raft domains, or perhaps both, remains unclear. Future directions could include testing whether PrP KO mice sufficiently form immunological synapses between T cells and APCs.

When engaged with opsonized antigens, CD21 and CD19 complex translocates to lipid rafts and reduces the signaling threshold to activate a B cell. CD19, a transmembrane protein, becomes phosphorylated and recruits Src family kinases to the membrane. Studies of CD19 transgenic mice reveal CD19 roles in B cell survival and activation. CD19 deficient mice reveal deficits in BCR signaling (Depoil et al. 2008) and elicit reduced IgG responses to vaccination (Gardby et al. 2001). Interestingly, CD19 over-expressing transgenic (hCD19TG) mice contain higher immunoglobulin levels in an isotype-dependent manner. Specifically, hCD19TG mice contain higher IgG2b levels,

yet lower IgG3 titers (Engel et al. 1995). We observe increased CD19 (Figure 5.8) and total serum IgG3 (Figure 5.4) in PrP^C deficient mice. CD19 augments B cell activation and antibody production, yet we report humoral impairments after vaccination in mice which overexpress CD19 yet lack PrP^C. Thus, CD19 overexpression in PrP KO mice does not compensate for the antibody impairments to vaccination seen in PrP KO mice. Perhaps CD19 cannot effectively recruit Src-family kinases Fyn and Lyn (Chalupny et al. 1995) or form lipid raft microclusters (Sohn et al. 2008) in the absence of PrP^C.

An alternative explanation to findings in this chapter could be PrP KO mice contain overall higher serum IgG levels due to mounting an antibody response against a concurrent infection. However, both strains of mice were age-matched, co-housed, and inoculated on the same days. We do not believe PrP KO mice were exposed to other pathogens, although we cannot entirely rule out this possibility.

Another possible explanation is that PrP KO mice effectively generate certain classes of immunoglobulin, but not others. For example, PrP^C may regulate certain isotype switching. CD40 ligation stimulates B cells to isotype switch, and we observe reduced Src phosphorylation in PrP KO mice downstream of CD40 cross-linking (Figure 5.3). Future experiments could involve longitudinal studies to determine precise isotype switching impairments, as well as T cell dependent and independent antigens. For example, crude heat-killed *E. coli* contains both T-independent antigens (LPS), as well as T-dependent antigens. Future experiments could test humoral responses to purified antigens. However, our findings suggest PrP^C plays a role in both responses because

IgM and CD40 cross-linking both at least partially relied on PrP^C. IgM cross-linking serves as a model for T-independent activation, whereas CD40 ligation generally involves interactions between T cells and antigen presenting cells.

The enclosed experiments used PrP KO Zurich-1 mice (Bueler et al. 1992) back-crossed on the FVB background (Prusiner et al. 1993). While these mice have proven useful in ascertaining the role of PrP^C in prion disease pathogenesis, Dr. Adriano Aguzzi argues effects observed in these mice may arise from transgenesis and back-crossing artifacts. Therefore, he generated TALEN PrP KO mice on the C57/Bl6 background which specifically targets small sequences in *Prnp* without off-target effects (Nuvolone et al. 2016). Therefore, we propose confirming the enclosed findings using the TALEN KO mice. Preliminary findings show the same trend with *in vitro* findings, although not statistically significant. Hurdles experienced thus far include large sample standard deviations, although perhaps optimizations in different mouse background strains are required.

Hou and colleagues (2001) published a seminal finding regarding mitochondrial antiviral-signaling protein (MAVS) aggregation in response to viral infection. Yuan and Hochschild (2017) reported the bacterial transcription terminator Rho no longer efficiently terminates transcription in its aggregated state. Further, yeast prions form in response to various environmental stressors. Thus, protein aggregation (“prion formation”) can serve normal, physiological functions in response to insults. We propose PrP^C, particularly considering its propensity to aggregate and misfold, may also

aggregate in response to immunological stressors. Interestingly, PrP^C is present in healthy mice mitochondria (Faris et al. 2017). In light of data presented in this chapter, among others, we hypothesize immunological stimuli cause PrP^C to internalize (Figure 5.1) and aggregate, and this response may involve mitochondria. If this hypothesis is indeed true, perhaps prion diseases arose from aberrant, non-resolvable misfolding in response to stressors. We began to optimize testing this hypothesis using semi-denaturing assays such as SDD-AGE, although PrP^C abundance in whole spleen limited detection capability. Further, PrP^C in normal (non-infected) brain ran in an aggregated state. Future experiments could involve testing varying concentrations of detergent and/or electrophoresis parameters.

In summary, we conclude PrP^C is the newest discovered member of the B cell co-receptor. We provide three lines of evidence: 1) PrP^C signals through similar SFKs as the B cell receptor and co-receptor (Mouillet-Richard et al. 2000; Shi et al. 2013; Pleiman et al. 1994; Chalupny et al. 1995); 2) SFK phosphorylation, calcium signaling, and humoral responses after at least partially rely on the presence of PrP^C (Figures 5.3 and 5.4); and 3) Purified PrP^C directly interacts with co-receptor member CD21 (Figure 5.6). Future directions could include testing direct interactions between PrP^C and other B cell co-receptor members. Experiments to address this include co-immunoprecipitation, surface plasmon resonance, and/or direct binding assays. We hypothesize PrP^C, a permanent lipid-raft resident, coordinates signaling partners to aid B cell activation. Intriguingly, Susan Pierce's group predicted a GPI-anchored member's presence in the B cell co-receptor (Cheng et al. 2001). We conclude this is PrP^C.

REFERENCES

- Ballerini C, Gourdain P, Bachy V, Blanchard N, Levavasseur E, Grégoire S, Fontes P, Aucouturier P, Hivroz C, Carnaud C. Functional implication of cellular prion protein in antigen-driven interactions between T cells and dendritic cells. *J Immunol*. 2006 Jun 15;176(12):7254-62. PubMed PMID: 16751368.
- Ballerini C, Gourdain P, Bachy V, Blanchard N, Levavasseur E, Grégoire S, Fontes P, Aucouturier P, Hivroz C, Carnaud C. Functional implication of cellular prion protein in antigen-driven interactions between T cells and dendritic cells. *J Immunol*. 2006 Jun 15;176(12):7254-62. PubMed PMID: 16751368.
- Bender HR, Kane S, Zabel MD. Delivery of Therapeutic siRNA to the CNS Using Cationic and Anionic Liposomes. *J Vis Exp*. 2016 Jul 23;(113). doi: 10.3791/54106. PubMed PMID: 27501362.
- Büeler H, Fischer M, Lang Y, Bluethmann H, Lipp HP, DeArmond SJ, Prusiner SB, Aguet M, Weissmann C. Normal development and behaviour of mice lacking the neuronal cell-surface PrP protein. *Nature*. 1992 Apr 16;356(6370):577-82. PubMed PMID: 1373228.
- Cashman NR, Loertscher R, Nalbantoglu J, Shaw I, Kascsak RJ, Bolton DC, Bendheim PE. Cellular isoform of the scrapie agent protein participates in lymphocyte activation. *Cell*. 1990 Apr 6;61(1):185-92. PubMed PMID: 1969332.
- Chalupny NJ, Aruffo A, Esselstyn JM, Chan PY, Bajorath J, Blake J, Gilliland LK, Ledbetter JA, Tepper MA. Specific binding of Fyn and phosphatidylinositol 3-kinase to the B cell surface glycoprotein CD19 through their src homology 2 domains. *Eur J Immunol*. 1995 Oct;25(10):2978-84. PubMed PMID: 7589101.
- Cheng PC, Cherukuri A, Dykstra M, Malapati S, Sproul T, Chen MR, Pierce SK. Floating the raft hypothesis: the roles of lipid rafts in B cell antigen receptor function. *Semin Immunol*. 2001 Apr;13(2):107-14. Review. PubMed PMID: 11308294.
- Cherukuri A, Cheng PC, Pierce SK. The role of the CD19/CD21 complex in B cell processing and presentation of complement-tagged antigens. *J Immunol*. 2001 Jul 1;167(1):163-72. PubMed PMID: 11418645.
- Depoil D, Fleire S, Treanor BL, Weber M, Harwood NE, Marchbank KL, Tybulewicz VL, Batista FD. CD19 is essential for B cell activation by promoting B cell receptor-antigen microcluster formation in response to membrane-bound ligand. *Nat Immunol*. 2008 Jan;9(1):63-72. Epub 2007 Dec 2. PubMed PMID: 18059271.
- Dürig J, Giese A, Schulz-Schaeffer W, Rosenthal C, Schmücker U, Bieschke J, Dührsen U, Kretzschmar HA. Differential constitutive and activation-dependent

expression of prion protein in human peripheral blood leucocytes. *Br J Haematol.* 2000 Mar;108(3):488-95. PubMed PMID: 10759704.

Engel P, Zhou LJ, Ord DC, Sato S, Koller B, Tedder TF. Abnormal B lymphocyte development, activation, and differentiation in mice that lack or overexpress the CD19 signal transduction molecule. *Immunity.* 1995 Jul;3(1):39-50. PubMed PMID: 7542548.

Faris R, Moore RA, Ward A, Race B, Dorward DW, Hollister JR, Fischer ER, Priola SA. Cellular prion protein is present in mitochondria of healthy mice. *Sci Rep.* 2017 Feb 2;7:41556. doi: 10.1038/srep41556. PubMed PMID: 28148964; PubMed Central PMCID: PMC5288712.

Gärdbby E, Chen XJ, Lycke NY. Impaired CD40-signalling in CD19-deficient mice selectively affects Th2-dependent isotype switching. *Scand J Immunol.* 2001 Jan;53(1):13-23. PubMed PMID: 11169202.

Genoud N, Behrens A, Miele G, Robay D, Heppner FL, Freigang S, Aguzzi A. Disruption of Doppel prevents neurodegeneration in mice with extensive Prnp deletions. *Proc Natl Acad Sci U S A.* 2004 Mar 23;101(12):4198-203. Epub 2004 Mar 8. PubMed PMID: 15007175; PubMed Central PMCID: PMC384718.

Haas KM, Hasegawa M, Steeber DA, Poe JC, Zabel MD, Bock CB, Karp DR, Briles DE, Weis JH, Tedder TF. Complement receptors CD21/35 link innate and protective immunity during *Streptococcus pneumoniae* infection by regulating IgG3 antibody responses. *Immunity.* 2002 Dec;17(6):713-23. PubMed PMID: 12479818.

Haas LT, Salazar SV, Kostylev MA, Um JW, Kaufman AC, Strittmatter SM. Metabotropic glutamate receptor 5 couples cellular prion protein to intracellular signalling in Alzheimer's disease. *Brain.* 2016 Feb;139(Pt 2):526-46. doi: 10.1093/brain/awv356. Epub 2015 Dec 14. PubMed PMID: 26667279; PubMed Central PMCID: PMC4840505.

Hasegawa M, Fujimoto M, Poe JC, Steeber DA, Tedder TF. CD19 can regulate B lymphocyte signal transduction independent of complement activation. *J Immunol.* 2001 Sep 15;167(6):3190-200. PubMed PMID: 11544305.

Hou F, Sun L, Zheng H, Skaug B, Jiang QX, Chen ZJ. MAVS forms functional prion-like aggregates to activate and propagate antiviral innate immune response. *Cell.* 2011 Aug 5;146(3):448-61. doi: 10.1016/j.cell.2011.06.041. Epub 2011 Jul 21. Erratum in: *Cell.* 2011 Sep 2;146(5):841. PubMed PMID: 21782231; PubMed Central PMCID: PMC3179916.

Li R, Liu D, Zanusso G, Liu T, Fayen JD, Huang JH, Petersen RB, Gambetti P, Sy MS. The expression and potential function of cellular prion protein in human lymphocytes. *Cell Immunol.* 2001 Jan 10;207(1):49-58. PubMed PMID: 11161453.

Liu J, Zhao D, Liu C, Ding T, Yang L, Yin X, Zhou X. Prion protein participates in the protection of mice from lipopolysaccharide infection by regulating the inflammatory process. *J Mol Neurosci*. 2015 Jan;55(1):279-287. doi: 10.1007/s12031-014-0319-2. Epub 2014 May 20. PubMed PMID: 24838383.

Lötscher M, Recher M, Hunziker L, Klein MA. Immunologically induced, complement-dependent up-regulation of the prion protein in the mouse spleen: follicular dendritic cells versus capsule and trabeculae. *J Immunol*. 2003 Jun 15;170(12):6040-7. PubMed PMID: 12794132.

Mabbott NA, Brown KL, Manson J, Bruce ME. T-lymphocyte activation and the cellular form of the prion protein. *Immunology*. 1997 Oct;92(2):161-5. PubMed PMID: 9415021; PubMed Central PMCID: PMC1364053.

Mouillet-Richard S, Ermonval M, Chebassier C, Laplanche JL, Lehmann S, Launay JM, Kellermann O. Signal transduction through prion protein. *Science*. 2000 Sep 15;289(5486):1925-8. PubMed PMID: 10988071.

Nuvolone M, Hermann M, Sorce S, Russo G, Tiberi C, Schwarz P, Minikel E, Sanoudou D, Pelczar P, Aguzzi A. Strictly co-isogenic C57BL/6J-Prnp^{-/-} mice: A rigorous resource for prion science. *J Exp Med*. 2016 Mar 7;213(3):313-27. doi: 10.1084/jem.20151610. Epub 2016 Feb 29. PubMed PMID: 26926995; PubMed Central PMCID: PMC4813672.

Petit CS, Besnier L, Morel E, Rousset M, Thenet S. Roles of the cellular prion protein in the regulation of cell-cell junctions and barrier function. *Tissue Barriers*. 2013 Apr 1;1(2):e24377. doi: 10.4161/tisb.24377. Review. PubMed PMID: 24665391; PubMed Central PMCID: PMC3887058.

Pleiman CM, Abrams C, Gauen LT, Bedzyk W, Jongstra J, Shaw AS, Cambier JC. Distinct p53/56lyn and p59fyn domains associate with nonphosphorylated and phosphorylated Ig-alpha. *Proc Natl Acad Sci U S A*. 1994 May 10;91(10):4268-72. PubMed PMID: 8183901; PubMed Central PMCID: PMC43766.

Politopoulou G, Seebach JD, Schmutz M, Schwarz HP, Aguzzi A. Age-related expression of the cellular prion protein in human peripheral blood leukocytes. *Haematologica*. 2000 Jun;85(6):580-7. PubMed PMID: 10870113.

Prusiner SB, Groth D, Serban A, Koehler R, Foster D, Torchia M, Burton D, Yang SL, DeArmond SJ. Ablation of the prion protein (PrP) gene in mice prevents scrapie and facilitates production of anti-PrP antibodies. *Proc Natl Acad Sci U S A*. 1993 Nov 15;90(22):10608-12. PubMed PMID: 7902565; PubMed Central PMCID: PMC47826.

Pulford B, Reim N, Bell A, Veatch J, Forster G, Bender H, Meyerett C, Hafeman S, Michel B, Johnson T, Wyckoff AC, Miele G, Julius C, Kranich J, Schenkel A, Dow S, Zabel MD. Liposome-siRNA-peptide complexes cross the blood-brain barrier and significantly decrease PrP on neuronal cells and PrP in infected cell cultures. *PLoS*

One. 2010 Jun 14;5(6):e11085. doi: 10.1371/journal.pone.0011085. PubMed PMID: 20559428; PubMed Central PMCID: PMC2885418.

Santuccione A, Sytnyk V, Leshchyns'ka I, Schachner M. Prion protein recruits its neuronal receptor NCAM to lipid rafts to activate p59fyn and to enhance neurite outgrowth. *J Cell Biol.* 2005 Apr 25;169(2):341-54. PubMed PMID: 15851519; PubMed Central PMCID: PMC2171870.

Sempou E, Biasini E, Pinzón-Olejua A, Harris DA, Málaga-Trillo E. Activation of zebrafish Src family kinases by the prion protein is an amyloid- β -sensitive signal that prevents the endocytosis and degradation of E-cadherin/ β -catenin complexes in vivo. *Mol Neurodegener.* 2016 Feb 9;11:18. doi: 10.1186/s13024-016-0076-5. PubMed PMID: 26860872; PubMed Central PMCID: PMC4748561.

Shi Q, Jing YY, Wang SB, Chen C, Sun H, Xu Y, Gao C, Zhang J, Tian C, Guo Y, Ren K, Dong XP. PrP octarepeats region determined the interaction with caveolin-1 and phosphorylation of caveolin-1 and Fyn. *Med Microbiol Immunol.* 2013 Jun;202(3):215-27. doi: 10.1007/s00430-012-0284-8. Epub 2013 Jan 3. PubMed PMID: 23283514.

Shyu WC, Harn HJ, Saeki K, Kubosaki A, Matsumoto Y, Onodera T, Chen CJ, Hsu YD, Chiang YH. Molecular modulation of expression of prion protein by heat shock. *Mol Neurobiol.* 2002 Aug;26(1):1-12. PubMed PMID: 12392052.

Sohn HW, Tolar P, Pierce SK. Membrane heterogeneities in the formation of B cell receptor-Lyn kinase microclusters and the immune synapse. *J Cell Biol.* 2008 Jul 28;182(2):367-79. doi: 10.1083/jcb.200802007. Epub 2008 Jul 21. PubMed PMID: 18644892; PubMed Central PMCID: PMC2483512.

Stuermer CA, Langhorst MF, Wiechers MF, Legler DF, Von Hanwehr SH, Guse AH, Plattner H. PrPc capping in T cells promotes its association with the lipid raft proteins reggie-1 and reggie-2 and leads to signal transduction. *FASEB J.* 2004 Nov;18(14):1731-3. Epub 2004 Sep 2. PubMed PMID: 15345693.

White MD, Farmer M, Mirabile I, Brandner S, Collinge J, Mallucci GR. Single treatment with RNAi against prion protein rescues early neuronal dysfunction and prolongs survival in mice with prion disease. *Proc Natl Acad Sci U S A.* 2008 Jul 22;105(29):10238-43. doi: 10.1073/pnas.0802759105. Epub 2008 Jul 16. PubMed PMID: 18632556; PubMed Central PMCID: PMC2474561.

Wortis HH, Teutsch M, Higer M, Zheng J, Parker DC. B-cell activation by crosslinking of surface IgM or ligation of CD40 involves alternative signal pathways and results in different B-cell phenotypes. *Proc Natl Acad Sci U S A.* 1995 Apr 11;92(8):3348-52. PubMed PMID: 7536930; PubMed Central PMCID: PMC42163.

Yuan AH, Hochschild A. A bacterial global regulator forms a prion. *Science*. 2017 Jan 13;355(6321):198-201. doi: 10.1126/science.aai7776. PubMed PMID: 28082594; PubMed Central PMCID: PMC5460984.

CHAPTER 6 – GENERATION OF PRION-SPECIFIC NANOBODIES: BIOCHEMICAL TOOLS AND POTENTIAL THERAPEUTICS TO COMBAT PRION DISEASE.

Summary

Four peptides, two heavy and two light chains, comprise canonical immunoglobulin G. However, camelids also generate heavy-chain only antibodies. Previous researchers generated molecular biology protocols to clone the variable domain of these heavy-chain antibodies which maintain full binding capacity and usually exhibit binding affinities within the low nanomolar range. Nanobodies preferentially bind three-dimensional epitopes, such as enzymatic clefts and perhaps the prions. Here we report immune library construction derived from an alpaca vaccinated with recombinant white-tailed deer prion protein. We identified a minimum of two clones which may preferentially bind prion-infected brain. Future directions include screening additional potentially reactive clones, as well as testing whether these nanobodies prevent or delay prion infection *in vitro* and *in vivo*. Further, we propose comparing binding capacities between different prion strains, if any. Collectively, data presented in this chapter outline a molecular biological approach to generate prion-specific antibody tools for diagnostics and perhaps therapeutic tools.

Introduction

Canonical G immunoglobulins are heterodimeric tetramers with both light and heavy chains (see Figure 6.1). Camelidae species, such as camels, llamas, and alpacas, generate these conventional antibodies, but also produce antibodies devoid of light

chains. These IgG₂ or IgG₃ heavy-chain antibodies (HCAbs) lack the constant heavy chain region CH1 (Hamers-Casterman et al. 1993) which anchors the light chain to the heavy chain (Padlan 1994). Thus, heavy-chain antibodies are much smaller than conventional antibodies yet maintain full binding capacity. Ghahroudi et al. (1997) reported a molecular biology technique which involved cloning the variable domain of the camel HCAb variable domain (VHH), later termed “nanobody.” Nanobody affinity analyses reveal dissociation constants (K_d) within the nanomolar range (Pain et al. 2015; Schoonaert et al. 2017), which are comparable to mouse monoclonal antibodies (van der Linden et al. 1999).

Potential nanobody applications seem boundless. Nanobody sequences share high homology with human variable domains, and are thus considered weakly immunogenic (Klarenbeek et al. 2015). Therefore, nanobodies may offer treatment opportunities which are limited in murine antibody treatments. Murine antibodies often prove successful after the first administration, but repeated administrations fail due to an immune response against the murine antibodies. Considering nanobodies share such high homology with human variable domains, it seems possible that repeated administration may bypass an immune response.

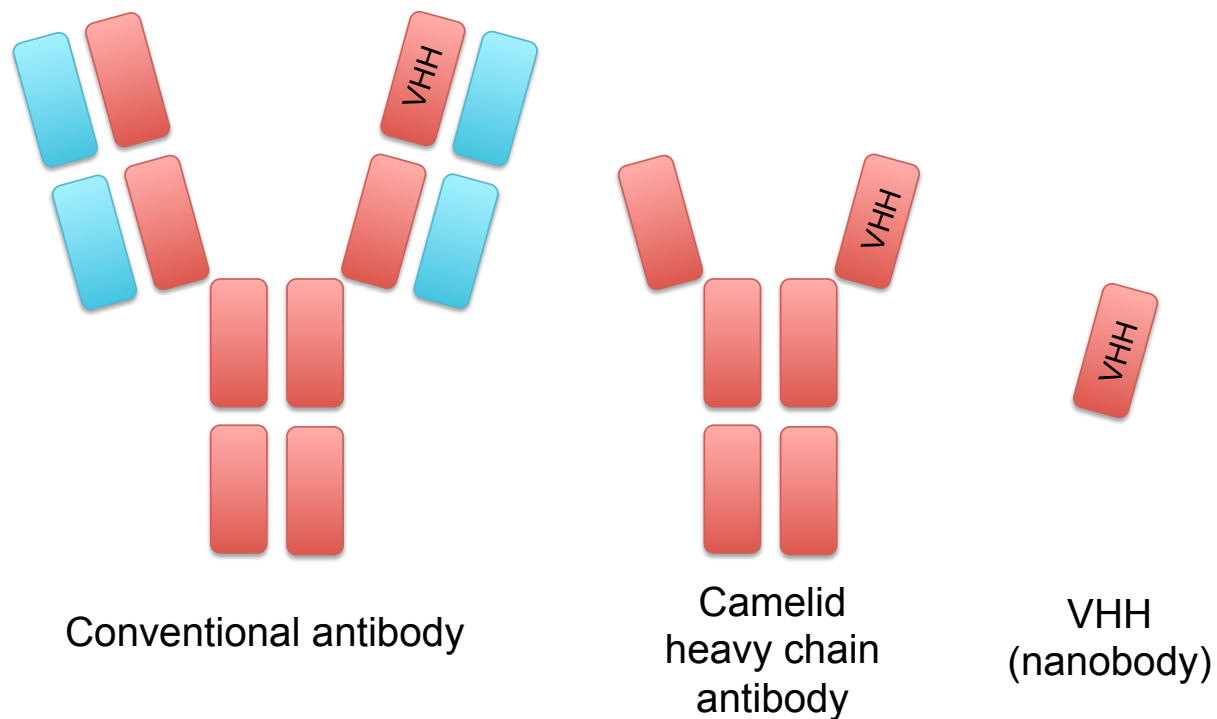


Figure 6.1. Cartoon diagram of camelid antibodies discussed in this chapter. Species from the Camelidae family generate conventional antibodies with both heavy (red) and light (blue) chains (left), as well as antibodies devoid of light chains (middle). Molecular biology techniques provide the ability to clone the variable heavy chain domain (VHH, right), which maintains high affinity interactions.

Nanobodies preferentially bind structural (3D) epitopes. Amyloidogenesis involves protein conformational changes which convert normally soluble proteins into an insoluble, aggregation-prone state. Considering nanobodies preferentially bind structural epitopes, perhaps they could provide mechanistic or therapeutic avenues to discriminate between native and misfolded forms and perhaps treat protein misfolding disorders. For example, Domanska et al. (2011) reported a nanobody clone which prevents β 2-microglobulin fibrillation *in vitro*. Revealing the epitope binding domain could not only provide structural information on exposed epitopes, but may also provide a therapeutic opportunity to prevent amyloidogenesis *in vivo*. For example, Guilliams et al. (2013) reported a nanobody-binding domain as soluble after fibrillation. These

findings may help identify exposed vs buried epitopes in amyloid and thus provide information regarding amyloid conformations and therapeutic targets. If these findings are translatable to other amyloid-prone proteins, such as the prion protein, perhaps nanobodies could not only provide mechanistic information on prion formation, but may also provide a therapeutic opportunity to combat disease.

Various *in vivo* data suggests nanobodies provide various disease therapeutic opportunities. Nanobody administration reduced viral replication and morbidity and mortality rates in a H5N1 influenza mouse model (Ibanez et al. 2011). Further, antibodies with basic isoelectric points (e.g. 9.4) can spontaneously cross the blood brain barrier (BBB, Li et al. 2012). While the large nature of conventional antibodies greatly impedes this process, nanobodies offer potential therapies for various neurological diseases and disorders. Therapies targeting central nervous system diseases, such as Alzheimer's Disease, Parkinson's Disease, prion diseases, etc, are limited due the difficulty in crossing the BBB. Further, the aforementioned diseases all contain a protein misfolding component. If nanobodies can spontaneously cross the BBB and recognize certain protein conformers, they may offer the cure-all for multiple CNS diseases.

Pardon et al. (2014) outlined a molecular biology protocol to clone the HCAb variable domain which generates 12-15 kD product termed nanobodies (see Figure 6.2). These nanobodies preferentially bind three-dimensional epitopes such as enzyme catalytic clefts (Li et al. 2012a), are weakly immunogenic due to high homology between human

and camelid variable domain framework region (Klarenbeek et al. 2015), and their small size provides therapeutic potentials.

Briefly, Pardon et al. (2014) outlined buffy coat RNA isolation and immune library construction via phage display (Figure 6.2). Camelid species generate robust HCAb responses after vaccination and several boosts. After the 6th or 7th boost, isolated buffy coat RNA contains HCAb mRNA which can be used to generate an immune library. Cloning VHH specific sequences into a phage display vector, followed by phage packaging and panning, can lead to identifying specific clones which produce HCAb against your targeted immunogen. After inducing protein expression and purifying putative clones, one can test specificity. Further, comparing sequence homology between clones can reveal whether these clones derived from the same B cell lineage.

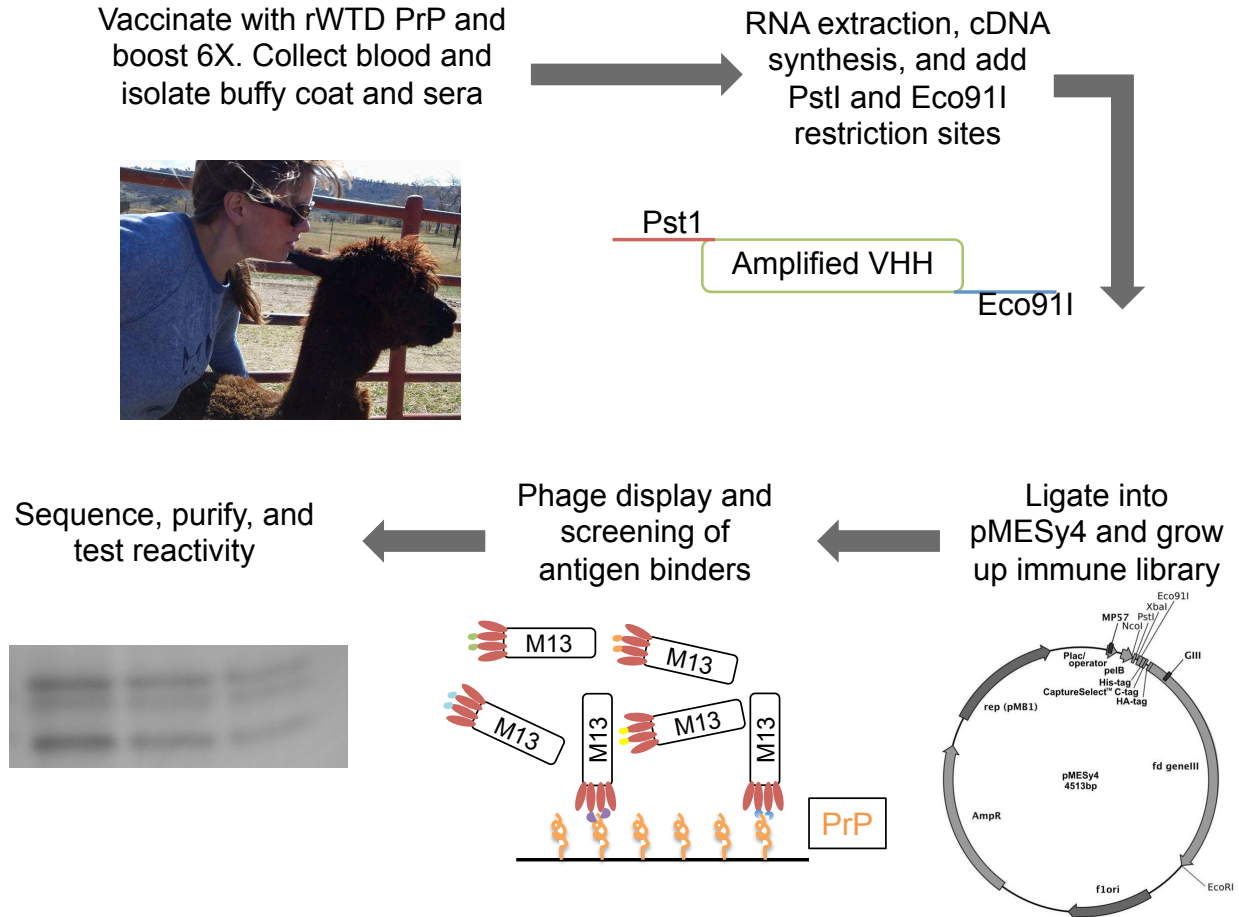


Figure 6.2. Nanobody library construction experimental design. Camelid species, such as alpacas, generate a robust antibody response after vaccination with recombinant white-tailed deer PrP (rWTD) and multiple boosts. Lymphocyte-concentrated blood fraction, termed buffy coat, contains antibody-producing B cells. RNA extracted from buffy coats contain PrP-specific nanobody transcripts. These sequences are reverse transcribed into cDNA, and VHH sequences are PCR-amplified to contain restriction enzyme sites. Using these restriction sites, nanobody-specific sequences are ligated into a phage display vector. This library is packaged into M13 helper phage, and antigen binders are selected after multiple pans of phage display. Putative clones are sequenced, purified, and screened for specificity.

Data presented in this chapter aimed to generate an immune library and clone nanobodies from an alpaca vaccinated with recombinant PrP (rPrP). While we encountered difficulties in immune library efficiency, we identified 12 clones which specifically recognize PrP. We screened 4 of the 12 potential candidate clones, and

present data which suggests two clones generate nanobodies which preferentially recognize infectious forms of PrP.

Materials and Methods

Alpacas. Alpacas were maintained by Dr. Dick Bowen at Colorado State University and accredited by the Association for Assessment and Accreditation of Lab Animal Care International and approved on January 14, 2016 by the Institutional Animal Care and Use Committee at Colorado State University (Protocol ID: 09-1580A). Alpacas were vaccinated and bled from the jugular vein by Dr. Valerie Johnson or Dr. Danielle Adney. A current graduate student in the Zabel laboratory, Savannah Rocha, extracted buffy coat RNA, reverse-transcribed RNA into cDNA, and amplified VHH-specific cDNA molecules via PCR. In a nested PCR reaction, Pst1 and Eco91I restriction sites were added to the ends of amplified VHH sequences (see her future dissertation for details). The following methods were performed as outlined in Pardon et al. (2014).

Seroconversion test via western blotting. To confirm a humoral response against the recombinant PrP vaccine, serum diluted 1:500 was probed against purified immunogen ran via western blotting. A polyclonal anti-camel antibody conjugated to HRP was used as the secondary antibody, and images were obtained after addition of chemiilluminiscent substrate. Savannah Rocha tested serum via ELISA under my supervision, and obtained a 120,000 reciprocal titer (data not shown). However, serum was highly reactive to *Prnp*-/- brain homogenate via western blotting (data not shown),

and we did not obtain observable differences between knockout and PrP^C-expressing brain homogenates via western blotting.

Immune library cloning. VHH-specific cDNA sequences with PstI/Eco91I recognition sequences were ligated into phage display vector pMESy4. pMESy4 (10 µg purified plasmid) was digested in a 250 µL reaction containing PstI, Eco91I, and XbaI. At the same time, amplified PCR product (3 µg) was digested in a 100 µL reaction with PstI and Eco91I. Test ligations with 30 ng of digested product ligated into 100 ng digested vector (3:1 molar ratio) and electroporated in TG1 cells yielded lower efficiency than outlined in Pardon et al. (2014). To determine ligation and amplification efficiency, individual colonies were suspended in 50 µL DEPC water and screened for nanobody insert via PCR using MP57 (5' TTATGCTTCCGGCTCGTATG 3') and GIII (5' CCACAGACAGCCCTCATAG 3') primers. The majority did not contain the proper sized insert. Therefore, we performed a large-scale ligation with a 6:1 molar ratio of product:vector in order to maximize the number of transformants in the immune library. The ligation products were purified with a PCR purification kit and electroporated into TG1 cells. Recovered cells (100 µL of 8 mL total) were diluted to determine effective library size, and the remaining cells were grown on large square (245 mm x 245 x 25 mm) bioassay dishes containing LB agar with 100 µg/mL ampicillin and 2% glucose. The immune library was recovered by adding 4 mL LB onto the plate and combining all colonies using a scraper. OD₆₀₀ values were obtained, and glycerol (20% v/v) stocks were made and stored at -80°C.

Phage packaging, amplification, and titering. Six OD₆₀₀ units of immune library glycerol stocks were grown at 37°C and 200 rpm to logarithmic phase in 60 mL 2X TY media containing 100 µg/mL ampicillin and 2% glucose. Culture was divided up into 10 mL aliquots and superinfected with ~10X phage: TG1 ratio, equating to 4x10¹⁰ plaque forming units (pfus) of M13 helper phage. Cells were incubated without shaking for 30 minutes at 37°C and centrifuged at 3,000 x g for 10 minutes. Pellets were resuspended in 50 mL 2X TY containing 100 µg/mL ampicillin and 25 µg/mL kanamycin and grown overnight at 37°C. Cultures were centrifuged at 3,000 x g for 20 minutes, and phage-containing supernatant (40 mL) was transferred to a fresh tube. Phage was precipitated by adding 10 mL 20% PEG6000 and 2.5M NaCl, inverting five times, and sitting on ice for 30 minutes. Precipitated phage particles were pelleted at 3,200 x g for 10 minutes at 4°C. Supernatant was discarded in bleach, and any remaining liquid on the pellet was removed by gently inverting the tubes over kim-wipes. Phage particles were resuspended in 1 mL ice-cold PBS and centrifuged at 20,000 x g at 4°C for 1 minute in a microcentrifuge (Telling lab) to pellet remaining bacteria. Supernatant was transferred to a fresh tube. Phage was re-precipitated by adding 250 µL PEG/NaCl buffer (above) to the supernatant, and tubes were inverted 10 times and sat on ice for 10 minutes. Phage was pelleted at 20,000 x g at 4°C for 15 minutes, and the supernatant was removed. Phage was resuspended in 1X PBS and centrifuged for 1 minute to remove any remaining bacterial cells. Supernatant containing amplified phage was titered in logarithmic-phase TG1 cells. Briefly, 90 µL logarithmic-phase TG1 cells were infected with 10 µL phage dilution, and 5 µL was plated on LB agar plates containing 100 µg/mL ampicillin and 2% glucose.

Phage panning to identify target-binders. To enrich phage particles which specifically bind PrP, we coated 1 µg recombinant white tailed deer PrP or Superblock on a microtiter plate (Nunc) in carbonate/bicarbonate buffer (SIGMA) at 4°C for 24+ hours and was washed with PBST (0.05% Tween 20). Note that pilot experiments included nonfat dry milk instead of Superblock as a negative control, but Superblock was determined to bind less phage particles nonspecifically. Further, we also employed various conformational tests, such as capturing PrP after coating anti-PrP (BAR224) antibody to the plate or first coating poly D-lysine. However, the final clones identified were screened against PrP coated to the microtiter plate. PrP-coated microtiter plates were blocked in 250 µL 2% NFDM (“blocking buffer”). Per selection or control well, 10¹¹ pre-packaged phage was pre-incubated with 10 µL blocking buffer and 100 µL PBS and was mixed by head-over-head rotation for 30 minutes. 100 µL of phage was incubated on PrP-coated wells for 2 hours at 700 rpm. Phage was removed by pipetting, and wells were washed 15 times with 250 µL PBST. Phage was trypsinized and transferred to microcentrifuge tubes containing PMSF to halt trypsin activity. Phage was titered as described above. Glycerol stocks were generated by infecting exponential-phase TG1 cells with 50 µL trypsinized phage and grown overnight in LB containing 100 µg/mL ampicillin and 2% glucose (“sublibrary”). Glycerol stocks were stored at -80°C. Subsequent rounds of panning further enriched the phage display library to select for clones which specifically recognize PrP. Glycerol stocks (500 µL) were grown to logarithmic growth, infected with phage, precipitated, etc, as described above.

Immune library master plate generation and analysis. Various dilutions of sublibrary cultures were plated on selective agar medium and grown for ~16 hours at 37°C. Individual colonies (96) were inoculated into each well of a 96-well round-bottom culture plate containing 100 µL 2X TY medium containing 100 µg/mL ampicillin, 2% glucose, and 10% glycerol. One well was inoculated with a Superblock-panned control, and one well was not inoculated with a colony. This master plate was grown overnight at 37°C without shaking. To obtain periplasmic extracts to screen via ELISA, 10 µL of the master plate was inoculated into medium, sealed with a gas-permeable screen, and grown for 3 hours at 37°C with shaking. IPTG addition (100 µL of 10 mM solution) induced nanobody expression, and the plate was shook at 37°C and 200 rpm for 4 hours. Cells were pelleted at 3,200 x g for 10 minutes, supernatants were discarded, and cells were lysed by freezing dry pellets at -20°C for 30 minutes. The plate was thawed at room temperature for 15 minutes, and pellets were resuspended in 100 µL PBS. Periplasmic extract (1:5) reactivity was screened via ELISA.

Nanobody specificity analysis. Soluble nanobodies were expressed in *E. coli* strain BL21. First, small amounts of A2, A9, B10, and B11 (identified by highest periplasmic extract reactivity) from master plate wells were scraped into selective LB medium and grown overnight. Plasmid was extracted using manufacturer's instructions. Plasmid was transformed into BL21 cells, and individual colonies were grown overnight in 10 mL LB containing 100 µg/mL ampicillin, 2% glucose and 1 mM MgCl₂. The next day, 3 mL of culture was inoculated into 330 mL TB media containing 100 µg/mL ampicillin, 0.1% glucose, and 1 mM MgCl₂ until O.D.₆₀₀ = 0.7. Nanobody expression was induced by

addition of 1 mM IPTG. After induction, cultures were centrifuged for 15 minutes at 9,000 x g. Pellets were resuspended in 15 mL ice-cold TES, incubated for 1 hr, and 30 mL TES/4 was added and incubated for 45 minutes. Periplasmic extract was collected after pelleting cellular debris for 30 minutes at 10,000 x g and 4°C. The His-tagged nanobodies were purified on an IMAC column per the manufacturer's instructions. We biotinylated the purified nanobodies, and screened for specificity via western blotting and ELISA using streptavidin conjugated to HRP for nanobody detection.

Nanobody sequence analysis. Clones A2, A9, A10, A12, B7, B8, B10, B11, C2, and E10 from master plate were grown up, and plasmid was purified according to the manufacturer's instructions. Plasmid and MP57 and GIII primers were sent to and sequenced by QuintaraBio. All sequence analysis, including alignments and protein translation, was performed using Serial Cloner software. Sequences from Schoonaert et al. (2017) were used to identify complementarity determining region number 3 (CDR3) sequences in the master plate nanobody sequences, and protein alignments were performed using Serial Cloner software.

Results

Robust alpaca seroconversion after vaccination and boosts. We tested immunoreactivity against purified immunogen via western blot (Figure 6.3). A serum dilution of 1:500 used as the primary antibody source was so reactive, one could see the chemiluminescent reaction develop with the naked eye. Future experiments should use much more dilute serum. Indeed, another researcher determined the serum to

contain a 120,000 reciprocal titer via ELISA (data not shown; generated by another researcher).

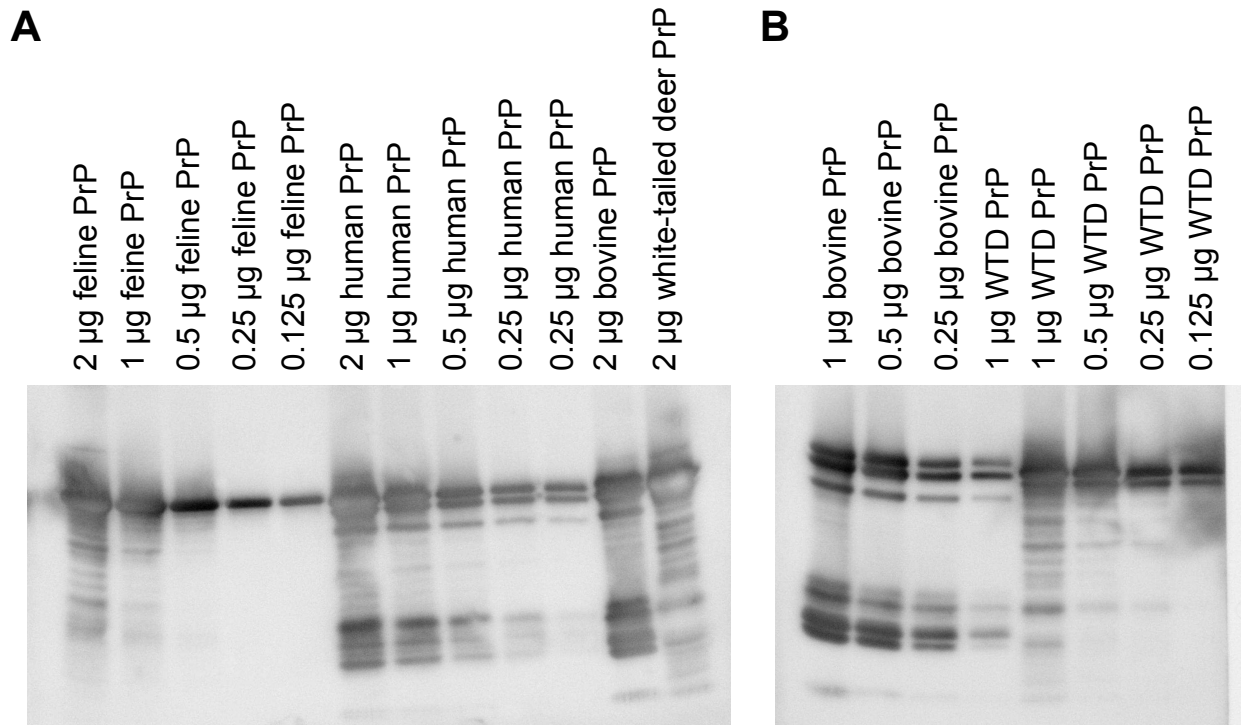


Figure 6.3. Alpaca serum contains highly-reactive antibodies after the 6th boost. Western blotting analysis reveal robust seroconversion after vaccination and boosts. Sera (1:500 dilution) detected purified recombinant PrP from various species (WTD: white-tailed deer). These particular western blots were so saturated, one could see the chemiluminescent reaction by the naked eye directly after substrate addition.

Cloning scheme for phage display. After determining the alpaca did indeed generate a robust antibody response, a fellow researcher extracted buffy-coat RNA, reverse transcribed into cDNA, and PCR-amplified VHH sequences to contain restriction enzyme sites (see Figure 6.2). These sequences were ligated into the pMESy4 phage display vector (Figure 6.4A). Briefly, the vector was cut with PstI, Eco91I, and XbaI, and the amplified PCR product was cut with PstI and Eco91I.

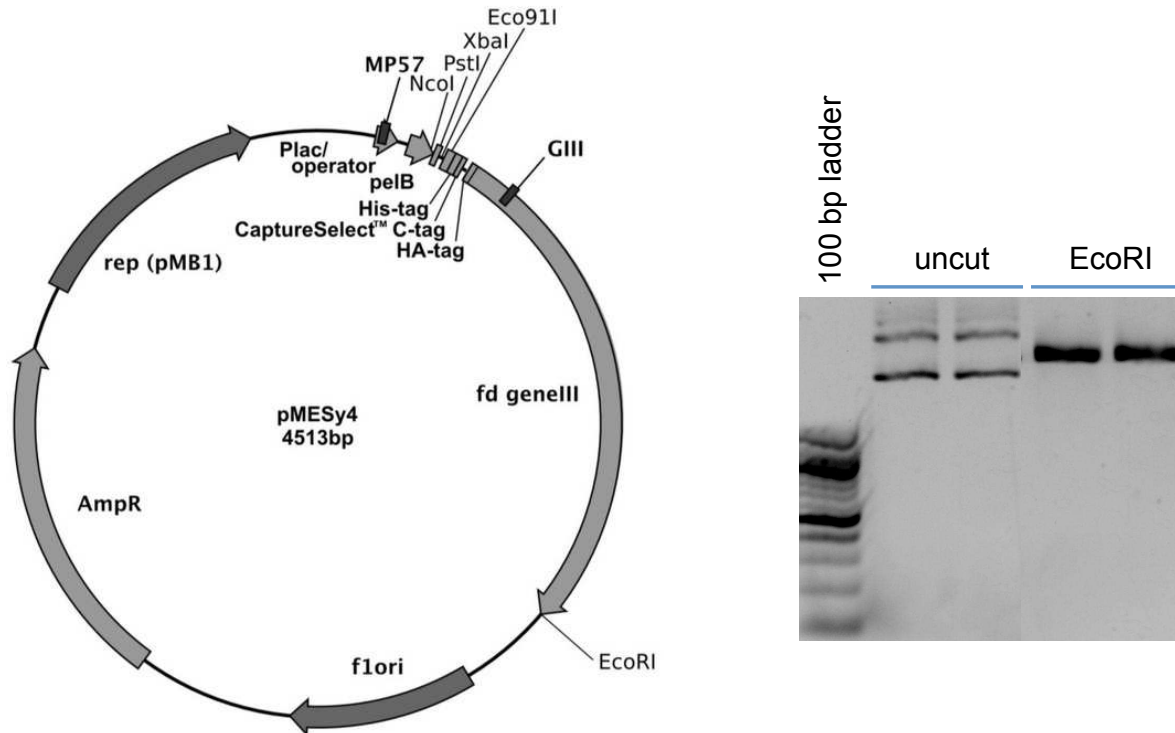


Figure 6.4. Phage display vector pMESy4 vector map and analysis. Nanobody-encoding VHH sequences are ligated into phage display vector map pMESy4 (left). We electroporated purified pMESy4 into TG1 cells, grew up, and purified plasmid. Agarose gel electrophoresis showed plasmid integrity and restriction enzyme site integrity (right).

Low percentage of nanobody-specific clones. PCR-amplified VHH sequences were ligated into pMESy4 at a 3:1 insert:vector molar ratio. Initial test screens reveal a small proportion of clones contained intact nanobody insert using MP57 and GIII primers (Figure 6.5). We hypothesize a number of nanobody sequences contained restriction-enzyme sites within the ligated VHH sequence. Thus, a digested, shorter sequence would be ligated into the vector. Indeed, it appears many clones contained shorter amplified sequences (Figure 6.5B).

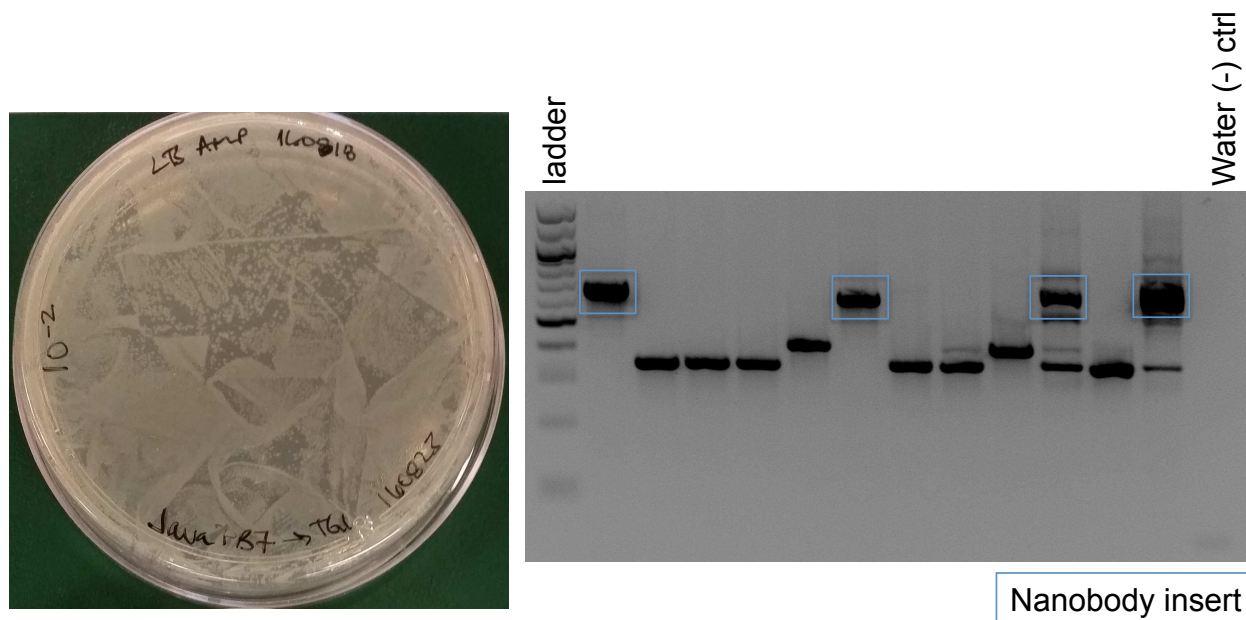


Figure 6.5. Initial screens show low percentage of clones containing true nanobody inserts. We performed a small-scale ligation and tested individual clones for nanobody-specific sequences. Digested insert was ligated into digested vector (3:1 insert:vector molar ratio) and electroporated into TG1 cells and plated on LB/Ampicillin agar plates (left). Individual colonies were screened for nanobody insert using MP57 and GIII primers (right). Each lane represents one clone, and bands highlighted with a blue box represent clones with true nanobody insert (~700bp).

Large-scale immune library construction. Pardon et al. (2014) described an efficient library containing 10^7 positive clones. Considering the small-scale test ligation showed less than 75% of clones contained true nanobody (Figure 6.5), we increased the molar concentration of insert:vector to 6:1 instead of 3:1. However, despite this change, we generated a less-than-ideal library, which we calculated to be 1.14×10^5 CFU/mL. We generated 3 mL of this library (or 342,000 total clones), equating to roughly 20-times less than the ideal library outlined in Pardon et al. (2014). However, we obtained a high phage titer (4.0×10^{12} CFU/mL, Figure 6.6C) after growing up and infecting the immune library stock.

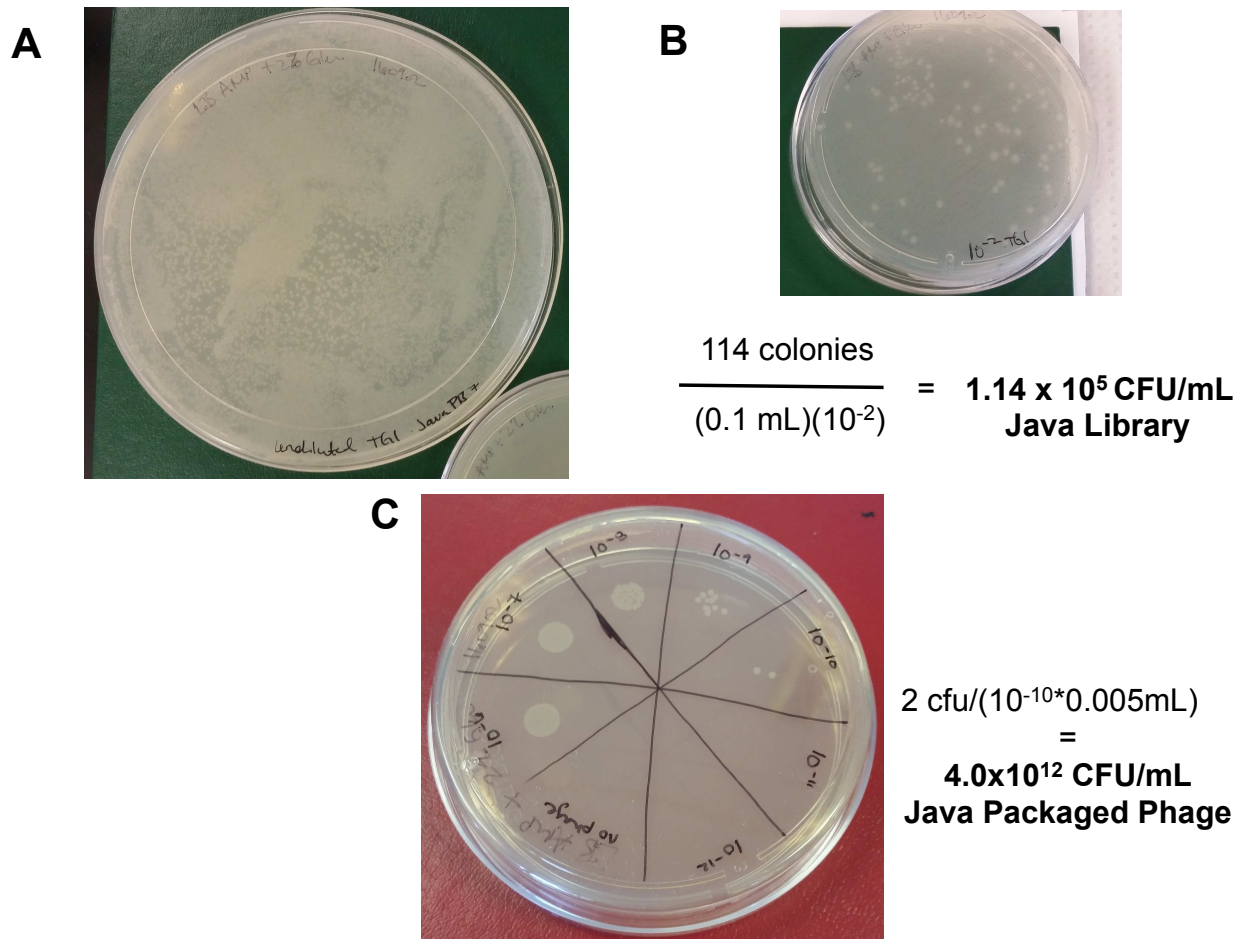


Figure 6.6. Large-scale library production and phage packaging. Due to the ligation test run inefficiency (Figure 6.5), we increased the insert:vector ratio to 6:1 and generated a library of 1.14×10^5 CFU/mL (A,B). We grew 6 OD⁶⁰⁰ units of immune library (A) to logarithmic phase and super-infected with M13 helper phage. Amplified and precipitated phage was titered in naïve TG1 cells (C) and generated a high titer of 4×10^{12} CFU/mL. Note this titering protocol outlined in Pardon et al. (2014) differs from traditional phage titering with plaque forming unit (pfu) readout. Therefore, titers are reported as CFU instead of PFU.

Phage-panning round 1. To enrich PrP-recognizing phage particles, we panned library phage particles (Figure 6.6) on a microtiter plate coated with recombinant WTD PrP or Superblock negative control. Pilot experiments also employed use of poly-D-lysine, capture antibody BAR224, or nonfat dry milk, although we observed a great deal of nonspecific binding, and thus chose to continue experiments with PrP or Superblock

alone. The first panning round did not show a difference between phage panned on PrP or negative controls (Figure 6.7). Therefore, we employed a second round of panning from phage particles grown up and precipitated from the first round (Figure 6.8). Phage panned on Superblock in round 1 did indeed positively pan on Superblock in round 2 (Figure 6.8), suggesting some immune library clones cross-react with the negative control Superblock. However, we obtained undefined enrichment between phage particles panned on PrP in round 1 panned on PrP or Superblock in round 2. Therefore, we did not continue subsequent rounds of panning in order to maintain library diversity.

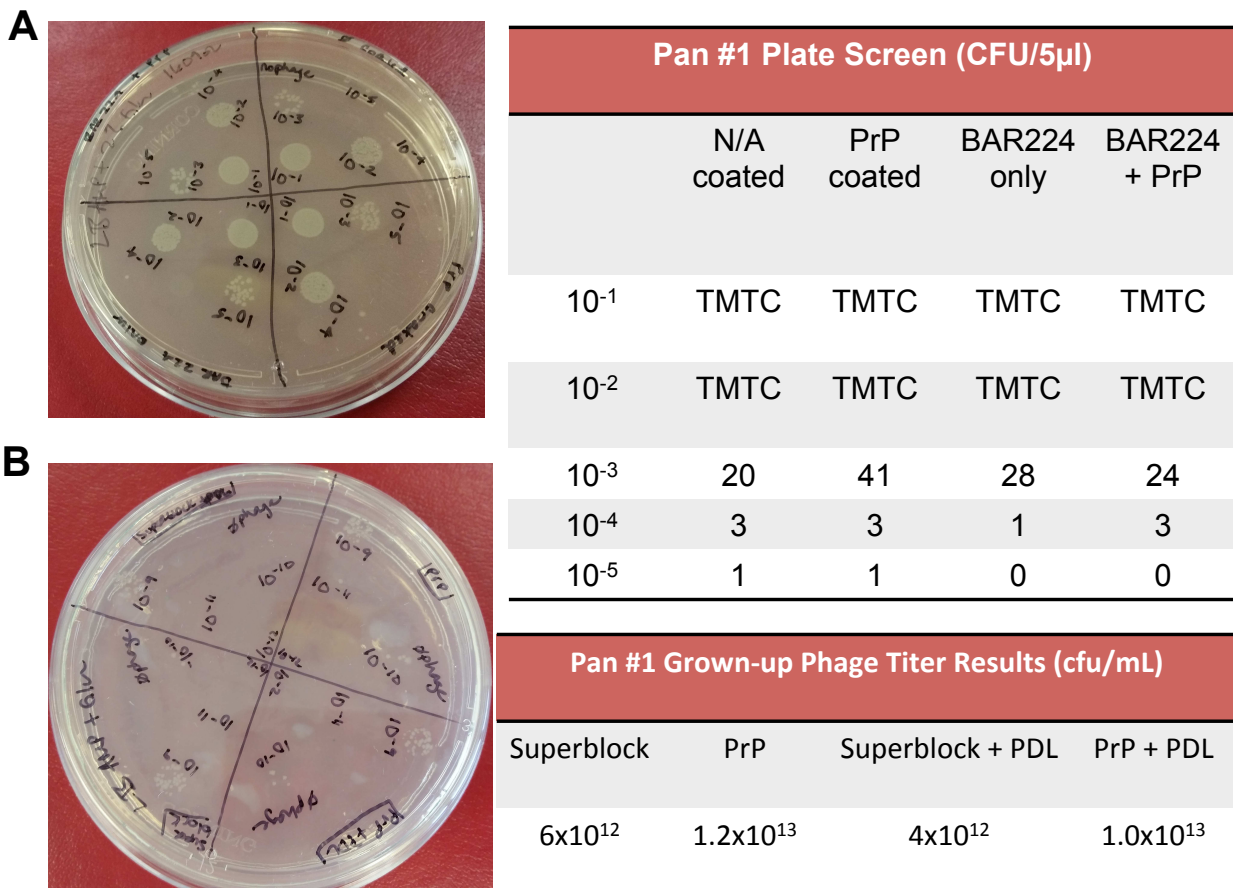


Figure 6.7. Phage panning round 1. To enrich phage particles which specifically recognize PrP, we panned phage particles from Figure 6.5C onto various conditions. We did not observe a difference between phage panned on PrP or the various negative controls (A). These data suggested a subsequent round of panning was required to

further enrich PrP-specific clones. We therefore grew up, precipitated, and titered phage (B) as previous.

A



Pan #2 Plate Screen (CFU/5 μ l)			
	SB phage panned SB	PrP phage panned on SB	PrP phage panned on PrP
10^{-1}	3	0	13
10^{-2}	0	0	3
10^{-3}	0	0	0

B

PrP-specific phage
panned on PrP
O.D. 0.9168



PrP-specific phage
panned on Superblock
O.D. 0.0251



Figure 6.8. Phage panning number 2 enriched specificity by an undefined amount. M13 helper phage amplified and precipitated from pan number 1 (Figure 6.7) was subsequently panned to enrich PrP-reactive clones. The number of colonies reduced as expected after subsequent panning rounds (A). Strikingly, phage particles panned on PrP were highly specific to PrP because panning on superblock did not yield any colonies (A), and the culture lacked turbidity after overnight growth (B). However, the immune library did contain phage which recognizes Superblock, because phage panned on Superblock in round 1 continued to recognize Superblock in round 2.

Master plate analysis. We infected TG1 cells with phage derived from the second round of phage panning (Figure 6.8) and allowed them to grow overnight. This overnight-grown culture was homogenously spread across selective medium, and individual colonies were inoculated into a 96 well plate containing media (“master plate”). Each

well (“clone”) was screened for nanobody insert via PCR with MP57 and GIII primers (Figure 6.9A). We observed 22 clones expressed the appropriately sized nanobody insert (Figure 6.9A), and periplasmic extract derived from these clones were assessed for PrP reactivity via ELISA. Four clones, A2, A9, B10, and B11, showed the highest reactivity with PrP (Figure 6.9B). Thus, we expressed and purified those nanobodies in BL21 cells to test using other biochemical techniques. However, the yield was lower than anticipated (Figure 6.9C). Therefore, future directions could involve transforming *E. coli* strain WK6 to generate higher quantities of soluble nanobody.

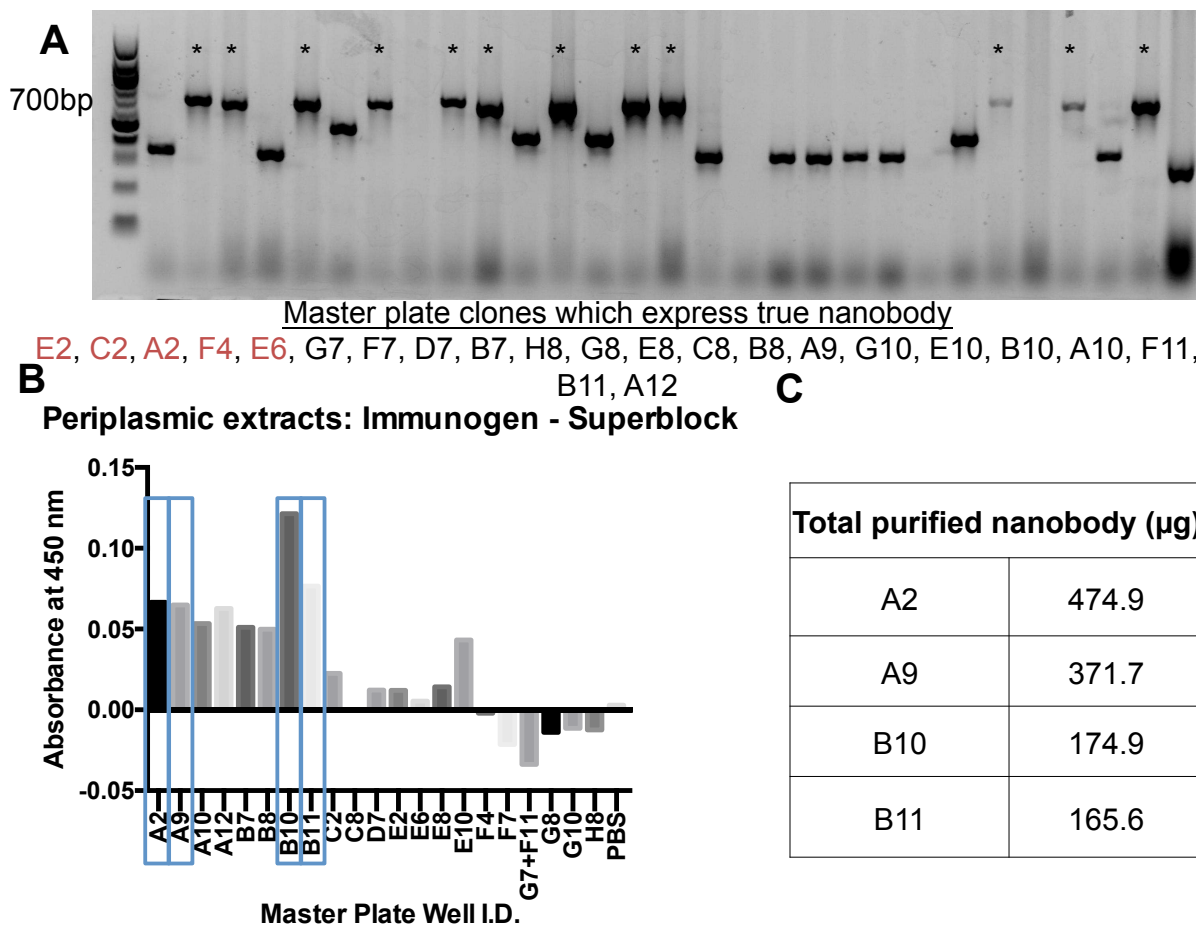


Figure 6.9. Library master plate analysis. Individual clones were screened for true nanobody insert using MP57 and GIII primers via PCR (A). Clones with asterisks (*)

contain the appropriately sized nanobody insert. Periplasmic extract (1:5) from these clones were screened for PrP reactivity via ELISA (B). We chose the four highest-reactive clones (blue boxes) to grow up, purify, (C) and screen via other biochemical techniques.

CDR3 sequence analysis. Pardon et al. (2014) grouped clones from the same B cell lineage based on level of CDR3 homology. If two CDR3 regions are the same length and share over 80% homology, they likely derived from the same B cell lineage and thus likely recognize the same epitope. We purified and sequenced plasmids from the 10 clones which reacted to PrP (Figure 6.8B) and analyzed the CDR3 homology using Serial Cloner. Briefly, we translated the nanobody sequence and identified CDR3 amino acids by comparing the framework sequences obtained from Schoonaert et al. (2017). We then performed each pairwise comparison and attempted to group clones which arise from the same B cell lineage. Comparisons highlighted in orange fit the parameters outlined in Pardon et al. (2014). Comparisons highlighted in green (**) likely do arise from the same B cell lineage, although the framework identification may have been shifted by one amino acid. Importantly, certain comparisons (*) may show high homology even though only a few amino acids aligned with each other. These comparisons should be ignored.

	A2	A9	A10	A12	B7	B8	B10	B11	C2	E10
A2		85*	77	71	71	70	63	100*	80	85*
A9			83	71	75	79	100*	78	100*	100*
A10				50	100*	67	85**	80*	100*	69
A12					80*	67	50	86*	71	100*
B7						63	100*	50	100*	88*
B8							67	75	67	73
B10								67	100*	100*
B11									100*	100*
C2										85**
E10										

Figure 6.10. CDR3 sequence homology analysis. Pardon et al. (2014) defined clones with CDR3 sequences with 80%+ sequence homology and identical length to derive from the same B cell lineage and likely share epitope binding domains. These homologous comparisons are highlighted in orange. Alignments highlighted in green represent comparisons which likely share the same B cell lineage, but either had one deleted amino acid in the middle and/or contained one N or C terminal additional amino acid. Comparisons with asterisks (*) are above 80% homology, yet are not the same length. For example, a 100%* comparison could have one or two aligned amino acids in the middle, but the other amino acids are not homologous.

Two clones may preferentially bind infectious brain homogenate. Based on periplasmic reactivity to recombinant PrP (Figure 6.9B), we selected four clones: A2, A9, B10, and B11 to make large batches of recombinant nanobodies in *E. coli* BL21 cells. We first

tested reactivity to purified immunogen loaded via western blotting (Figure 6.11A), and indeed observe signal from all nanobodies tested. However, these nanobodies nonspecifically bind various brain proteins via western blotting (data not shown), and we did not observe signal in PK-treated samples, indicating these nanobodies either: do not recognize PrP in the PK-resistant core or they preferentially recognize 3D epitopes which are only revealed in non-denatured forms. Indeed, we provide evidence of the latter because we observe higher reactivity in brains which express PrP than in PrP KO brain via ELISA (Figure 6.11C).

Surprisingly, however, we were unable to observe discernable difference in PrP signal via flow cytometry (Figure 6.11B). These data suggest either: these nanobodies do not recognize mouse prion protein, or perhaps they specifically recognize infectious prions. While we observed background signal in PrP KO brain via ELISA with most of the clones, we obtained promising data from clones A9 and B11. A9 appears to specifically recognize infected brain (RML5 or E2), and B11 appears to specifically recognize elk PrP, both from infected and non-infected brain. However, non-infected brains were homogenized with buffer containing Triton X-100 (NBH), whereas infected brains (RML5 or E2) were homogenized in PBS only. Future directions should involve comparing infected to non-infected when the homogenates are prepared with the same buffers.

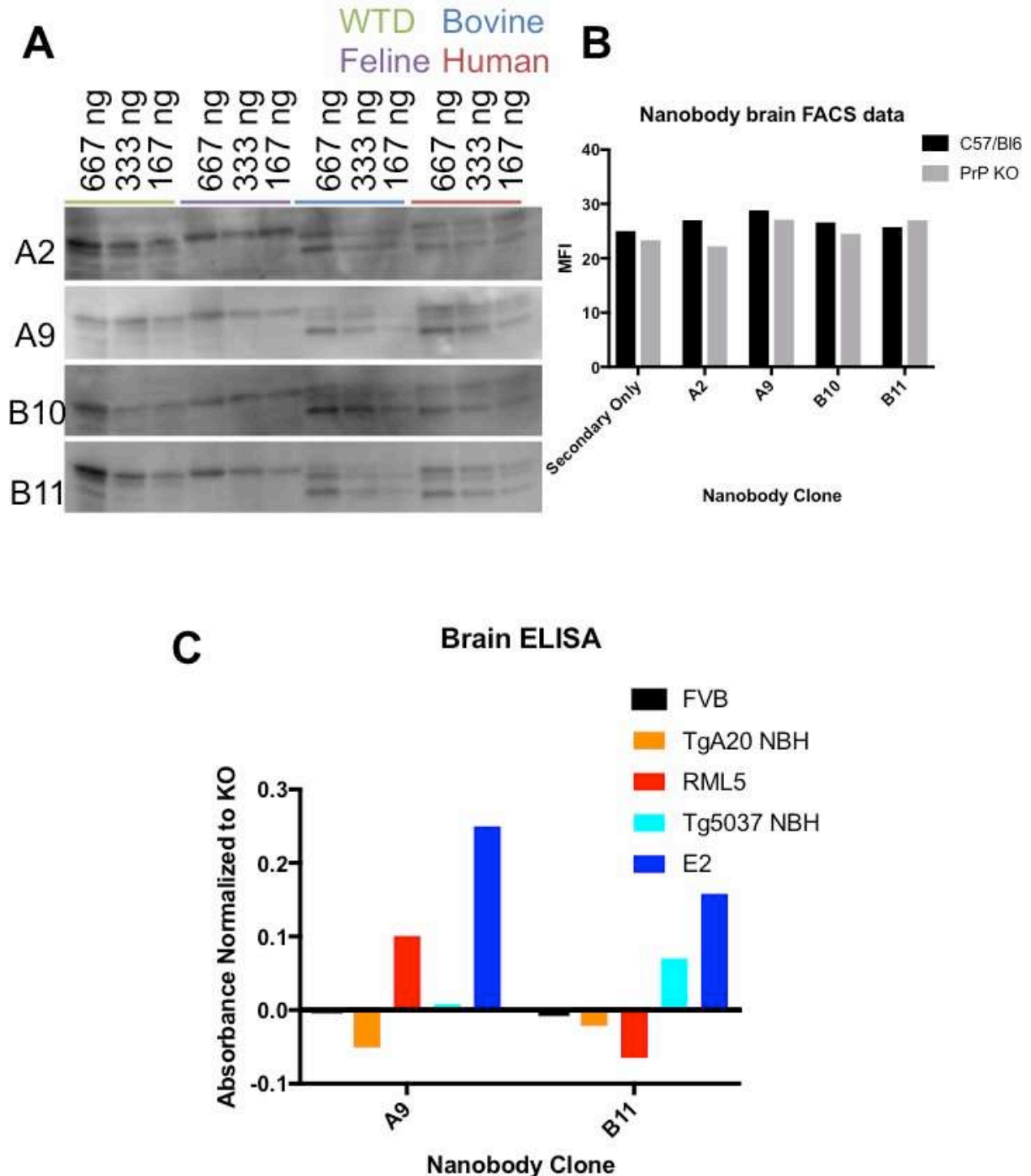


Figure 6.11. Two positive clones may specifically recognize infected brain. We chose clones A2, A9, B10, and B11 to purify and test for specificity. While all four clones recognize purified recombinant PrP from various species via western blotting (A), we observe little nanobody signal differences between wild type and PrP KO mouse brains via flow cytometry (B). However, A9 appears to preferentially bind infected brain (RML5: mouse-adapted scrapie; E2: chronic wasting disease isolate E2), and B11 appears to be cervid specific (Tg5037: transgenic mice expressing elk PrP)

Discussion

Nanobodies could function to delay prion disease in a number of ways. Nanobodies may bind prions and render them innocuous. For example, nanobodies could bind prions and prevent the PrP^C:prion interaction. Alternatively, nanobodies could bind PrP^C, perhaps promote internalization, and thus reduce prion substrate (PrP^C) needed for propagation. However, future studies on whether nanobodies induce internalization are required. Lastly, similarly to Domanska et al. (2011), one could engineer nanobodies which bind domain(s) important for amyloidogenesis. Perhaps such a nanobody could bind PrP^C and limit or prevent conversion to PrP^{Sc}. However, future studies are required to determine if nanobodies generated in this chapter prevent fibrillation. As discussed previously, PrP^C spontaneously aggregates with shaking and low pH. One could incubate the enclosed nanobodies with PrP^C under aggregation-prone conditions and determine whether nanobodies limit the generation of PK-resistant aggregates. If so, translating these findings *in vivo* may limit or prevent the onset of prion disease.

Recently, Ilijina et al (2017) reported nanobodies inhibit alpha-synuclein fibrillation. Specifically, incubating alpha-synuclein oligomers with two nanobody clones, NbSyn2 and NbSyn87, resulted in fewer fibrils, as well as increased sensitivity to PK digestion. Perhaps nanobodies against both PrP^C and infectious prions (similarly to clone B11), may prevent the PrP^C:PrP^{Sc} interaction and thus delay or prevent prion propagation. We would also like to test the hypothesis nanobody clone A9 specifically recognizes infectious prions only. Testing differences (if any) between outcome after treatment with

A9 or B11 may help determine whether targeting PrP^C or the misfolded form is most promising for combating prion disease. Previous studies suggest targeting PrP^C, either transiently or permanently, could reduce the substrate needed for prion propagation and thus delay disease. However, these treatments would eliminate the normal function of PrP^C as discussed in Chapter 5. For example, targeting PrP^C may render a patient immunosuppressed. Therefore, we suggest targeting misfolded prions instead of PrP^C. We believe nanobodies, such as clone A9, could provide such an avenue. Future directions could involve testing the capacity of B11 or A9 to prevent *in vitro* fibrillation and/or prion disease *in vivo*.

The concept of prion strains emerged after Bessen and Marsh (1992) reported differential clinical outcomes after inoculation with transmissible mink encephalopathy (TME). The two prion strains, termed hyper (HY) or drowsy (DY) TME, are manifested with shorter incubation times and hyperactive behavior versus long incubation times and lethargic behavior, respectively. Further, work from the Telling lab suggests chronic wasting disease prions may exhibit strain-like behavior. Certain CWD prions exhibit differential histological patterns, such as bilateral or unilateral hemisphere deposition, yet exhibit nearly identical resistance to chemical denaturation (Angers et al. 2010). The strain phenomenon remains elusive. We hypothesize strains arise from different conformations of PrP^{Sc}. Therefore, one could utilize nanobodies to probe for conformational differences between prion strains. If so, one could use nanobodies to diagnose and/or ascertain strain prevalence.

In summary, data presented in this chapter aimed to generate alpaca-derived nanobodies. These nanobodies may provide useful for understanding structural differences between prions, as well as potentially used to inhibit prion formation *in vitro* and *in vivo*. Future directions include epitope mapping, fibrillation assays with or without nanobodies, as well as testing whether these nanobodies limit or prevent prion propagation *in vivo*. With the ability to cross the BBB, we propose nanobodies are viable tools to combat various neurological diseases and disorders.

REFERENCES

Angers RC, Kang HE, Napier D, Browning S, Seward T, Mathiason C, Balachandran A, McKenzie D, Castilla J, Soto C, Jewell J, Graham C, Hoover EA, Telling GC. Prion strain mutation determined by prion protein conformational compatibility and primary structure. *Science*. 2010 May 28;328(5982):1154-8. doi: 10.1126/science.1187107. Epub 2010 May 13. PubMed PMID: 20466881; PubMed Central PMCID: PMC4097672.

Arbabi Ghahroudi M, Desmyter A, Wyns L, Hamers R, Muyldermans S. Selection and identification of single domain antibody fragments from camel heavy-chain antibodies. *FEBS Lett*. 1997 Sep 15;414(3):521-6. PubMed PMID: 9323027.

Bessen RA, Marsh RF. Identification of two biologically distinct strains of transmissible mink encephalopathy in hamsters. *J Gen Virol*. 1992 Feb;73 (Pt 2):329-34. PubMed PMID: 1531675.

Domanska K, Vanderhaegen S, Srinivasan V, Pardon E, Dupeux F, Marquez JA, Giorgetti S, Stoppini M, Wyns L, Bellotti V, Steyaert J. Atomic structure of a nanobody-trapped domain-swapped dimer of an amyloidogenic beta2-microglobulin variant. *Proc Natl Acad Sci U S A*. 2011 Jan 25;108(4):1314-9. doi: 10.1073/pnas.1008560108. Epub 2011 Jan 10. PubMed PMID: 21220305; PubMed Central PMCID: PMC3029709.

Guilliams T, El-Turk F, Buell AK, O'Day EM, Aprile FA, Esbjörner EK, Vendruscolo M, Cremades N, Pardon E, Wyns L, Welland ME, Steyaert J, Christodoulou J, Dobson CM, De Genst E. Nanobodies raised against monomeric α -synuclein distinguish between fibrils at different maturation stages. *J Mol Biol*. 2013 Jul 24;425(14):2397-411. doi: 10.1016/j.jmb.2013.01.040. Epub 2013 Apr 1. PubMed PMID: 23557833.

Ibañez LI, De Filette M, Hultberg A, Verrips T, Temperton N, Weiss RA, Vandeveldel W, Schepens B, Vanlandschoot P, Saelens X. Nanobodies with in vitro neutralizing activity protect mice against H5N1 influenza virus infection. *J Infect Dis*. 2011 Apr 15;203(8):1063-72. doi: 10.1093/infdis/jiq168. PubMed PMID: 21450996.

Klarenbeek A, El Mazouari K, Desmyter A, Blanchetot C, Hultberg A, de Jonge N, Roovers RC, Cambillau C, Spinelli S, Del-Favero J, Verrips T, de Haard HJ, Achour I. Camelid Ig V genes reveal significant human homology not seen in therapeutic target genes, providing for a powerful therapeutic antibody platform. *MAbs*. 2015;7(4):693-706. doi: 10.1080/19420862.2015.1046648. PubMed PMID: 26018625; PubMed Central PMCID: PMC4622956.

Li JW, Xia L, Su Y, Liu H, Xia X, Lu Q, Yang C, Reheman K. Molecular imprint of enzyme active site by camel nanobodies: rapid and efficient approach to produce abzymes with alliinase activity. *J Biol Chem*. 2012 Apr 20;287(17):13713-21. doi:

10.1074/jbc.M111.336370. Epub 2012 Feb 28. PubMed PMID: 22374998; PubMed Central PMCID: PMC3340132.

Li T, Bourgeois JP, Celli S, Glacial F, Le Sourd AM, Mecheri S, Weksler B, Romero I, Couraud PO, Rougeon F, Lafaye P. Cell-penetrating anti-GFAP VHH and corresponding fluorescent fusion protein VHH-GFP spontaneously cross the blood-brain barrier and specifically recognize astrocytes: application to brain imaging. *FASEB J*. 2012 Oct;26(10):3969-79. doi: 10.1096/fj.11-201384. Epub 2012 Jun 22. PubMed PMID: 22730440.

Padlan EA. Anatomy of the antibody molecule. *Mol Immunol*. 1994 Feb;31(3):169-217. Review. PubMed PMID: 8114766.

Pain C, Dumont J, Dumoulin M. Camelid single-domain antibody fragments: Uses and prospects to investigate protein misfolding and aggregation, and to treat diseases associated with these phenomena. *Biochimie*. 2015 Apr;111:82-106. doi: 10.1016/j.biochi.2015.01.012. Epub 2015 Feb 3. Review. PubMed PMID: 25656912.

Pardon E, Laeremans T, Triest S, Rasmussen SG, Wohlkönig A, Ruf A, Muyldermans S, Hol WG, Kobilka BK, Steyaert J. A general protocol for the generation of Nanobodies for structural biology. *Nat Protoc*. 2014 Mar;9(3):674-93. doi: 10.1038/nprot.2014.039. Epub 2014 Feb 27. PubMed PMID: 24577359; PubMed Central PMCID: PMC4297639.

Schoonaert L, Rué L, Roucourt B, Timmers M, Little S, Chávez-Gutiérrez L, Dewilde M, Joyce P, Curnock A, Weber P, Hausteraete J, Hassanzadeh-Ghassabeh G, De Strooper B, Van Den Bosch L, Van Damme P, Lemmens R, Robberecht W. Identification and characterization of Nanobodies targeting the EphA4 receptor. *J Biol Chem*. 2017 Jul 7;292(27):11452-11465. doi: 10.1074/jbc.M116.774141. Epub 2017 May 19. PubMed PMID: 28526745; PubMed Central PMCID: PMC5500810.

van der Linden RH, Frenken LG, de Geus B, Harmsen MM, Ruuls RC, Stok W, de Ron L, Wilson S, Davis P, Verrips CT. Comparison of physical chemical properties of llama VHH antibody fragments and mouse monoclonal antibodies. *Biochim Biophys Acta*. 1999 Apr 12;1431(1):37-46. PubMed PMID: 10209277.

OVERALL SUMMARY

Prions encipher disease information by structurally perverting native host protein. While prion researchers made great strides since Stanley Prusiner coined the term prion in 1982, many questions remain unaddressed. For example: which host proteins facilitate disease transmission? What is the function of the properly-folded, cellular prion protein? Lastly, are there ways to combat prion disease? Data presented in this dissertation aimed to (at least partially) address these questions. Factor H (fH) limits autoimmunity by binding host proteins and preventing Complement deposition. In Chapter 2, we show fH binds misfolded prions and aids in disease transmission because fH-deficient mice propagate fewer prions in the lymphoreticular system and resist disease longer than their Factor H sufficient cohorts. These data suggest preventing the Factor H:prion interaction may prolong survival times. Likewise, we show in Chapters 3 and 4 Complement protein C1q and receptors CD21/35 directly binds prion amyloid. Alternative splicing generates CD21 and CD35, and the relative importance of each splice variant in prion disease remained unknown. In Chapter 3, we provide evidence CD21 promotes prion disease more-so than CD35 and highlights specific cell-type roles in prion pathogenesis. Further, we show soluble CD21 may provide a therapeutic avenue to combat prion disease *in vivo*. Previous reports suggest C1q promotes scrapie, but we show an opposite trend in a CWD mouse model. However, human error and perhaps inappropriate comparisons limit the interpretations presented in Chapter 4. In Chapter 5, we assessed the role of the prion protein, PrP^C, in eliciting adaptive immunity. We report B cell activation, from early events such as SRC phosphorylation

and calcium mobilization to antibody production partially relies on PrP^C expression. Lastly, we generated an immune library from an alpaca vaccinated with recombinant prion protein in Chapter 6. After cloning the variable domain and generating ~15 kD nanobodies, initial screening suggests two clones may preferentially bind the misfolded form of PrP. Next steps include testing whether these nanobodies prevent prion infection *in vitro* and *in vivo*. Collectively, data presented in this dissertation not only highlight Factor H and CD21 as host proteins which promote prion disease, but also provide tools and reagents to potentially combat prion disease.